

**CYP1A1 AND CYP1B1 EXPRESSION AND FREE ZINC LEVELS IN  
ENDOTHELIAL CELLS ARE DIFFERENTIALLY REGULATED BY PRO-  
ATHEROGENIC VERSUS ANTI-ATHEROGENIC SHEAR STRESS**

A Dissertation  
Presented to  
The Academic Faculty

By

Daniel Elridge Conway

In Partial Fulfillment  
Of the Requirements for the Degree  
Doctor of Philosophy in Biomedical Engineering

Georgia Institute of Technology and Emory University

May, 2009

**CYP1A1 AND CYP1B1 EXPRESSION AND FREE ZINC LEVELS IN  
ENDOTHELIAL CELLS ARE DIFFERENTIALLY REGULATED BY PRO-  
ATHEROGENIC VERSUS ANTI-ATHEROGENIC SHEAR STRESS**

Approved by:

Dr. Larry McIntire, Advisor  
Wallace H. Coulter Department of  
Biomedical Engineering  
*Georgia Institute of Technology and  
Emory University School of Medicine*

Dr. Suzanne Eskin  
Wallace H. Coulter Department of  
Biomedical Engineering  
*Georgia Institute of Technology and  
Emory University School of Medicine*

Dr. Craig Marcus  
Department of Environmental &  
Molecular Toxicology  
*Oregon State University*

Dr. Hanjoong Jo  
Wallace H. Coulter Department of  
Biomedical Engineering  
*Georgia Institute of Technology and  
Emory University School of Medicine*  
Division of Cardiology  
*Emory University School of Medicine*

Dr. W. Robert Taylor  
Wallace H. Coulter Department of  
Biomedical Engineering  
*Georgia Institute of Technology and  
Emory University School of Medicine*  
Division of Cardiology  
*Emory University School of Medicine*

Date approved: February 17, 2009

*To my family*

## ACKNOWLEDGEMENTS

I would like to express my deep gratitude to the many people who have given me invaluable support for this work and my graduate studies. I would first like to thank my advisors, Dr. Larry McIntire and Dr. Suzanne Eskin for creating a supporting environment for me to pursue my thesis research, and for their knowledge, direction, and personal guidance. I also very much appreciate the support and guidance of the rest of my thesis committee, Dr. W. Robert Taylor, Dr. Hajoong Jo, and Dr. Craig Marcus. I would like to thank Dr. Taylor, Dr. Diana Weiss and J. David Vega for giving me access to human coronary artery samples. I would also like to thank Dr. Jo and Chih-Wen Ni for giving me access to mice and teaching me how to perform mouse aorta isolation and *en face* staining. I also want to thank Dr. Marcus for providing me with access to CYP1A1 and CYP1B1 antibodies, a wealth of P450 knowledge, and for his frequent and patient mentoring.

I would like to thank the current and former members of the McIntire lab for their training, frequent discussions of data and hypotheses, and personal support. In particular I wish to thank Yumiko Sakurai for her technical assistance and expertise in Western blotting and immunohistochemistry. I also wish to acknowledge Marcie Williams for her work on the reversing flow project, specifically for her role in performing the microarray analysis of the reversing flow experiments and for her participation in designing the reversing flow system and monocyte adhesion assay. In addition I want to thank Dr. Andrew Yee for his mentoring and training and for his assistance in developing the

reversing flow system. Finally I want to thank the undergraduate students who have contributed to my thesis project, Blaise MacEachern, Matt Goette, Courtney Mitchell, and Ankit Shah.

I want to thank Dr. Phil Santangelo for his advice on measuring and quantitating changes in free zinc. I also want to thank the undergraduate lab managers, Joe Polinsky and Dr. Essy Behraves, for their very helpful discussion and for allowing me virtually unrestricted access to the undergraduate laboratory equipment and supplies.

I wish to thank the National Science Foundation for providing me with a Graduate Research Fellowship. Additionally, I would like to thank my undergraduate advisor, Dr. Antonios Mikos for his support in editing my graduate fellowship application. I would also like to acknowledge the National Institutes of Health for the funding of my research.

Lastly, I wish to express my deep gratitude to my entire family for their continued support. Thank you to my parents for providing me with the enthusiasm for science when I was a young child. I also would like to thank my wife, Christy, for her continued support and friendship.

# TABLE OF CONTENTS

ACKNOWLEDGEMENTS .....	iv
LIST OF TABLES .....	viii
LIST OF FIGURES.....	ix
LIST OF SYMBOLS ABBREVIATIONS .....	xi
SUMMARY .....	xv
CHAPTER 1: THESIS RATIONALE .....	1
1.1 Introduction.....	1
Specific Aim 1: Determine the effects of the carotid sinus wall shear stress on endothelial cell function.....	4
Specific Aim 2: Characterize the regulation of and determine the functional contributions of CYP1A1 and CYP1B1 to the human endothelial cell shear stress response.....	5
Specific Aim 3: Characterize the regulation of and determine the functional contributions of free zinc to the human endothelial cell shear stress response.....	7
CHAPTER 2: REVERSING SHEAR STRESS PROMOTES A MORE INFLAMMATORY AND PROLIFERATIVE PHENOTYPE IN ENDOTHELIAL CELLS THAN STEADY SHEAR STRESS .....	9
2.1 Introduction.....	9
2.2 Methods.....	11
2.3 Results.....	16
2.4 Discussion .....	34
CHAPTER 3: EXPRESSION OF CYP1A1 AND CYP1B1 IN HUMAN ENDOTHELIAL CELLS: REGULATION BY FLUID SHEAR STRESS .....	40
3.1 Introduction.....	40
3.2 Methods.....	42

3.3 Results .....	47
3.4 Discussion .....	56
CHAPTER 4: FREE INTRACELULAR ZINC IS REDUCED UNDER REVERSING SHEAR STRESS .....	62
4.1 Introduction .....	62
4.2 Methods.....	65
4.3 Results.....	68
4.4 Discussion .....	75
CHAPTER 5: CONCLUSIONS.....	78
5.1 Summary .....	78
5.2 Future Work .....	80
APPENDIX A: CALCULATION OF WALL SHEAR STRESS .....	83
APPENDIX B: SUPPLEMENTARY MICROARRAY TABLES .....	89
REFERENCES.....	97

## LIST OF TABLES

Table 2.1: Number of Differentially Expressed Genes Between Conditions .....	18
Table 2.2: Top 10 Genes Up- and Down-Regulated by Fluid Flow .....	21
Table 2.3: Genes regulated by flow reversal.....	28
Table B.1: Complete list of genes regulated by high shear component.....	89
Table B.2: Complete list of genes regulated by low shear stress.....	89

## LIST OF FIGURES

Figure 2.1	Wall shear stress of the carotid sinus used in the reversing flow system. ....	11
Figure 2.2	Schematic of the reversing flow system. ....	12
Figure 2.3	Comparison of <i>in vitro</i> parallel plate shear stress to <i>in vivo</i> shear stress.....	16
Figure 2.4	Changes in endothelial cell morphology by differences in shear stress. ....	17
Figure 2.5	Proportional Venn diagram of differentially expressed genes in a comparison of RF, HSS, and LSS to static culture.....	20
Figure 2.6	ECs exposed to fluid flow cluster on a branch separate from ECs grown in static culture. ....	22
Figure 2.7	Venn diagram of differentially expressed genes in a comparison of RF to HSS, RF to LSS, and HSS to LSS. ....	23
Figure 2.8	Hierarchical clusters of functional groups up-regulated by low average shear stress.....	25
Figure 2.9	Hierarchical clusters of functional groups up-regulated by low average shear stress.....	26
Figure 2.10	Hierarchical clusters of functional groups up- and down-regulated by reversing flow. ....	29
Figure 2.11	qRT-PCR Confirmation of Microarray Results.....	31
Figure 2.12	Cell proliferation is inhibited by high shear stress compared to low average shear stress and reversing shear stress. ....	32
Figure 2.13	THP-1 cells have greater adhesion to ECs exposed to reversing flow .....	33
Figure 3.1	Time course of CYP1A1 and CYP1B1 mRNA and protein expression under shear stress .....	48
Figure 3.2	Effect of shear stress on CYP1A1 and CYP1B1 activity .....	49
Figure 3.3	Effect of shear stress magnitude on CYP1A1 and CYP1B1 mRNA and protein expression .....	50
Figure 3.4	Effect of shear stress pattern on CYP1A1 and CYP1B1 mRNA and protein expression.....	52

Figure 3.5 Effect of siRNA knockdown of CYP1A1 and CYP1B1 gene expression.....	53
Figure 3.6 Expression of AhR and CYP1A1 protein in mouse aorta .....	54
Figure 3.7 Expression of CYP1A1 and CYP1B1 protein in human coronary artery endothelial cells <i>in vivo</i> .....	55
Figure 4.1 Free zinc levels in HUVEC after 24 hours shear stress.....	69
Figure 4.2 Pseudocolor of free zinc levels in HUVEC after 24 hours shear stress.....	70
Figure 4.3 Flow cytometry measurement of free zinc in HUVEC.....	71
Figure 4.4 Inhibition of nitric oxide attenuates the free zinc increase by shear stress.....	72
Figure 4.5 Metallothionein and Znt-1 expression is regulated by shear stress. ....	73
Figure 4.6 Expression of metallothionein protein in mouse aorta .....	74
Figure 4.7 Possible mechanisms for shear stress mediated changes in free zinc.....	76

## LIST OF SYMBOLS ABBREVIATIONS

18S	18 Svedberg Sub-unit of Ribosomal Ribonucleic Acid
AhR	Aryl hydrocarbon receptor
ANOVA	Analysis of Variance
APOL3	Apolipoprotein L-III
BrdU	Bromodeoxyuridine
CCNB3	Cyclin B3
CCNE2	Cyclin E2
CD31	Platelet Endothelial Cell Adhesion Molecule 1
CD34	Hematopoietic Progenitor Cell Antigen
CD58	Lymphocyte Function-associated Antigen, Type 3
CDC20	Cell Division Cycle 20
cDNA	Complementary Deoxyribonucleic Acid
CDK2	Cyclin-dependent Kinase 2
CRIP1	Cysteine-rich Intestinal Protein 1
cRNA	Complementary Ribonucleic Acid
Ct	Cycle Threshold
CVD	Cardiovascular Disease
CYP	Cytochrome P450
CYP1	Cytochrome P450, Family 1
CYP1A1	Cytochrome P450, Family 1, Subfamily A, Member 1

CYP1B1	Cytochrome P450, Family 1, Subfamily B, Member 1
DAVID	Database for Annotation, Visualization and Integrated Discovery
EC	Endothelial Cells
eNOS	Endothelial Nitric Oxide Synthase
FITC	Fluorescein Isothiocyanate
G <sub>1</sub> phase	Gap 1 Phase
G <sub>2</sub> phase	Gap 2 Phase
HAEC	Human Aortic Endothelial Cells
HDL	High-density lipoprotein
HSS	High Steady Shear Stress
HUVEC	Human Umbilical Vein Endothelial Cells
Hz	Hertz
ICAM-1	Inter-Cellular Adhesion Molecule 1
IgG	Immunoglobulin G
kDa	Kilodalton
KLF2	Kruppel-like Factor 2
LDL	Low-density Lipoprotein
L-NAME	L-N <sup>G</sup> -Nitroarginine methyl ester
LSS	Low Steady Shear Stress
Luciferin-CEE	Luciferin-6' Chloroethyl Ether
MEF2A	Mads Box Transcription Enhancer Factor 2, Polypeptide A
MMP	Matrix Metalloproteinase
MMP-2	Matrix Metalloproteinase 2

MMP-9	Matrix Metalloproteinase 9
M phase	Mitosis Phase
MT	Metallothionein
MT1	Metallothionein, Family 1
MT1E	Metallothionein, Family 1, Member E
MT1F	Metallothionein, Family 1, Member F
MT1G	Metallothionein, Family 1, Member G
MT2A	Metallothionein, Family 2, Member A
MTF-1	Metal-regulatory Transcription Factor 1
NF- $\kappa$ B	Nuclear Factor Kappa-light-chain-enhancer of Activated B Cells
NO	Nitric Oxide
NPR1	Natriuretic Peptide Receptor A
p	P-value
P450	Cytochrome P450
PBS	Phosphate Buffered Solution
PRIM2A	Primase Polypeptide 2A
PTH1H	Parathyroid Hormone-like Hormone
Q	Volumetric flow rate
qRT-PCR	Quantitative Real Time Polymerase Chain Reaction
RF	Reversing Flow
RNA	Ribonucleic Acid
RRM1	Ribonucleotide Reductase M1
S phase	Synthesis Phase

SDS-PAGE	Sodium Dodecyl Sulfate Polyacrylamide Gel Electrophoresis
SEM	Standard Error of the Mean
siRNA	Small Interfering Ribonucleic Acid
STAT	Static
THP-1	Human Acute Monocytic Leukemia Cell Line
TMS	2,3',4,5'-Tetramethoxystilbene
TPEN	N,N,N',N'-tetrakis-(2-pyridylmethyl)-ethylenediamine
VCAM-1	Vascular Cell Adhesion Molecule 1
VLDL	Very Low-density Lipoprotein
Znt-1	Solute Carrier Family 30, Member 1; SLC30A1
$\gamma$	Shear Rate
$\mu$	Viscosity
$\tau_w$	Wall Shear Stress

## SUMMARY

Understanding the molecular basis of the modulation of vascular cell phenotype by mechanical forces (stresses induced by blood flow and vascular wall strain) is an area of great significance in vascular biology. It is hypothesized that exposing endothelial cells to steady or non-reversing pulsatile shear stress produces a healthy, anti-atherogenic endothelium, whereas a reversing pulsatile shear stress promotes an unhealthy, pro-atherogenic endothelium. To further investigate this hypothesis, a novel parallel plate flow chamber system was used to expose human endothelial cells to a pro-atherogenic reversing shear stress waveform designed to simulate the wall shear stress at the carotid sinus, a region prone to atherosclerosis. Cells exposed to this reversing shear stress were compared to cells exposed to high levels of steady shear stress (15 dynes/cm<sup>2</sup>), low steady shear stress (1 dyne/cm<sup>2</sup>, the time-average of the carotid shear stress), and static culture conditions. Functional analysis confirmed previous findings that reversing shear stress increases cell proliferation and monocyte adhesion. Microarray results indicate that although there are unique sets of genes controlled by both low average shear stress and by reversing flow, more genes were controlled by low average shear stress. We propose that low-time average shear stress, and not fluid reversal/oscillation, may be the more significant mechanical force. The reversing shear stress system was also used to investigate two shear stress-responsive genes, CYP1A1 and CYP1B1. Both were maximally up-regulated at arterial steady shear stresses of at least 15 dynes/cm<sup>2</sup> and reversing pulsatile shear stress attenuated expression of both genes. Furthermore, AhR

nuclear localization and CYP1A1 protein expression correlate with the flow patterns in the mouse aortic arch. The data strongly suggest that the AhR/CYP1 pathway promotes an anti-atherogenic phenotype in the endothelium. Finally, as a result of observed changes in zinc-binding and zinc transporter proteins, changes in free zinc were measured under different shear stresses. High steady shear stress dramatically increases the levels of free zinc in endothelial cells as compared to cells grown in static culture. This increase in free zinc is attenuated under reversing shear stress and low steady shear stress, which correlates with an increase in zinc-binding metallothionein proteins and zinc exporter Znt-1. Overall, the findings provide further insight into endothelial responses to mechanical forces and may be important in understanding mechanisms of atherosclerotic development and localization to regions of disturbed flow.

## CHAPTER 1: THESIS RATIONALE

### 1.1 Introduction

According to the Heart Disease and Stroke Statistics published by the American Heart Association, cardiovascular disease (CVD) remains the primary cause of mortality in both women and men in the United States. It is estimated that 80 million American adults (approximately 1 in 3) suffer from one or more types of CVD, which includes high blood pressure, coronary heart disease, heart failure, and stroke.<sup>1</sup> CVD claims more lives each year than the next four leading causes of death (cancer, chronic lower respiratory diseases, accidents, and diabetes mellitus) combined. The estimated direct and indirect cost of CVD for 2009 is \$475.3 billion.<sup>1</sup>

Mechanical forces resulting from blood flow directly affect cellular functions and morphology and thus, the physiology of the cardiovascular system.<sup>2</sup> The forces to which cells of the blood vessels are subjected directly include wall shear stress and circumferential strain. Disruption or distortion of these forces affects local cellular homeostasis and may prime the area for development of pathology. Sites of atherosclerosis in humans have been shown to be non-random, and are strongly correlated with curved or branched sites in the vasculature that, as a result of their geometry, experience low time-averaged shear stress, shear stress reversal, and spatial and temporal gradients in shear stress.<sup>3, 4</sup>

The flow of blood over the endothelium generates viscous drag forces in the direction of flow. The resulting tangential force exerted per unit area of vessel surface at

the blood–endothelium surface defines shear stress. Mathematically, the product between the viscosity ( $\mu$ ) and the velocity gradient at the wall, also known as the wall shear rate ( $\gamma$ ), equates to wall shear stress ( $\tau_w$ ) (Equation 1).

$$\tau_w = \mu\gamma \quad (1)$$

With ventricular contraction, momentum propagates as waves down the aorta, diminishing in amplitude with increasing distance from the heart. Pulsatility is generated by the pumping action of the heart, and gives rise to pulsatile shear stress and cyclic strain. Typical mean arterial values of shear stress range from 6 to 40 dyn/cm<sup>2</sup>.<sup>5,6</sup> While pulsing down the arterial tree, blood flow remains mostly laminar; however, it often becomes complex and/or disturbed (reversing and/or recirculating) at areas of arterial branching, triggering spatial and/or temporal gradients in shear stress.

Endothelial cells have been studied extensively for their ability to respond to changes in shear stress. Two *in vitro* systems have been developed to characterize the response of endothelial cells to a variety of shear stresses: the parallel plate flow chamber and the cone and plate system. In the parallel plate model, cells are grown on a glass slide and mounted onto a polycarbonate parallel plate flow chamber, separated only by a silicone gasket.<sup>7</sup> This gasket creates a very small gap height through which tissue culture medium is circulated. The geometric dimensions are known, allowing for the calculation of the fluid shear stress from the flow rate. For a Newtonian fluid flowing through a parallel-plate flow chamber with a rectangular geometry, the steady, laminar shear stress at the wall is:

$$\tau_w = \frac{6\mu Q}{bh^2} \quad (2)$$

in which  $\tau_w$  = wall shear stress,  $\mu$  = viscosity,  $Q$  = flow rate,  $b$  = channel width, and  $h$  = channel height. By varying the chamber geometry, the flow rate, or the viscosity, the entire physiological range of wall shear stresses can be investigated. The flow rate is varied using a syringe pump or gravity driven system to provide the desired wall shear stress across the cells. The cone and plate viscometer system consists of a tissue culture dish as the plate and a fixed angle cone mounted to a motor that imparts an angular velocity. For small cone angles, the shear rate (and therefore the shear stress) is essentially constant throughout the flow field. Since the dimensions of this system are also characterized, the fluid shear stress can be calculated for a given angular velocity.

Endothelial cells, in either of these *in vitro* shear stress systems, exposed to long-term (24 hours or greater) steady shear stress at arterial levels (10-25 dynes/cm<sup>2</sup>), as well as pulsatile non-reversing shear stress, have been shown to produce a more anti-inflammatory and anti-proliferative phenotype than when exposed to pulsatile reversing conditions or low shear stress, or to static culture.<sup>8-11</sup> Acute responses to arterial shear stress include release of signaling molecules such as nitric oxide and prostacyclin, phosphorylation of membrane proteins, and activation of GTPases and tyrosine kinases.<sup>12</sup>

<sup>13</sup> Released signaling molecules, such as prostacyclin and nitric oxide, can in turn act on smooth muscle cells to mediate vasorelaxation. Response of endothelial cells to arterial level shear stresses of 24 hours or longer include alignment of the actin cytoskeleton, movement of the microtubule organizing center toward the direction of flow, and cell elongation and alignment in the direction of flow.<sup>14, 15</sup>

Endothelial cells respond differently to reversing or oscillatory shear stress as compared to non-reversing shear stress. Steady or non-reversing shear stress transiently

induces pro-inflammatory and proliferative pathways, which are subsequently down-regulated by long-term exposure to shear stress. However, oscillatory or reversing shear stress results in sustained activation of these pathways, leading to the hypothesis that under steady shear stress cells adapt and down-regulate these pathways, whereas under disturbed flow the continued changes in flow magnitude and direction lead to sustained activation.<sup>8, 11, 14</sup> The increases in cell proliferation, lipid metabolism, and inflammation observed in endothelial cells exposed to reversing shear stress *in vitro* suggest that *in vivo* disturbed hemodynamics may prime local sites for atherosclerosis. Consistent with biochemical differences, cells do not elongate or align in the direction of flow at sites of atherosclerosis.

The overall goal of this thesis project was to investigate the effects of pro-atherogenic shear stress on endothelial cells, using a physiological shear stress waveform in an existing parallel plate model. Microarray analysis and functional assays were performed on endothelial cells exposed to either pro-atherogenic or anti-atherogenic shear stress. Two shear stress responsive genes, CYP1A1 and CYP1B1, were characterized for their response to different forms of fluid shear stress. As a result of observed changes in zinc-binding and zinc transporter proteins, changes in free zinc were measured under different shear stress regimens.

**Specific Aim 1: Determine the effects of the carotid sinus wall shear stress on endothelial cell function**

It is hypothesized that exposing endothelial cells to steady or non-reversing pulsatile shear stress produces a healthy, anti-atherogenic endothelium, whereas a

reversing pulsatile shear stress promotes an unhealthy, pro-atherogenic endothelium.<sup>3, 8</sup>

Some of the earliest studies comparing anti-atherogenic *non-reversing* arterial shear stress to pro-atherogenic *reversing* arterial shear stress modeled the reversing shear stress in the form of a sine wave. However, simulations of the wall shear stress of the carotid sinus have shown the wall shear stress is not harmonic, but is a more complex waveform.<sup>16, 17</sup> Additionally, these studies did not address whether the low time-average shear stress or the fluid reversal were responsible for observed changes in endothelial gene expression and function

A new parallel plate flow chamber system was developed that is capable of reproducing the wall shear stress at the carotid sinus (a region prone to the development of atherosclerosis). Cells exposed to this reversing shear stress were compared to cells exposed to high levels of steady shear stress (15 dynes/cm<sup>2</sup>), low steady shear stress (1 dyne/cm<sup>2</sup>, the time-average of the carotid shear stress), and static culture conditions. Global gene changes were measured using microarray analysis, and functional assays performed to examine changes in cell proliferation and inflammation.

**Specific Aim 2: Characterize the regulation of and determine the functional contributions of CYP1A1 and CYP1B1 to the human endothelial cell shear stress response**

Previous microarray studies of human endothelial cells exposed to steady shear stress show CYP1A1 and CYP1B1 as two of the most dramatically changed genes when compared to static controls.<sup>16, 18-23</sup> CYP1A1 and CYP1B1 are classically recognized as enzymes that metabolize exogenous halogenated or polycyclic aromatic compounds for

elimination.<sup>24, 25</sup> CYP1A1 and CYP1B1 enzymes can also modulate cellular levels of a variety of lipid signaling molecules, including arachidonic acid and retinoic acid metabolites that can directly affect gene expression and vascular homeostasis.<sup>26</sup> Recent work has shown that CYP1B1 is involved in the generation of retinoic acid during chick embryogenesis.<sup>27</sup> Mutations of CYP1B1 in humans are associated with glaucoma,<sup>28</sup> and CYP1B1 (-/-) mice have abnormalities in their ocular drainage structure that resemble those in human glaucoma patients.<sup>29, 30</sup> The ability of both genes to affect lipid signaling, and the association of CYP1B1 mutations with a human pathology strongly suggest that CYP1A1 and CYP1B1 have important endogenous roles in the maintenance of homeostatic functions.

Because CYP1A1 and CYP1B1 have been primarily studied for their response to environmental toxins, their functional contribution to the endothelial cell as well as to the shear stress response remains unknown. To further investigate physiological role of these two genes, the effects of duration, magnitude and pattern of shear stress on CYP1A1 and CYP1B1 expression in human endothelial cells are described, toward the goal of understanding the role(s) of these genes in pro-atherogenic or anti-atherogenic endothelial cell functions. The expression of CYP1A1 and CYP1B1 in endothelial cells *in vivo* has been examined to provide confirmation of their constitutive expression and regulation by shear stress.

### **Specific Aim 3: Characterize the regulation of and determine the functional contributions of free zinc to the human endothelial cell shear stress response**

Zinc is a trace metal and essential nutrient. Within a cell, zinc binds with high affinity to metalloenzymes, structural proteins, and transcription factors, making the intracellular concentration of free (unbound) zinc typically very low.<sup>31</sup> Zinc has been estimated to be required for the function of more than 2000 transcription factors and 300 enzymes, making many signaling pathways dependent on zinc. Zinc has also been shown to have anti-atherogenic properties, although the mechanisms remain unclear.

Epidemiological studies of zinc have shown that in some populations low zinc serum levels are associated with coronary artery disease.<sup>32</sup> Zinc has also been found to reduce the development of atherosclerosis in rabbits<sup>33-35</sup>. LDL (-/-) mice fed a zinc deficient diet had increased VLDL and HDL,<sup>36</sup> increased vascular cell adhesion molecule (VCAM-1) protein expression,<sup>36</sup> increased monocyte adhesion,<sup>37</sup> and up-regulation of nuclear factor  $\kappa$ B (NF- $\kappa$ B) in cultured endothelial cells.<sup>38</sup> Zinc has been shown to be required in the activation of the transcription factor nuclear factor, erythroid derived 2, like-2 (nrf-2) by hydrogen peroxide;<sup>31</sup> nrf-2 is responsible for the activation of antioxidant response element (ARE) genes such as hemeoxygenase-1 (HO-1).

A recent microarray study by our group showed the MT1 family, and MT2A to be differentially regulated by non-reversing pulsatile shear stress compared to steady shear stress.<sup>9</sup> Our unpublished microarray data, as well as published microarray data by Dai et al.,<sup>16</sup> showed increased MT1 and MT2A mRNA expression in HUVEC exposed to reversing shear stress compared to cells exposed to non-reversing shear stress. Regulation

of metallothioneins by shear stress was also reported by Ohura et al. who showed a downregulation of metallothionein expression in cells exposed to turbulent flow in comparison to high steady laminar flow.<sup>18</sup> These differences indicate that metallothionein expression is highly sensitive to variations in shear stress.

Cells subjected to different shear stress regimes were examined for intracellular changes in free zinc. Changes in expression levels of zinc binding and zinc transporting proteins were also examined. Experiments in which nitric oxide production is inhibited were performed to assess the role of nitric oxide in free zinc changes.

## CHAPTER 2: REVERSING SHEAR STRESS PROMOTES A MORE INFLAMMATORY AND PROLIFERATIVE PHENOTYPE IN ENDOTHELIAL CELLS THAN STEADY SHEAR STRESS

*N.B.: Work in this chapter was generated as a joint project with Marcie Williams, a fellow graduate student in the McIntire Lab. I participated jointly with Marcie in the design of the reversing shear stress system and monocyte adhesion assay experiments. I performed the flow validation, shear stress experiments and RNA isolation, and BrdU cell proliferation experiments. Marcie was responsible for the microarray analysis.*

### 2.1 Introduction

Atherosclerosis is typically localized to the carotid artery sinus, the coronary arteries, the abdominal aorta, and the superficial femoral arteries.<sup>39</sup> These regions have complex blood flow patterns which include flow reversal during each cardiac cycle, leading to the hypothesis that disturbed hemodynamic patterns are atherogenic. Such differences in hemodynamics alter the gene expression profile and ultimately the structure and function of endothelial cells, resulting in modulation of both endothelial cell responses to blood borne factors and endothelial cell interactions with underlying smooth muscle cells, thus increasing the likelihood of atherogenesis.<sup>3, 8</sup>

Some of the earliest studies comparing “anti-atherogenic” *non-reversing* arterial shear stress to “pro-atherogenic” *reversing* arterial shear stress modeled the reversing shear stress in the form of a sine wave. However, simulations of the wall shear stress of

the carotid sinus have shown the wall shear stress is not harmonic, but is a more complex waveform.<sup>16, 17</sup> This waveform has a low average shear stress of  $\sim 1$  dyne/cm<sup>2</sup> with peak shear stresses as high as  $\pm 11$  dyne/cm<sup>2</sup>. Previous studies used high steady shear stress and static conditions as controls for comparison to the proatherogenic waveform.<sup>16, 18, 20</sup> These studies did not address whether the low average shear stress or the flow reversal found at the wall of the carotid sinus was responsible for observed increases in atherogenesis.

To address the limitations of previous studies, we developed a parallel plate reversing flow system that accurately recreates the physiological form of the reversing shear stress at the carotid sinus wall. Using human umbilical vein endothelial cells (HUVEC), we compared the effects of this shear profile to the effects of steady arterial shear stress (15 dynes/cm<sup>2</sup>). Based on our previous work showing few differences between non-reversing pulsatile and steady shear stress,<sup>9, 40</sup> we chose a steady shear stress of 15 dynes/cm<sup>2</sup> to approximate shear stress in the arteries. We also included a steady low shear stress control (1 dyne/cm<sup>2</sup>) to distinguish gene and functional changes that were due to the application of a low average shear stress. Functional analysis confirmed previous findings that reversing shear stress increases cell proliferation and monocyte adhesion; increased cell proliferation was found to be dependent on low average shear stress whereas monocyte adhesion was found to be dependent on fluid reversal. Microarray results indicate that although there are unique sets of genes controlled by both low average shear stress and by reversing flow, more genes were controlled by low average shear stress. We propose that low-time average shear stress, and not fluid reversal/oscillation, may be the more significant mechanical force on endothelial cells.

## 2.2 Methods

### *Reversing Shear Stress System*

The shear stress profile used in this study (Figure 2.1) was based on a computer simulation of the wall shear stresses at the carotid bifurcation (time-average 1 dyne/cm<sup>2</sup>, maximum +11 dynes/cm<sup>2</sup>, minimum -11 dynes/cm<sup>2</sup>, 1 Hz).<sup>17</sup> A custom flow system was designed to reproduce this waveform in a parallel plate flow system (Figure 2.2). The flow profile was split into two separate waveforms: the steady component of the waveform (-1 dyne/cm<sup>2</sup>) and the reversing component of the waveform which had a time-averaged shear stress of 0 dynes/cm<sup>2</sup>. A standard syringe pump (Harvard Apparatus 33 Twin Syringe Pump) was used to apply the continuous shear stress component. A 1 mL glass syringe (Becton Dickinson) was mounted to a linear motor (MX80L, Parker Motion). The linear motor controller (ACR9000, Parker Motion) was programmed to deliver the reversing flow component.

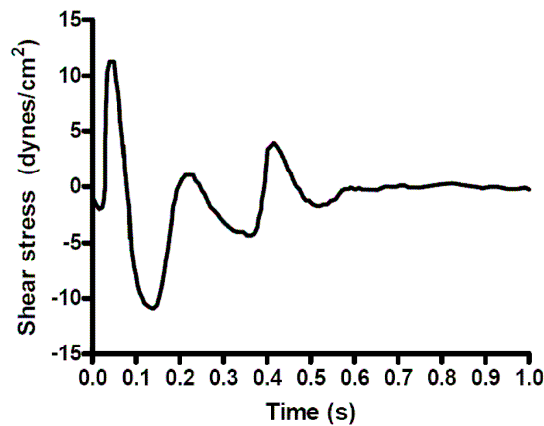


Figure 2.1 Wall shear stress of the carotid sinus used in the reversing flow system. A previously published computer simulation<sup>17</sup> was used to obtain the wall shear stress at the carotid sinus. This shear stress profile was used for the reversing flow system.

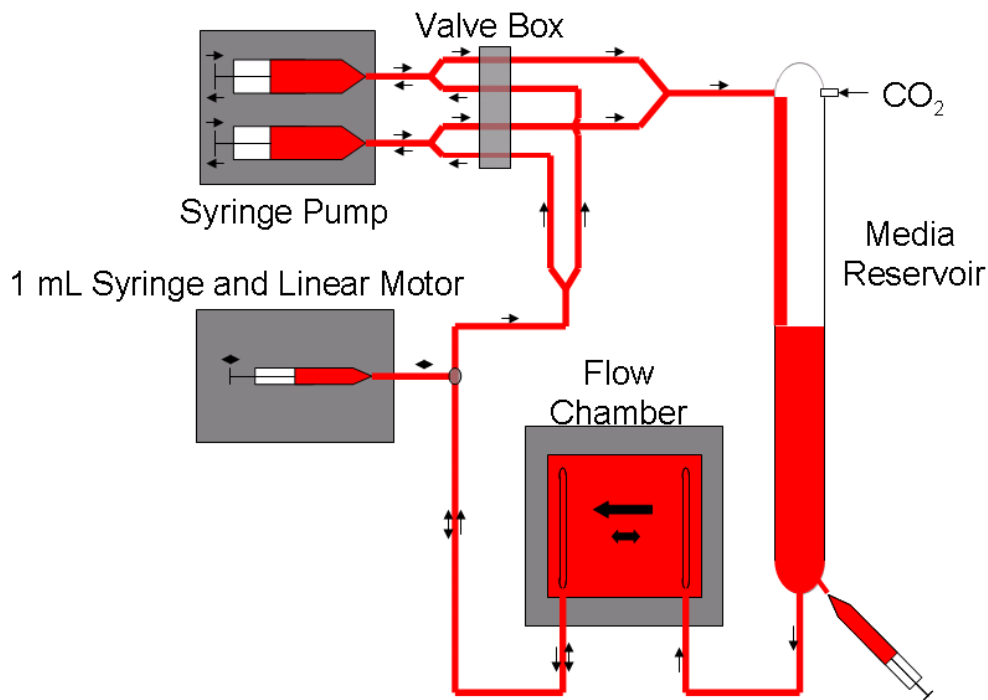


Figure 2.2 Schematic of the reversing flow system.

To validate the reversing flow system, latex beads (6  $\mu\text{m}$ , Bangs Laboratory) were tracked (Metamorph, Molecular Devices) under high-speed video microscopy (1000 frames per second, (Phantom V4.2, Vision Research) to directly measure the flow rate through the chamber. The focal plane of the microscope was selected to be the center of the parallel plate flow chamber and the velocity of the beads was assumed to represent the maximum velocity through the chamber. Wall shear stress was calculated using Equation 3 ( $V_{\text{max}}$  is the maximum velocity,  $b$  is the height of the flow chamber, and  $\mu$  is the viscosity of the media):

$$\tau_w = \frac{4V_{\text{max}}\mu}{b} \quad (3)$$

The full derivation of Equation 3 is in Appendix A.

### *Experimental Protocol*

HUVEC (passages 3-5) (Lonza) were grown to confluence on glass slides,<sup>41</sup> mounted on a parallel plate flow chamber, and exposed to one of four conditions for 24 hours: reversing flow using the newly designed system (RF, 1 dyne/cm<sup>2</sup> +/- 11 dyne/cm<sup>2</sup>), arterial high steady shear stress (HSS, 15 dynes/cm<sup>2</sup>), low steady shear stress (LSS, 1 dyne/cm<sup>2</sup>), and static treatment.

### *RNA Isolation and qRT-PCR*

Immediately after exposure to shear stress total RNA was extracted using TRIzol (Invitrogen); RNA was further purified with DNase (Qiagen) and RNeasy MinElute Cleanup Kit (Qiagen), according to manufacturers' instructions. The integrity and quantity of the RNA were verified with UV spectrophotometry, accepting only RNA with a 260/280 ratio greater than 1.9.

Total RNA from each sample was reverse transcribed into cDNA using SuperScript II (Invitrogen). cDNA was purified with Micro Bio-Spin P-30 Chromatography Columns (BioRad), and diluted in RT-PCR Grade Water (Ambion). Pre-designed PCR primers and Quantitect SYBR Green PCR Master Mix were purchased from Qiagen. Primers were added to the master mix at a ratio of 1:5. Each reaction was performed with 4 µl of diluted cDNA and 6 µl of primers in the master mix. The qRT-PCR reactions were performed on a MyIQ (BioRad) with a 15 minute activation step at 95 °C; 50 cycles at 94 °C for 15 seconds, 55 °C for 30 seconds, 72 °C for 30 seconds; and a ramped melting cycle. Samples were normalized based on 18S expression. Fold

changes were determined using the  $\Delta\Delta C_t$  method. qRT-PCR was used to verify gene expression from RNA isolated from five independent experiments.

#### *Microarray Analysis of Gene Expression Changes*

Microarray hybridization and imaging were performed at the Morehouse School of Medicine Functional Genomics Core Facility. Briefly, RNA was linearly amplified to cRNA using Cy3 labeled CTP and a Low RNA Input Fluorescent Linear Amplification Kit (Agilent) according to the manufacturer's instructions. Cy3-labeled cRNA for each sample was hybridized to a 44k Whole Human Genome Microarray (Agilent) according to the manufacturer's instructions. Slides were dried under nitrogen and scanned on an Agilent DNA Microarray Scanner. Microarray images were analyzed with Agilent Feature Extraction Software according to the manufacturer's instructions.

Microarray images were analyzed with Agilent Feature Extraction Software according to the manufacturer's instructions. Genes were flagged as either present, marginal, or absent based on criteria such as image saturation, uniformity, population outlier, and uniformity of background. GeneSpring GX 10 software was used to further analyze the microarray data. One way ANOVA assuming equal variances was applied followed by a post-hoc Student-Neuman-Keuls test with a false discovery rate of 5%. Differentially expressed genes were identified as those genes having adjusted p-values of less than 0.05 and flags marked as present or marginal in at least 50% of the samples for conditions with fold changes of at least 1.5 fold.

### *Analysis of Cell Proliferation*

Shear stress experiments were performed in the presence of 10  $\mu$ M bromodeoxyuridine (BrdU) (EMD Biosciences). Cells were fixed in 4% paraformaldehyde, treated with 2N HCl and 0.1% Triton-X, stained using a rat anti-BrdU antibody (Abcam), followed by staining using goat anti-rat Alexa Fluor 563 (Invitrogen) and Hoechst (Invitrogen). Standard fluorescent microscopy was used to image the cells. ImageJ (NIH) was used to count BrdU stained cells and Hoechst stained cells from the same frame. For each experimental condition 8 frames were analyzed for each experimental replicate with a total of 5 replicates. The percentage of cells that divided under shear stress was determined by dividing the BrdU positive cells by the total number of cells as measured by the Hoechst staining.

### *Monocyte Adhesion Assay*

Monocyte adhesion assays were performed on HUVEC pretreated for 24 hours with one of the four shear stress conditions. Cell tracker orange stained THP-1 (Human acute monocytic leukemia cell line) cells ( $10^6$  cells/mL) were perfused across the pretreated HUVEC at 1 dyne/cm<sup>2</sup> for 5 minutes, stopping the flow for 30 seconds, and rinsing with media for an additional 5 minutes. The number of adherent cells was then counted in ten frames for each replicate.

## 2.3 Results

High-speed video tracking of latex beads through the parallel plate chamber allowed for measurement of the average flow rate and the calculation of the wall shear stress in the chamber. Figure 2.3 provides a visual comparison of the wall shear stress within our parallel plate flow chamber to the *in vivo* shear stress at the wall of the carotid sinus as determined by computer simulations performed by Perktold and Rappitsch.<sup>17</sup> This comparison shows that our system accurately recreates the *in vivo* reversing shear stress found at the wall of the carotid sinus. Because this area of the vasculature is particularly prone to atherosclerosis, validation of our system's ability to model flow within the carotid sinus indicates that our system is appropriate for studying the effects of this altered flow type on endothelial cells.

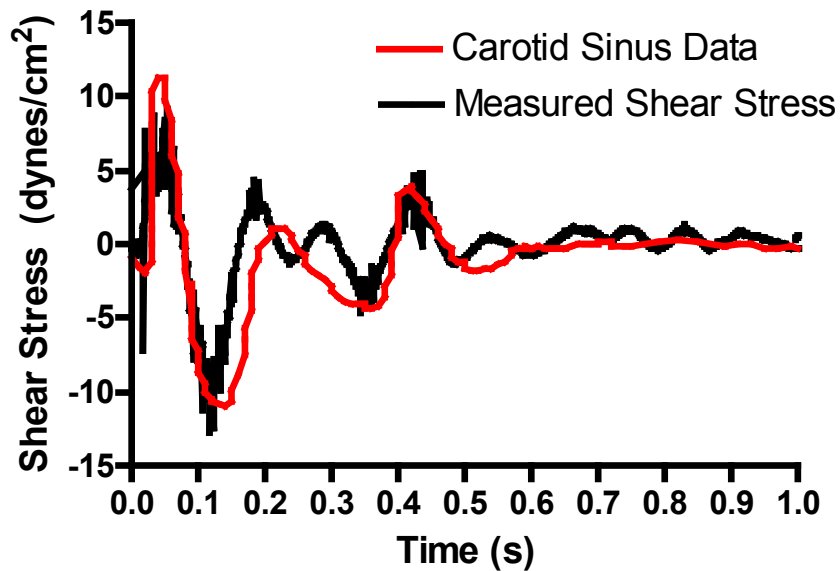


Figure 2.3 Comparison of *in vitro* parallel plate shear stress to *in vivo* shear stress. *In vitro* parallel plate shear stress was estimated by tracking latex beads within the flow chamber using high speed video microscopy. *In vivo* shear stress was estimated by Perktold and Rappitsch<sup>17</sup> using computer simulations of fluid flow within the carotid sinus.

ECs treated with steady shear stress of 15 dyne/cm<sup>2</sup> for 24 hours aligned parallel to the flow direction (Figure 2.4). ECs exposed to 1 dyne/cm<sup>2</sup> were randomly aligned and slightly elongated in comparison to static conditions. Under reversing flow, the cells exhibited a cobblestone morphology, which is similar to that seen under static conditions.

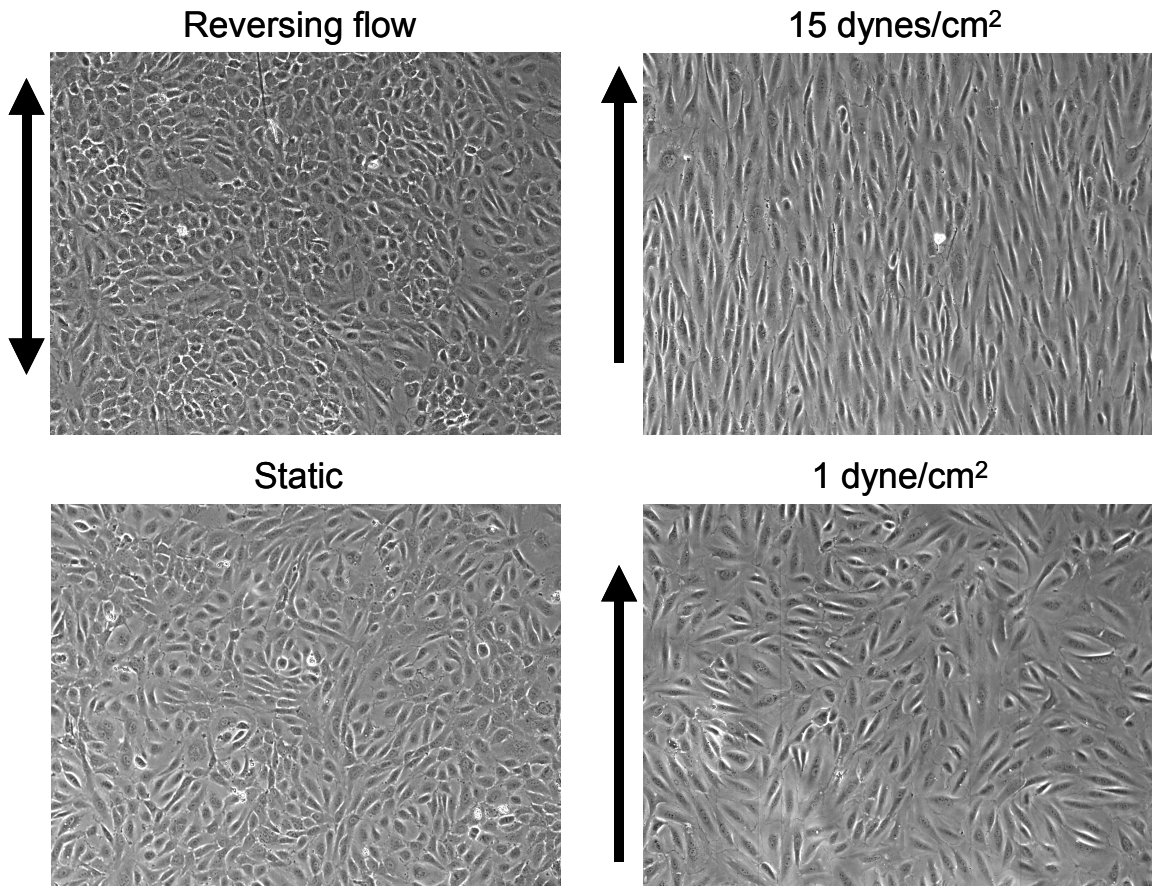


Figure 2.4 Changes in endothelial cell morphology by differences in shear stress. Phase contrast images of ECs exposed to 15 dynes/cm<sup>2</sup> shear stress for 24 h reveal an elongated morphology which is aligned with shear stress. ECs exposed to 1 dyne/cm<sup>2</sup> have an elongated morphology but do not align with shear stress. ECs exposed to reversing flow exhibit a cobblestone like morphology that is very similar to the morphology of cells grown under static conditions.

A comparison of HUVEC exposed to 24 hours of reversing flow (RF), high steady shear (HSS), low steady shear (LSS), and static culture (STAT) was performed with a whole human genome microarray. One-way ANOVA with a false discovery rate of 5% revealed 4767 genes with statistically significant differences between at least two of the treatment conditions. A post hoc Student-Newman-Keuls test was performed to determine which conditions were significantly different from each other for each gene. Differentially expressed genes were identified as those that passed the Student-Newman-Keuls test and had flags present or marginal in at least 50% of the samples for conditions having greater than 1.5 fold changes in expression between at least two of the four HUVEC treatment conditions. A total of 4017 differentially expressed genes were identified. Table 2.1 contains the number of differentially expressed genes between each condition.

Table 2.1: Number of Differentially Expressed Genes Between Conditions

	Static	HSS	LSS
HSS	3,026	--	--
LSS	2,998	194	--
RF	3,102	365	57

ECs exposed to fluid flow differentially expressed over 3000 genes as compared to ECs exposed to static conditions. This high number of differentially expressed genes compared to static was independent of the type of fluid flow that ECs were exposed to. On the other hand, a comparison of gene expression between fluid flow types revealed

that the largest number of differentially expressed genes can be found in a comparison of reversing flow to high shear stress, with 365 differentially expressed genes. When reversing flow was compared to low shear stress, less than 100 genes were found to be differentially expressed.

Differentially expressed genes for each of the 3 flow conditions compared to static are shown on the proportional Venn diagram in Figure 2.5.<sup>42</sup> 57 % of the total number of genes found in these three comparisons are differentially expressed in all of the shear stress conditions. Further examination of these genes shows that there is 100% agreement for all of the flow conditions in the direction of differential expression as compared to static. This indicates that exposure to shear stress determines whether these genes will be up- or down-regulated as compared to the static condition. Thus, the type of shear stress that ECs are exposed to regulates the value of the fold change rather than the direction of the fold change that occurs when comparing gene expression in shear stress conditions to static conditions. Table 2.2 contains a list of twenty genes that are most up- and down-regulated by fluid flow as compared to static.

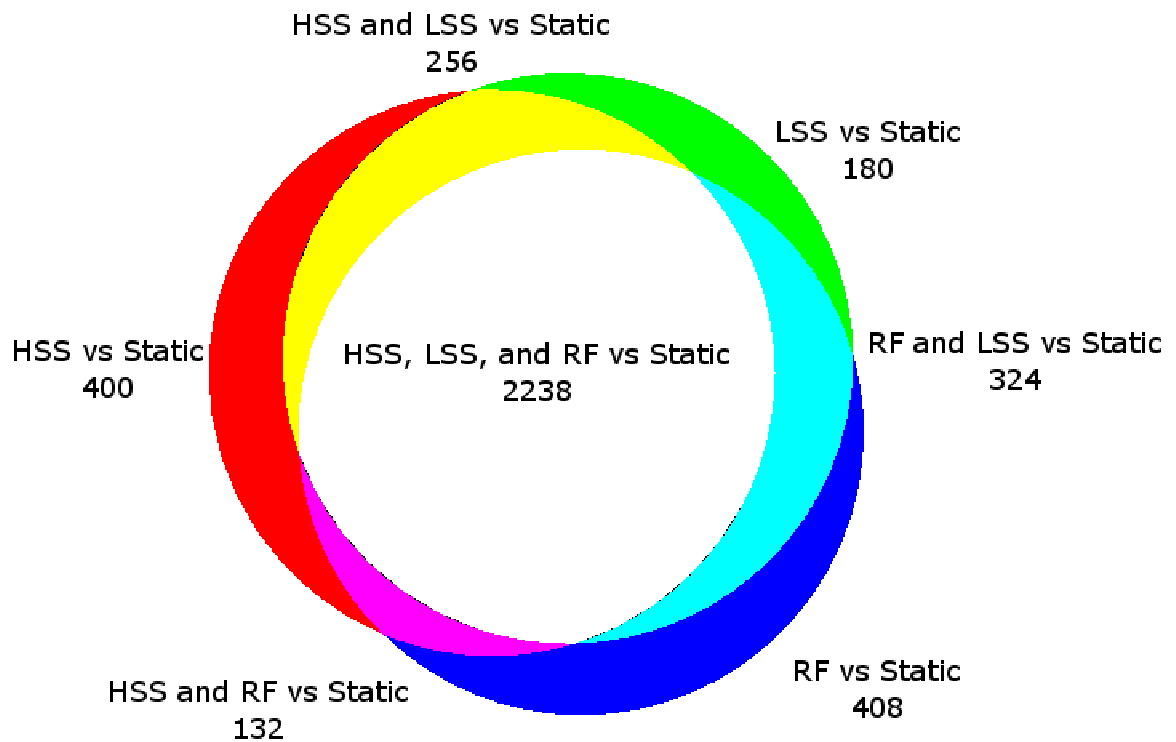


Figure 2.5 Proportional Venn diagram of differentially expressed genes in a comparison of RF, HSS, and LSS to static culture. Genes found within the white area of the Venn diagram are differentially expressed by all three fluid flow types as compared to static culture

Table 2.2: Top 10 Genes Up- and Down-Regulated by Fluid Flow

<b>Gene Symbol</b>	<b>Gene Name</b>	<b>Average Fold Change* (Flow vs Static)</b>
CLEC1B	C-type lectin domain family 1, member B	121.2
GPR83	G protein-coupled receptor 83	57.2
CYP1B1	Cytochrome P450, family 1, subfamily B, polypeptide 1	54.1
KCNK3	Potassium channel, subfamily K, member 3	39.8
MYOM3	Myomesin family, member 3	38.7
BDKRB2	Bradykinin receptor B2	36.1
GPR92	G protein-coupled receptor 92	27.6
IL11	Interleukin 11	22.4
ID2	Inhibitor of DNA binding 2	20.8
FREM3	FRAS1 related extracellular matrix 3	20.6
CD34	CD34 molecule	-32.7
XLKD1	Extracellular link domain containing 1	-38.0
PPP1R9A	Protein phosphatase 1 regulatory subunit 9A	-42.0
PRND	Prion protein 2	-50.3
CHRNA1	Cholinergic receptor nicotinic alpha 1	-50.5
DHRS3	Dehydrogenase/reductase (SDRfamily) member 3	-62.4
CYP26B1	Cytochrome P450, family 26, subfamily B, polypeptide 1	-68.0
KIT	v-kit Hardy Zuckerman 4 feline sarcoma viral oncogene homolog	-76.0
MYO5C	Myosin VC	-89.9
C10Orf10	Chromosome 10 Open reading frame 10	-143.1

\*Fold changes represent the average of the average fold change in comparison to static for reversing flow, high shear stress, and low shear stress.

Hierarchical clustering applied to the four EC culture conditions provides further evidence that the largest differences in gene expression are seen between ECs exposed to fluid flow of any type and ECs grown under static conditions. Figure 2.6 reveals that HSS, LSS, and RF cluster on a branch separate from static culture. From there HSS and LSS cluster separately from RF, indicating that ECs exposed to high shear stress or low shear stress are more similar to each other in terms of gene expression than ECs exposed to reversing flow.

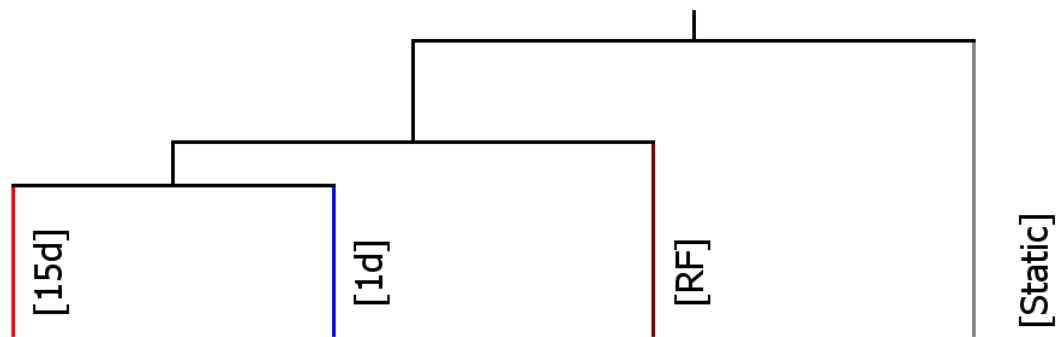


Figure 2.6 ECs exposed to fluid flow cluster on a branch separate from ECs grown in static culture.

In Table 2.1 the greatest number of differentially expressed genes is found in a comparison of RF and HSS, with 365 differentially expressed genes. Comparison of HSS to LSS showed 194 genes were differentially expressed, while only 57 genes were differentially expressed when RF and LSS were compared. These differences in the number of differentially expressed genes are indicative of the large changes in EC phenotype that can be found between ECs growing on the wall of the carotid sinus and ECs located in other regions of the vasculature which do not experience blood flow disturbances caused by curvature of the vessels or branching. The Venn diagram shown in Figure 2.7 depicts the overlap among these three comparisons.

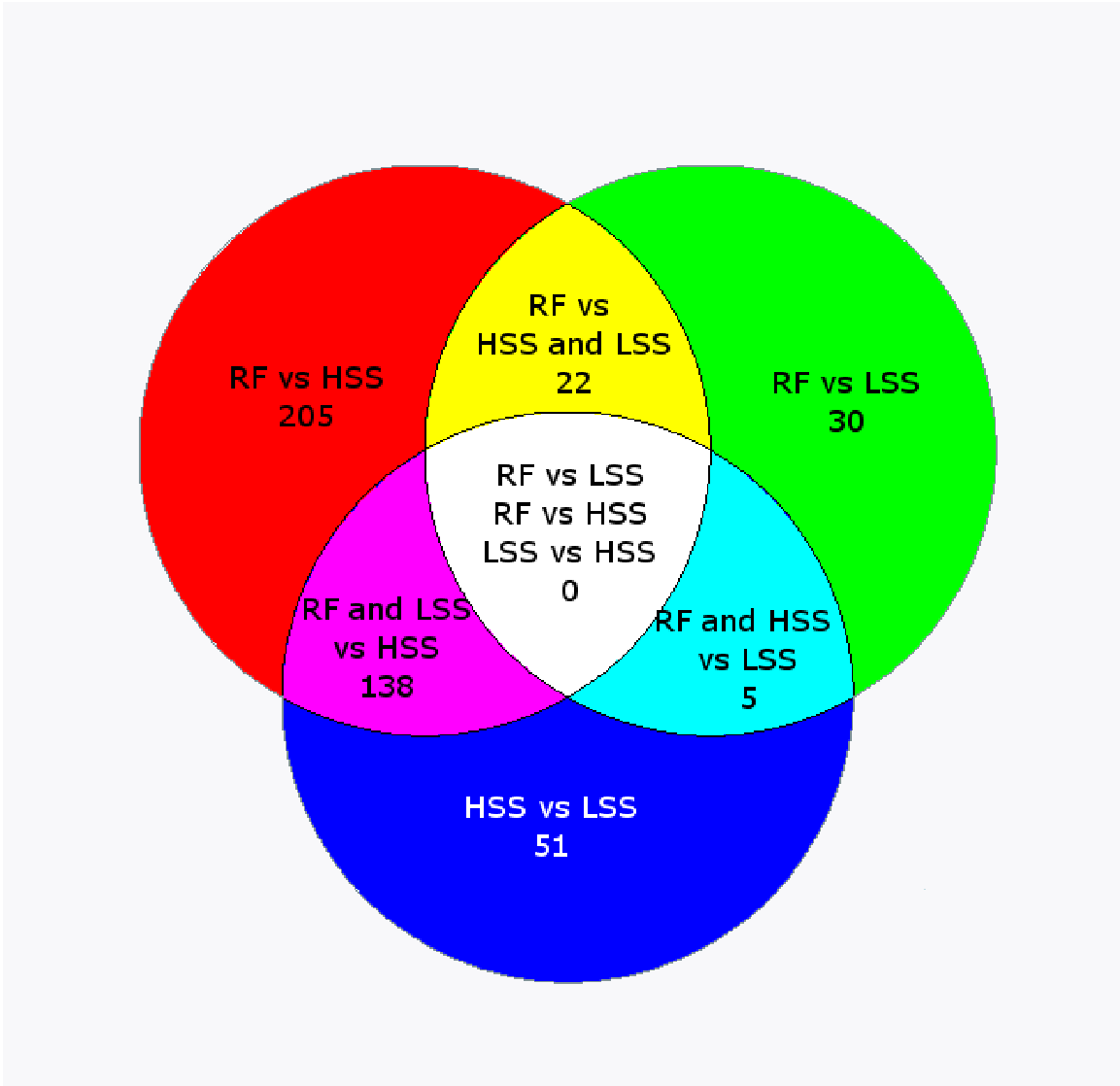


Figure 2.7 Venn diagram of differentially expressed genes in a comparison of RF to HSS, RF to LSS, and HSS to LSS. Differentially expressed genes found in the purple region of overlap are regulated by low average flow while genes found within the yellow region of overlap are regulated by flow reversal. Genes located within the light blue area are regulated by high average shear stress.

In our study there are two conditions that have low average shear stress, LSS and RF. Examination of the purple portion of Figure 2.7 shows that when either LSS or RF is compared to HSS there are 138 genes that are found in both lists. Further examination shows that in all of these genes both LSS and RF generate the same direction of either up- or down-regulation compared to HSS. Based on this similar response to both LSS and RF as compared to HSS, these genes can be termed "regulated by low average shear stress" (Appendix Table B.2). DAVID functional annotation clustering was used to group down-regulated and up-regulated genes based on function. These functional groups are shown in Figure 2.8 and Figure 2.9 as hierarchical clusters of associated genes and conditions.

These hierarchical clusters include down-regulation by low average shear stress of genes associated with anatomical structure development, cell communication, response to external stimuli, blood vessel morphogenesis, chemical homeostasis, hydrolase activity, and actin filament organization (Figure 2.8). Genes up-regulated by low average shear stress were associated with metallothioneins and cell cycle phase, in particular the M phase (Figure 2.9).

## Down-regulated by Low Average Shear

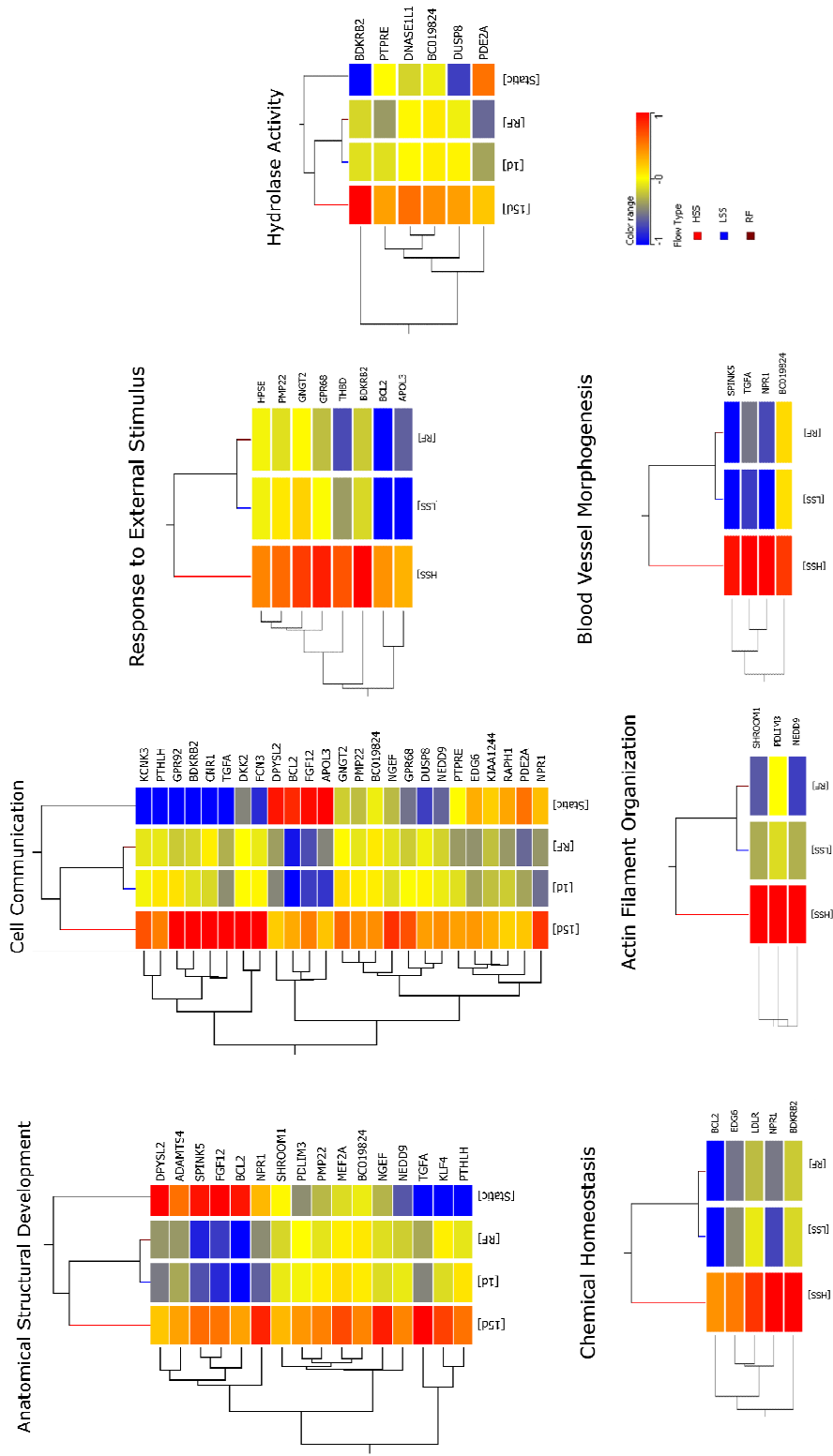


Figure 2.8 Hierarchical clusters of functional groups up-regulated by low average shear stress. Flow conditions and genes associated with functional groups identified by DAVID were clustered according to expression patterns. The color range shown is indicative of the normalized natural log transformed signal values for each gene.

## Up-Regulated by Low Average Shear Stress

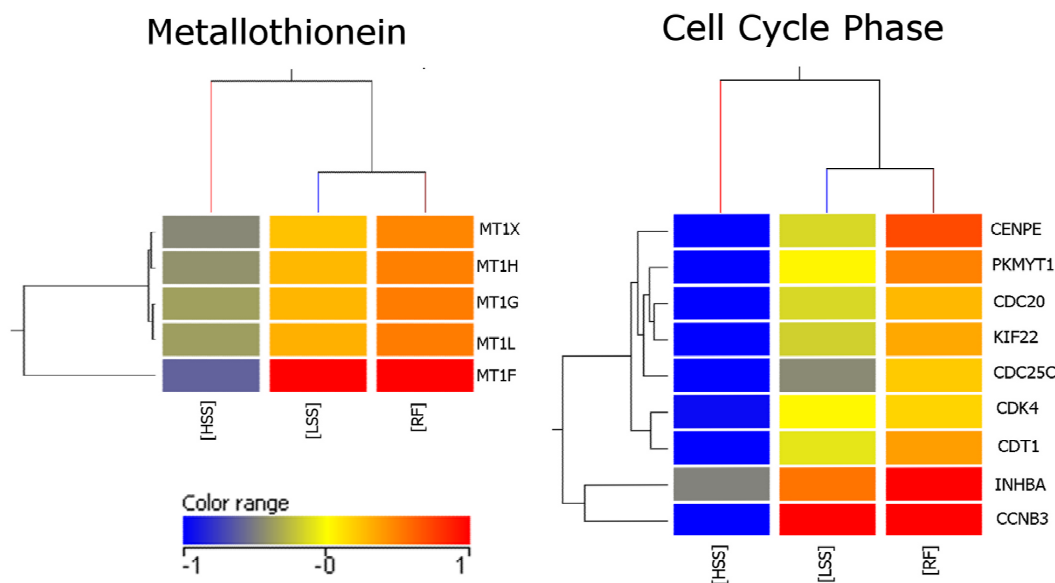


Figure 2.9 Hierarchical clusters of functional groups up-regulated by low average shear stress.

Flow conditions and genes associated with functional groups identified by DAVID were clustered according to expression patterns. The color range shown is indicative of the normalized natural log transformed signal values for each gene.

These hierarchical clusters show clustering of both genes and conditions associated with functional groups regulated by low average shear stress. In all of the hierarchical clusters shown, ECs exposed to reversing flow and ECs exposed to low shear stress cluster on a branch which is separate from ECs exposed to high shear stress. It should be noted that clustering of the reversing flow and low shear stress conditions on a single branch is in contrast to the clustering results obtained when all of the genes on the microarray were incorporated into the clustering algorithm. This is a further indication that these genes are regulated by low average shear stress.

In our study RF was compared to both HSS and LSS. The yellow portion of Figure 2.7 shows that there are 22 genes which overlap between these two comparisons. 100% of the genes showed similar directions of up- or down-regulation in response to reversing flow as compared to both HSS and LSS. Based on this these genes can be termed "regulated by reversing flow" (Table 2.3). DAVID functional annotation clustering was used to group these genes based on function. Differentially regulated functional groups are shown in Figure 2.10 as hierarchical clusters of associated genes and conditions. In these hierarchical clusters, ECs exposed to reversing flow clustered on a branch separate from ECs exposed to high shear stress or low shear stress. This pattern coincides with the clustering results obtained from analysis of the entire array as shown in Figure 2.6.

Further examination of Figure 2.7 shows that in the light blue section there are 5 genes that overlap (Table B.1). This portion of the Venn diagram represents genes that are differentially expressed in a comparison of HSS to LSS and RF to LSS. In this case both HSS and RF have been exposed to high shear stresses for at least some period of time during each cycle. As with the other genes in overlapping lists described previously, exposure to HSS and RF induced differential expression compared to LSS in the same direction of either up- or down-regulation. Thus, these 5 genes may be regulated by exposure to high shear stress despite the fact that the average shear stress applied to RF is low.

Table 2.3: Genes regulated by flow reversal

Gene Symbol	Gene Name	Fold Change (RF/HSS)
AK023086	Unannotated	3.1
GGTLA1	gamma-glutamyltransferase-like activity 1	2.5
PRIM2A	primase, polypeptide 2A	2.5
FLJ14712	Unannotated	2.4
CCNE2	Cyclin E2	2.4
CEP55	centrosomal protein 55kDa	2.1
APOM	apolipoprotein M	1.9
RRM1	ribonucleotide reductase M1 polypeptide	1.9
KRTAP19-1	keratin associated protein 19-1	1.8
ATAD5	ATPase family, AAA domain containing 5	1.8
PIF1	PIF1 5'-to-3' DNA helicase homolog	1.8
KIF21A	kinesin family member 21A	1.8
BC020241	Unannotated	1.8
C21orf2	chromosome 21 open reading frame 2	1.7
CASC5	cancer susceptibility candidate 5	1.7
JPH2	junctophilin 2	1.7
PRKACB	protein kinase, cAMP-dependent, catalytic, beta	1.6
BC017350	Unannotated	-1.6
THC2731337	Unannotated	-1.7
MGA	Unannotated	-1.7
CDC42EP3	CDC42 effector protein (Rho GTPase binding) 3	-1.8
SLC26A2	Solute carrier family 26 (sulfate transporter), member 2	-1.8
THC2722466	Unannotated	-1.9
CCR3	chemokine (C-C motif) receptor 3	-2.0
BX111338	Unannotated	-2.3
ATF7	activating transcription factor 7	-2.3
A_24_P607751	Unannotated	-2.6
AL117571	Unannotated	-2.6
AL832806	Unannotated	-2.7
A_23_P64962	Unannotated	-2.7
FGF16	fibroblast growth factor 16	-2.8
BE184906	Unannotated	-2.8
DB041606	Unannotated	-3.1
KBTBD2	kelch repeat and BTB (POZ) domain containing 2	-3.2
THC2727548	Unannotated	-3.2
ZNF585A	zinc finger protein 585A	-3.2
SOCS2	suppressor of cytokine signaling 2	-3.3
THC2751803	Unannotated	-3.4
DKKL1	dickkopf-like 1 (soggy)	-3.5
RP11-93B10.1	Unannotated	-3.8
SLC5A8	Solute carrier family 5 (iodide transporter), member 8	-4.4
ANK1	Homo sapiens ankyrin 1, erythrocytic (ANK1), transcript variant 3, mRNA [NM_000037]	-5.3

## Regulated by Reversing Flow

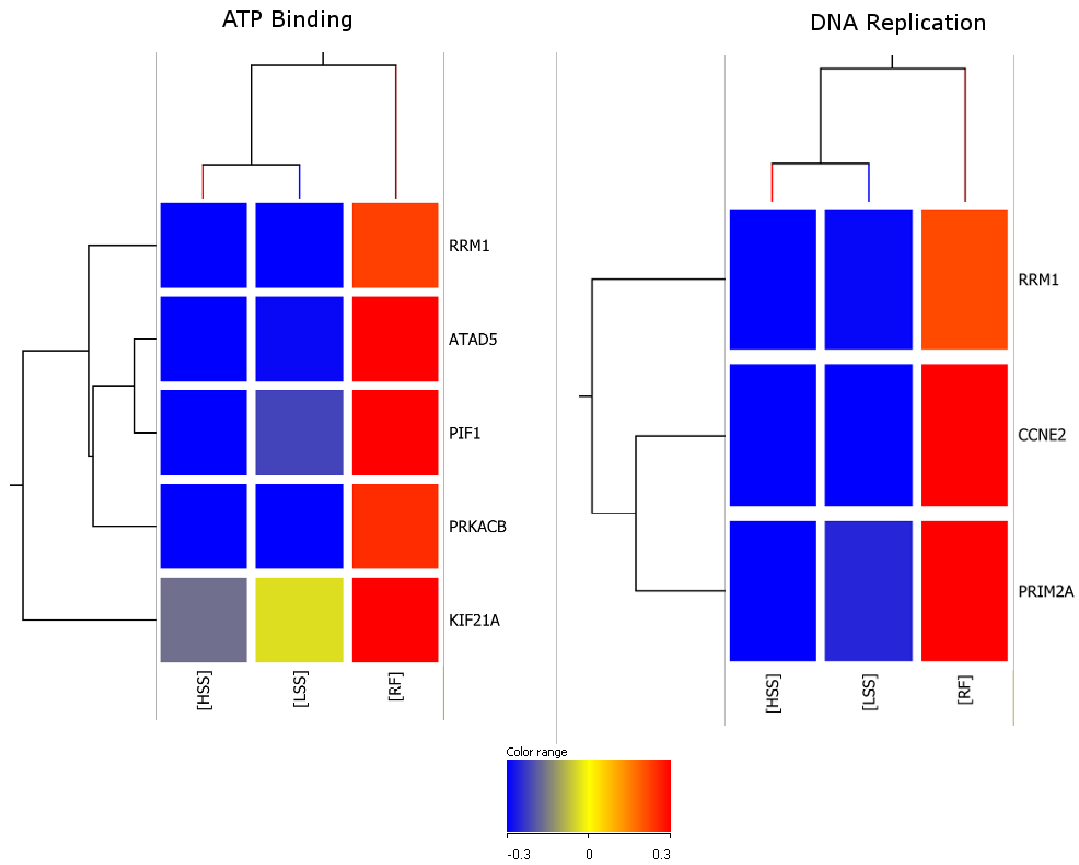


Figure 2.10 Hierarchical clusters of functional groups up- and down-regulated by reversing flow. Flow conditions and genes associated with functional groups identified by DAVID were clustered according to expression patterns. The color range shown is indicative of the normalized natural log transformed signal values for each gene.

Microarray data was confirmed with qRT-PCR on two genes up-regulated by low average shear stress, metallothionein 1F (MT1F) and cyclin B3 (CCNB3), along with two genes down-regulated by low average shear stress, Kruppel-like factor 2 (KLF2) and natriuretic peptide receptor A (NPR1). Additionally, two genes up-regulated by reversing flow, primase polypeptide 2A (PRIM2A) and cyclin E2 (CCNE2), were chosen for qRT-PCR confirmation. Comparisons of qRT-PCR data and microarray data are shown in Figure 2.11. The genes regulated by low average shear stress had very similar changes in expression as measured by either qRT-PCR or microarray. Of the two genes which were up-regulated by reversing flow, only PRIM2A had qRT-PCR data similar to microarray data. CCNE2 showed no significant change in expression between the three flow conditions when measured by qRT-PCR.

To further investigate cell cycle changes, cells exposed to either static culture, HSS, LSS, or RF were assayed for cell proliferation via incubation with BrdU followed by staining for BrdU incorporation into the DNA. Although static control cultures had the greatest fraction of BrdU positive cells, comparisons among the shear stress conditions showed that the number of BrdU positive cells was increased over two-fold under reversing shear stress and 1 dyne/cm<sup>2</sup> when compared to 15 dynes/cm<sup>2</sup> (Figure 2.12). This data indicates that exposure of ECs to shear stress causes inhibition of cell proliferation. In comparison to HSS, both RF and LSS cause increased cell proliferation in ECs, indicating that low time average shear stress is involved in regulating cell division.

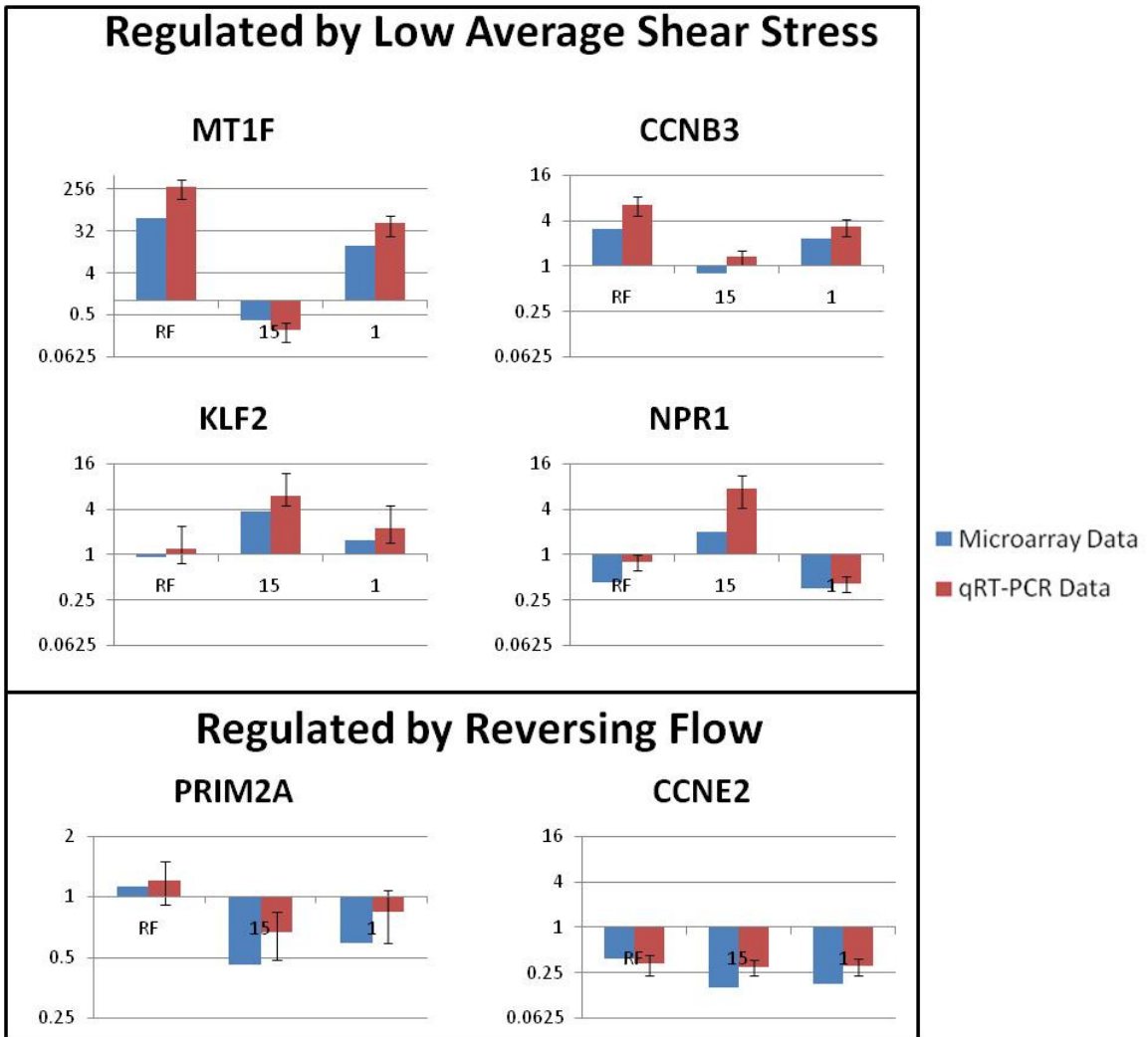


Figure 2.11 qRT-PCR Confirmation of Microarray Results

Four genes regulated by low average shear stress and two genes regulated by reversing flow were chosen for confirmation of microarray results with qRT-PCR. Blue bars are microarray data and red bars are qRT-PCR data. Note that not all axes share the same value.

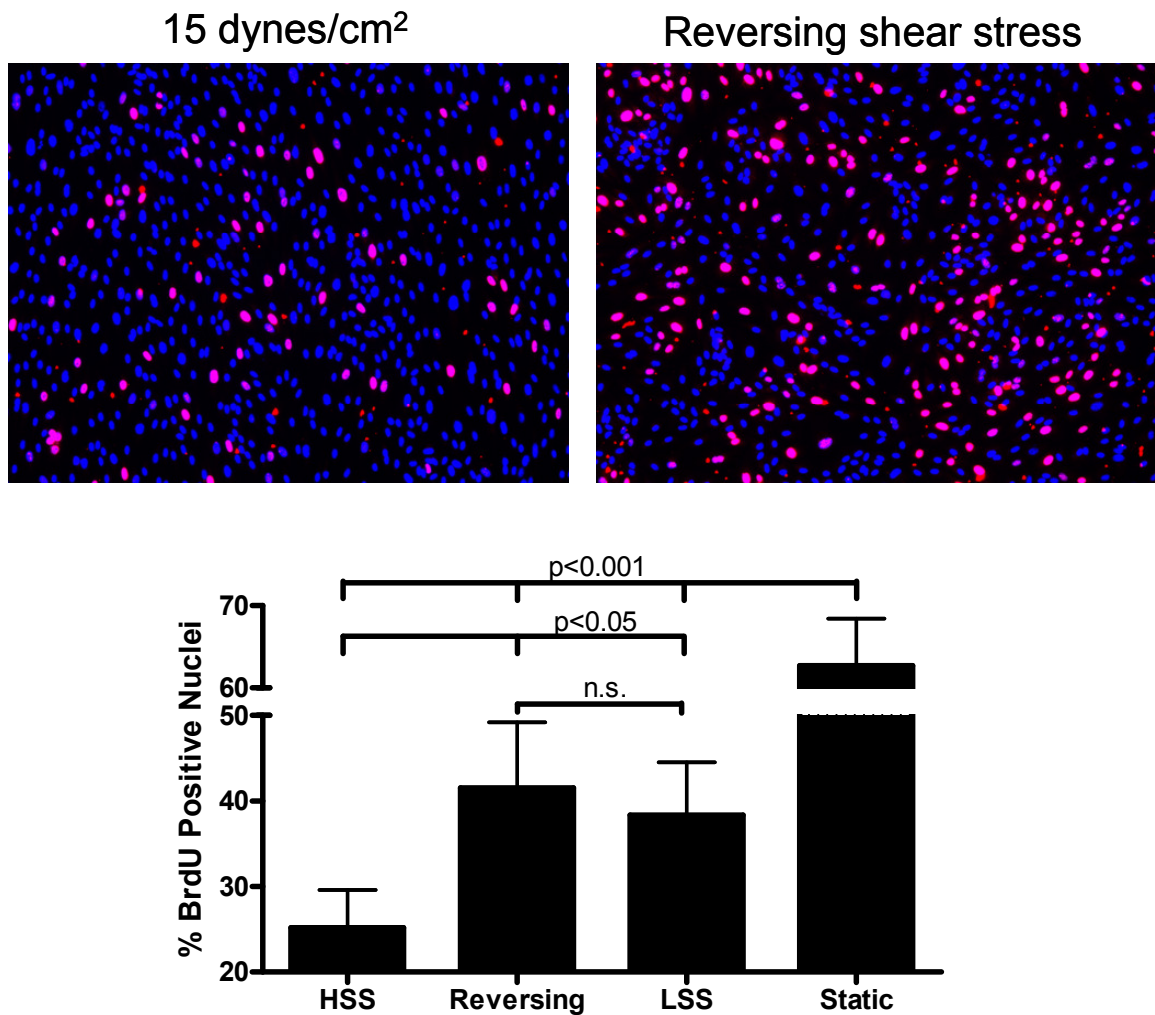


Figure 2.12 Cell proliferation is inhibited by high shear stress compared to low average shear stress and reversing shear stress. ECs were stained for BrdU incorporation (red) and the presence of nuclear DNA using Hoechst 33258 (blue) following culture in either static or flow conditions. Nuclei appearing pink are indicative of positive staining for both DNA and BrdU. Top: Representative image of ECs cultured under 15 dynes/cm<sup>2</sup> or reversing flow for 24 hours and stained for BrdU incorporation and nuclear DNA. Bottom: Fluid flow caused a reduction in BrdU incorporation. Exposure to high shear stress caused the greatest reduction in BrdU incorporation. The percentage of nuclei which stained positively for BrdU was determined by counting nuclei in 5 experiments with 8 frames per experiment .

To assess the ability of reversing shear stress to lead to increased inflammation and leukocyte recruitment, a monocyte adhesion assay was performed on HUVEC pretreated with each of the shear stress conditions. Significantly increased monocyte adhesion was observed under reversing flow, but not under other conditions (Figure 2.13).

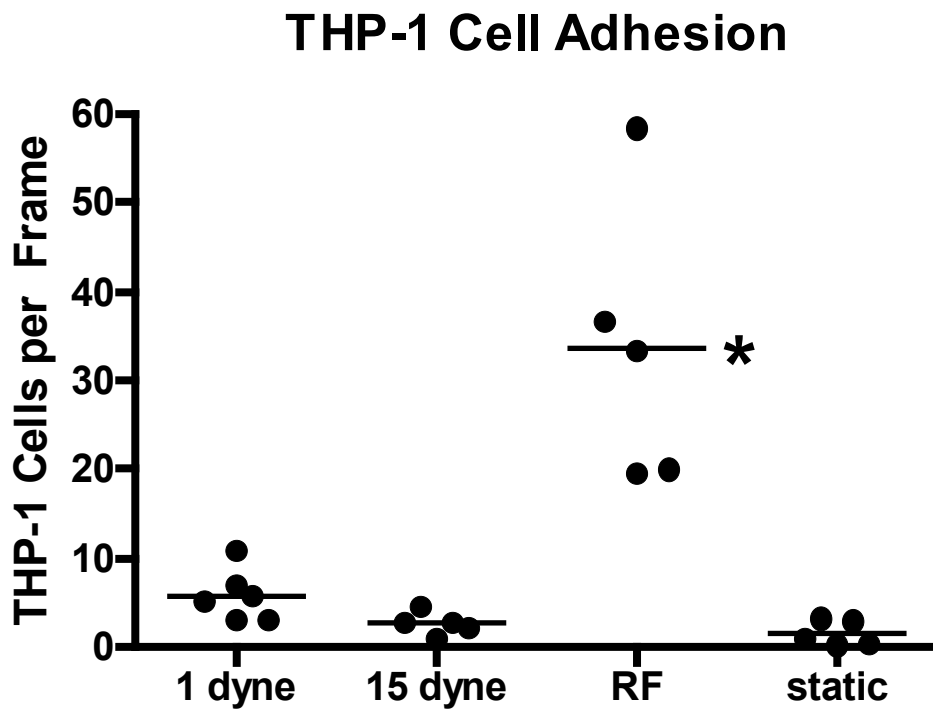


Figure 2.13 THP-1 cells have greater adhesion to ECs exposed to reversing flow THP-1 cells were counted in 10 frames each of five to six separate experiments. Dots shown on the graph represent the average number of adherent cells in each experiment. The line shown on the graph represents the median number of adherent cells for all experiments. Significance was assessed using ANOVA followed by Tukey's post-hoc test. \*  $p < 0.001$  between reversing flow and all three other conditions.

## 2.4 Discussion

We describe herein the design and application of a novel reversing shear stress system using a parallel plate flow chamber. Other studies have used a variety of parallel plate or cone and plate systems to study the effects of either disturbed or oscillating flow on endothelial cell gene expression.<sup>16, 18, 20, 43-45</sup> Some of these studies comparing the effects of steady shear stress to reversing shear stress have modeled the reversing shear stress waveform as an oscillating sine wave function. While this is a simpler shear stress to implement in an *in vitro* system, the physiological shear stress is not harmonic, and includes much more rapid changes in shear stress direction. Also, the time-average shear stress in some models was set at zero,<sup>44</sup> and as a result there was no net forward movement across the cells, a situation that does not occur *in vivo*. Another limiting factor of previous studies is the lack of a steady low shear stress control, which would allow for differentiation of responses that are due only to time-average low shear stress from those due to fluid shear stress reversal.

The shear stress profile chosen for our system was based on computer simulated data of the shear stress at the carotid sinus<sup>17</sup> and is similar to that of the atheroprone waveform developed by Dai, et al.<sup>16</sup> However, unlike the system by Dai, et al., we designed our system to use a parallel plate chamber instead of a cone and plate. A parallel plate chamber allowed us to perform a flow-based monocyte adhesion assay on cells pre-treated with different shear stress conditions. Although we have chosen to use this system to model the reversing shear stress at the carotid sinus, the linear motor can be easily programmed to deliver other equally complex shear stress waveforms.

With this system we investigated changes in cell morphology, gene expression, cell proliferation, and monocyte adhesion under reversing flow as compared to high shear stress, low shear stress, and static culture. ECs exposed to reversing flow exhibited a cobblestone like appearance in contrast to ECs exposed to high shear stress which were elongated and aligned with flow. Similar differences in cell morphology are seen *in vivo* when comparing porcine ECs found in the descending thoracic aorta (undisturbed unidirectional flow) and porcine ECs found adjacent to a branch of the aorta (separated disturbed flow),<sup>46</sup> providing further evidence that our reversing flow system mimics *in vivo* fluid flow disturbances found in branching regions of the vasculature.

In our system, fluid flow induced differential gene expression in approximately 7% of all human genes. This number of differentially expressed genes is similar to, although slightly higher, than previous reports which indicate that shear stress affects between 1% and 6% of genes.<sup>18-20, 45, 47</sup> Differences in the number of genes reported as differentially expressed can be attributed to microarray analysis techniques, microarray platforms, and differences in experimental setup. In our system a comparison of fluid flow to static flow revealed that 57% of differentially expressed genes were similarly up- or down-regulated by high shear stress, low shear stress, and reversing flow as compared to static flow. This indicates that up- or down-regulation of these genes is controlled simply by the presence of flow while the type of flow determines the magnitude of response rather than the direction of response as compared to static culture. This is further validated in Figure 2.6 by clustering of the three flow conditions on a branch separate from static culture.

In order to validate our microarray data, we have compared our data to data from other groups who have looked at a comparison of endothelial cell gene expression under shear stress and static culture. Our data comparing high shear stress to static culture confirmed 72 percent of the genes reported by Ohura et al. to be up-regulated by in HUVEC by 15 dynes/cm<sup>2</sup> laminar shear stress as compared to static culture.<sup>18</sup> McCormick et al. reported transcriptional changes in HUVEC exposed to 25 dynes/cm<sup>2</sup>. Our data confirmed differential expression for 47 percent of the genes reported by McCormick et al. which had fold changes of at least 1.5 fold at 24 hours.<sup>19</sup> This agreement of our data with previously published reports on steady shear stress provides further validation of our microarray results.

Comparisons of ECs exposed to different fluid flow regimes are more relevant to understanding vascular pathologies than comparison to static culture because static culture is not representative of a known physiological state. Therefore gene expression of ECs exposed to reversing flow, high shear stress, and low shear stress were compared. Comparison of reversing flow to high shear stress identified 365 differentially expressed genes between the two conditions. The reversing flow profile which we used has a low time averaged shear stress of approximately 1 dyne/cm<sup>2</sup>. Therefore, further comparisons were performed to determine whether differential gene expression was induced by low average shear stress or flow reversal. 138 genes were identified as being regulated by low average shear stress, while only 22 genes were identified as being regulated by flow reversal.

Flow reversal caused up-regulation of three genes related to DNA replication (Figure 2.10). RRM1 is a gene which encodes for one of two subunits that make up

ribonucleotide diphosphate reductase, an enzyme required for the production of deoxyribonucleotides prior to DNA synthesis.<sup>48</sup> CCNE2 encodes for cyclin E2 which regulates CDK2 activity and is involved in the G1 to S phase transition.<sup>49</sup> Finally, PRIM2A is responsible for synthesis of small RNA primers necessary for Okazaki fragments made during DNA replication.<sup>50</sup> Up-regulation of these genes by flow reversal may play an important role in regulating cell proliferation.

The reversing flow profile which we have studied is similar to the “athero-prone” waveform studied by Dai et al.<sup>16</sup> This group used a cone and plate device to apply either athero-prone reversing flow or athero-protective pulsatile non-reversing flow to ECs. This group found 159 genes which were differentially regulated in a comparison of ECs exposed to either athero-prone or athero-protective flow profiles. In our system a comparison of reversing flow to high shear stress revealed differential regulation of 13 of these same genes. Our data further reveals that 10 of these 13 genes are regulated by low average shear stress rather than flow reversal (APOL3, CD34, CD58, CRIP1, CYP1B1, KLF2, MEF2A, PTHLH, CDC20, and metallothioneins).

We have recently further examined CYP1B1 expression and confirmed regulation of CYP1B1 by low average shear stress (see Chapter 3).<sup>41</sup> KLF2 has been shown to be attenuated under reversing shear stress as compared to non-reversing shear stress<sup>16</sup>; however, other published work has shown KLF2 is also equally attenuated under low shear stress<sup>51, 52</sup> supporting our observation that KLF2 is regulated by low average shear stress. Regulation of metallothioneins was also reported by Ohura et al. who examined the effects of turbulent flow in comparison to high steady laminar flow<sup>18</sup>; however, in their system turbulent flow caused down-regulation of metallothionein expression while

in our system reversing shear stress caused up-regulation of metallothioneins. Our lab has also shown metallothioneins to be one of the few gene groups differentially regulated by non-reversing pulsatile shear stress compared to steady shear stress.<sup>9</sup> These differences indicate that metallothionein expression is highly sensitive to variations in endothelial shear stress, which may be important for regulation of downstream signaling events.

Our results indicate that a number of genes which regulate the cell cycle are up-regulated by low average shear stress in comparison to high steady shear stress. We performed an analysis of BrdU incorporation in order to assess the effects of differential expression of these genes on cell cycle progression. The increased BrdU incorporation suggests that cell cycle progression can be upregulated under reversing shear stress. Interestingly similar results were observed for the low shear stress control, suggesting that the time-average low shear stress may regulate cell cycle progression.

We also observed increased monocyte adhesion to ECs following exposure to reversing shear stress. This increase in monocyte adhesion was not found in ECs following exposure to low steady shear stress, indicating that fluid reversal is responsible for the development of a more adhesive and activated endothelial cell phenotype. Previous studies of EC exposure to oscillatory flow have shown a similar increase in monocyte adhesion.<sup>43, 44, 53</sup> These studies examined monocyte adhesion following a 45 minute incubation with ECs exposed to oscillatory shear stress. In our study we have examined monocyte adhesion under flow; monocytes were perfused across ECs at 1 dyne/cm<sup>2</sup> for five minutes and an assessment of monocyte rolling or firm adhesion revealed no binding between the flowing monocytes and the ECs. However, when fluid

flow was stopped for 30 seconds and then returned to 1 dyne/cm<sup>2</sup>, monocytes firmly adhered to ECs exposed to reversing flow and did not firmly adhere to ECs grown in static culture or exposed to high or low steady shear stress. These data indicate that flow reversal fails to induce expression of selectins or other molecules involved in initial leukocyte binding; however, exposure to reversing flow leads to increased firm adhesion likely mediated by integrin ligands such as ICAM1 and VCAM1.

In summary we have developed a physiological reversing shear stress system which can be used to reproduce the wall shear stress at the carotid sinus. Using a low steady shear stress control, we show that most gene expression changes in cells exposed to reversing shear stress are regulated by the low average shear stress and not fluid shear stress reversal. We also show that low average shear stress is the major force responsible for increases in cell proliferation as compared to cells exposed to arterial levels of steady shear stress. Interestingly, we showed increased monocyte adhesion only in cells exposed to reversing shear stress. Our findings provide further insight into endothelial responses to mechanical forces and may be important in understanding mechanisms of atherosclerotic development and localization to regions of disturbed flow.

## **CHAPTER 3: EXPRESSION OF CYP1A1 AND CYP1B1 IN HUMAN ENDOTHELIAL CELLS: REGULATION BY FLUID SHEAR STRESS**

*N.B.: This chapter has been published (Conway et al., Expression of CYP1A1 and CYP1B1 in human endothelial cells: Regulation by fluid shear stress. Cardiovascular Research, 2009).*

### **3.1 Introduction**

Cytochrome P450s are a class of membrane bound hemoproteins which, when complexed with a NADPH-cytochrome P450 reductase and cytochrome b<sub>5</sub>, oxidize, peroxidize or reduce endogenous fatty acids and steroids, as well as exogenous xenobiotics and pharmaceutical compounds.<sup>54</sup> Cytochrome P450, family 1, subfamily A, polypeptide 1 (CYP1A1) and cytochrome P450, family 1, subfamily B, polypeptide 1 (CYP1B1) are classically recognized as enzymes that metabolize exogenous compounds for elimination.<sup>24, 25</sup> Halogenated aromatic hydrocarbons and polycyclic aromatic hydrocarbons have been shown to be strong exogenous inducers of CYP1A1 and CYP1B1 genes by binding to and activating the aryl hydrocarbon receptor (AhR), a ligand-activated basic helix-loop-helix transcription factor, which translocates from the cytoplasm to the nucleus upon activation.<sup>55</sup> Recently, endogenous activators have been found for the AhR, which can also lead to increased CYP1A1 and CYP1B1 transcription.<sup>56, 57</sup> In addition, CYP1A1 and CYP1B1 enzymes can modulate cellular levels of a variety of lipid signaling molecules, including arachidonic acid and retinoic

acid metabolites that can directly affect gene expression and vascular homeostasis.<sup>26</sup>

Recent work has shown that CYP1B1 is involved in the generation of retinoic acid during chick embryogenesis.<sup>27</sup> Mutations of CYP1B1 in humans are associated with glaucoma,<sup>28</sup> and CYP1B1 (-/-) mice have abnormalities in their ocular drainage structure that resemble those in human glaucoma patients.<sup>29, 30</sup> The ability of both genes to affect lipid signaling, and the association of CYP1B1 mutations with a human pathology strongly suggest that CYP1A1 and CYP1B1 have important endogenous roles in the maintenance of homeostatic functions.

Microarray studies showed that gene expression of both CYP1A1<sup>16, 19, 23</sup> and CYP1B1<sup>16, 18-23</sup> are dramatically up-regulated by arterial levels of shear stress in cultured human endothelial cells. Han et al. recently showed that the AhR is involved in CYP1A1 expression under laminar shear stress.<sup>58</sup> The most highly up-regulated genes in our array studies under both steady shear stress<sup>19</sup> and pulsatile non-reversing shear stress<sup>9</sup> were CYP1A1 and CYP1B1. We postulated that their increases under shear stress resulted from unidirectional arterial shear stresses, and that low steady shear stress or reversing pulsatile shear stress would not up-regulate either gene.

To better characterize the increased expression of CYP1A1 and CYP1B1 genes and proteins in human aortic and human umbilical vein endothelial cells (HAEC and HUVEC, respectively) subjected to shear stress, we modeled the flow pattern in the common carotid sinus, a region prone to atherosclerosis, to examine the effects of this flow regimen on CYP1A1 and CYP1B1 gene and protein expression *in vitro*. We demonstrate that these genes are maximally up-regulated at arterial steady shear stresses of at least 15 dynes/cm<sup>2</sup> and that reversing pulsatile shear stress attenuated expression of

both genes. Furthermore, AhR nuclear localization and CYP1A1 protein expression correlate with the flow patterns in the mouse aortic arch. Our results strongly suggesting that the AhR/CYP1 pathway promotes an anti-atherogenic phenotype in the endothelium.

### **3.2 Methods**

#### *Cell culture and shear stress experiments*

Pooled HUVEC or single donor HAEC (Lonza, Walkersville, MD, USA) were grown in M199 media (Mediatech, Manassas, VA, USA) supplemented with 20% (v/v) FBS (Hyclone), 50 ug/ml endothelial mitogen (Biomedical Technologies, Stoughton, MA, USA), 2mM L-glutamine (Mediatech), 2.5 U/ml heparin sodium (American Pharmaceutical Partners, Schaumburg, IL, USA), 50 U/ml penicillin, and 50 µg/ml streptomycin (Mediatech) at 37°C in humidified 5% CO<sub>2</sub>/95% air. Different lots of pooled HUVEC were used for each experimental replicate. Passage 3 to 5 HUVEC or passage 6 HAEC were seeded (20,000 cells/cm<sup>2</sup>) onto 0.5 M NaOH treated glass slides (Corning, Corning, NY, USA) coated with 1% bovine gelatin (Sigma, St. Louis, MO, USA) and crosslinked with 0.5% glutaraldehyde (Electron Microscopy Sciences, Hatfield, PA, USA).

Steady shear stress experiments were performed with a parallel plate flow chamber as previously described.<sup>7</sup> After 36-48 hours confluent slides were mounted in parallel plate chambers and subjected to shear stress using a constant head flow loop. Shear stress experiments were performed at 37°C, in 5% CO<sub>2</sub>/95% air, using the same media as for cell culture. A system was developed based on computer simulated data<sup>17</sup> to produce a reversing shear stress pattern that mimics the *in vivo* conditions at the carotid

sinus wall. The waveform has a time-averaged shear stress of  $-1 \text{ dyne/cm}^2$ , a maximum shear stress at  $+11 \text{ dynes/cm}^2$ , a minimum shear stress of  $-11 \text{ dynes/cm}^2$ , and a cycle frequency of 1 Hz.

#### *siRNA transfection*

Cells were transfected 48 hours prior to shear stress with 100 nM CYP1A1 (sense: 5'-gguaucacaaaauguguaatt-3') or CYP1B1 (sense: 5'-gggcccaaugaaauuuuauatt-3') siRNA (Silencer Pre-designed siRNAs, Ambion, Austin, TX, USA) using Oligofectamine reagent (Invitrogen, Carlsbad, CA, USA) according to the manufacturer's instructions. siRNA sequences chosen knocked down target gene expression by at least 75%. Control cells were transfected with 100 nM Cy3 labeled nonsense siRNA (Silencer negative control #1, Ambion). Transfection was verified using fluorescent microscopy.

#### *Quantitative Real-time PCR and Western blotting*

Immediately after exposure to shear stress, total RNA and protein were extracted using TRI-zol (Invitrogen); RNA was further purified with DNase (Qiagen, Valencia, CA, USA) and RNeasy MinElute Cleanup Kit (Qiagen), according to manufacturers' instructions. The integrity and quantity of the RNA were verified with UV spectrophotometry, accepting only RNA with a 260/280 ratio greater than 1.9.

For quantitative real-time PCR (qRT-PCR), total RNA was reverse transcribed into cDNA with SuperScript II (Invitrogen) according the manufacturer's instructions. The resulting cDNA was purified through Micro Bio-Spin P-30 Chromatography Columns (BioRad) and diluted 1:20. qRT-PCR primers used were CYP1A1 (forward:

5'-cactgtcaaggatgagccagcagtag-3', reverse: 5'-gctgggtcagaggcaatggagaaactt-3'); CYP1B1 (forward: 5'-ggtgaccagcccaacctgcctatg-3', reverse: 5'-tctgctggtcaggctcctgttgatgag-3'); thrombospondin-1 (forward: 5'-gggggcgtcaatgacaatttc-3', reverse: 5'-gccaatgtagtagtgcgat-3'); and 18S (QuantumRNA Classical II, Ambion). qRT-PCR reactions and analysis were performed on a MyiQ (BioRad, Hercules, CA, USA) using iQ SYBR Green Supermix (BioRad) according to the manufacturer's instructions. The qRT-PCR reactions and analysis were performed on a MyiQ (BioRad) with a 3 min initial denaturation step at 95°C; 45 cycles (30 cycles for 18S) at 95°C for 5 s, 60°C for 10 s, 72°C for 60 s/kbp product and a ramped melting cycle. Absolute concentrations were quantified from Ct values with a linear standard curve.

Protein concentration was quantified with DC Protein Assay (Bio-Rad) using BSA standards. Equal amounts of protein were resolved by SDS-PAGE in 7.5% Tris-HCl precast polyacrylamide gels (Bio-Rad) under reducing conditions with Laemmli sample buffer and electro-transferred onto polyvinyl difluoride membranes. After blocking with 5% nonfat dry milk, membranes were probed either with rabbit-anti-human CYP1A1 (1:1000, Santa Cruz, Santa Cruz, CA, USA), rabbit-anti-human CYP1B1 (1:1000, previously characterized<sup>59</sup>). Bound primary antibodies were labeled with either sheep anti-mouse or donkey anti-rabbit immunoglobulin conjugated with horseradish peroxidase (GE Healthcare, Buckinghamshire, UK) and detected with enhanced chemiluminescence (ECL Plus, GE Healthcare). Membranes were then re-probed with mouse anti-human  $\beta$ -actin (1:5000, Clone A-15, Sigma, St. Louis, MO, USA) to normalize protein loading. Band intensities were quantified by densitometry with the EDAS 1D Imaging System (Kodak, Rochester, NY, USA).

### *CYP1A1 and CYP1B1 activity assay*

Combined CYP1A1 and CYP1B1 activity was measured using the CYP1A1/CYP1B1 P450 Glo Assay (Promega, Madison, WI, USA).<sup>60</sup> Cells were exposed to 25 dynes/cm<sup>2</sup> for 48 hours. Following shear stress the media was replaced with media containing 100 µM luciferin-6' chloroethyl ether (luciferin-CEE), and cells were cultured for an additional 3 hours under static conditions. Media was then incubated 1:1 with the manufacturer-supplied luciferase developing reagent for 20 minutes and luminescence measured (Victor 3 plate reader, Perkin-Elmer, Waltham, MA, USA). CYP1B1 activity was inhibited with 1 µM 2,3',4,5'-tetramethoxystilbene (TMS) (Cayman Chemical, Ann Arbor, MI, USA) added to the media simultaneously with the luciferin-CEE. Luminescence was normalized to total protein (DC Protein Assay, Bio-Rad).

### *Mouse Aorta Immunohistochemistry*

C57BL/6 mice (6 to 8 week-old males, The Jackson Laboratory, Bar Harbor, ME, USA) were euthanized by CO<sub>2</sub> inhalation, and the aortas were perfusion-fixed with 10% formalin. The aortas were carefully cleaned *in situ*, and the arches and thoracic aortas were dissected and stained with anti-AhR IgG (1:100, gift of R. Pollenz, University of South Florida)<sup>61</sup> or anti-CYP1A1 IgG (1:100, gift from F. Guengerich, Vanderbilt University)<sup>62</sup> antibodies. Immunoreactive AhR and CYP1A1 were detected with goat anti-rabbit IgG (1:250, Alexa Fluor 568, Invitrogen). Along with primary antibody, all samples were counterstained with antibody against CD31 using rat anti-

mouse IgG (1:100, Santa Cruz), followed by counterstaining with goat anti-rat IgG (1:250, Alexa Fluor 488). The aortas were opened and separated into regions of lesser curvature, greater curvature, and thoracic artery. *En face* images were collected with a LSM 510 META confocal microscope (Zeiss, Jena, Germany).<sup>63</sup> The investigation conforms with the *Guide for the Care and Use of Laboratory Animals* published by the US National Institutes of Health (NIH Publication No. 85-23, revised 1996). Approval for use of animal studies was provided by the Emory University Institutional Animal Care and Use Committee.

#### *Human Coronary Artery Immunohistochemistry*

Frozen sections of human coronary artery explants from patients undergoing heart transplants were prepared<sup>64</sup> and stained with either rabbit anti-human CYP1A1 (1:100, gift from F. Guengerich, Vanderbilt University)<sup>62</sup> or rabbit anti-human CYP1B1 (1:100, previously characterized<sup>59</sup>). Along with primary antibody, all samples were counterstained with antibody against mouse anti-human CD31 (1:500, Clone WM59, BD Biosciences, San Jose, CA USA) for endothelial cell identification. Immunoreactive CYP1A1 and CYP1B1 were detected with goat anti-rabbit IgG (1:250, Alexa Fluor 568, Invitrogen). CD31 was detected with goat anti-mouse IgG (1:1000, Alexa Fluor 488, Invitrogen). Nuclei were counterstained with Hoechst. Images were viewed with a Nikon Eclipse TE2000-U fluorescence microscope and acquired with a Retiga EXi cooled CCD camera (Qimaging, Surrey, BC Canada). The investigation conforms with the principles outlined in the Declaration of Helsinki. Approval for use of human tissue was granted by the Emory University School of Medicine Institutional Review Board.

### *Statistics*

Results are expressed as mean±standard error of the mean (SEM). All measures of significance were performed using either Student's t-test or one-way analysis of variance (ANOVA) with post-hoc analysis using Tukey's multiple comparison test as indicated. Values of  $p < 0.05$  are considered significant.

### **3.3 Results**

A time course of the response of CYP1A1 and CYP1B1 genes to 25 dynes/cm<sup>2</sup> was performed at 1, 2, 4, 8, 24, 48, and 72 hours and compared to cells cultured under static conditions (Figure 3.1). Shear stress up-regulated CYP1A1 and CYP1B1 mRNA in a time-dependent manner. Following 24 hours of 25 dynes/cm<sup>2</sup>, CYP1A1 mRNA was up-regulated 32.1±5.0 fold and CYP1B1 mRNA was up-regulated 428.9±82.6 fold. CYP1A1 protein was not quantifiable in static cultures and at 1, 2, 4, and 8 hours, but was observed at 24-72 hours under 25 dynes/cm<sup>2</sup>. CYP1B1 protein was elevated time-dependently, reaching maximal induction of 5.6±1.5 fold at 48 hours. Static controls isolated at each time point (0-72 hours) showed no significant differences in CYP1A1 and CYP1B1 mRNA expressions (data not shown).

Total CYP1A1 and CYP1B1 activity, measured by dechloroethylation of luciferin-6' chloroethyl ether, was 7.2±1.0 fold higher in cells shear stressed for 48 hours at 25 dynes/cm<sup>2</sup> compared to static controls (Figure 3.2). Shear stressed cells simultaneously treated with the CYP1B1 inhibitor (1 μM TMS) had a 3.5±1.1 fold increase in activity over static cells, a decrease of over 50 percent when compared to

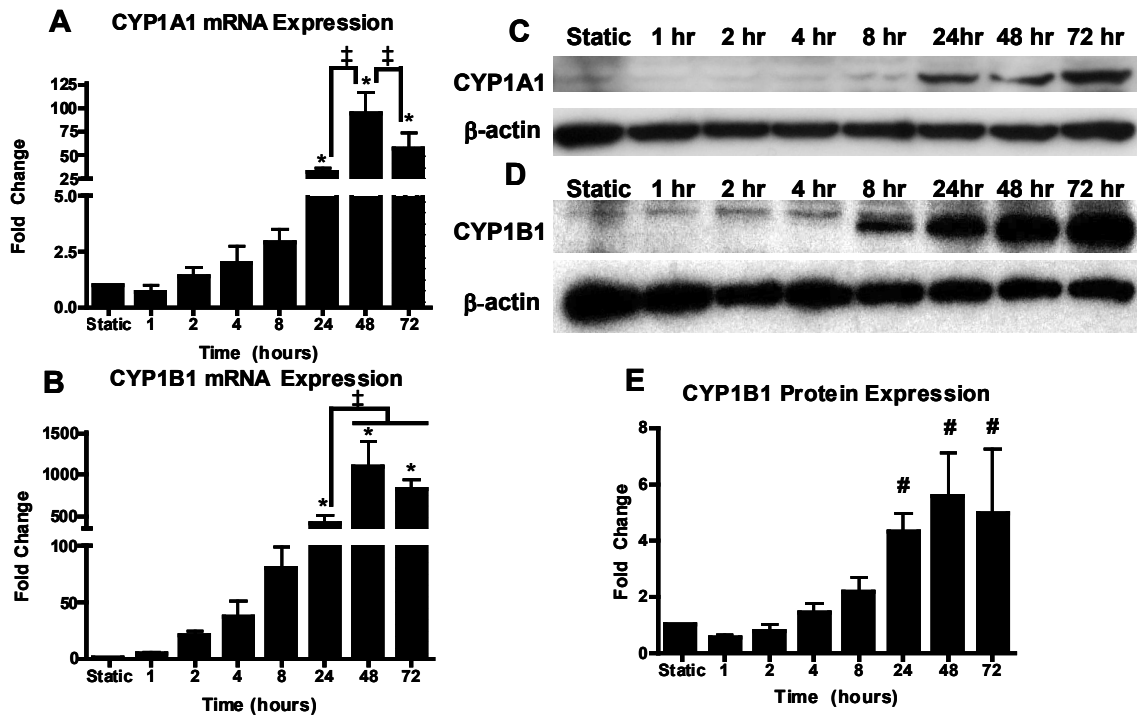


Figure 3.1 Time course of CYP1A1 and CYP1B1 mRNA and protein expression under shear stress. HUVEC were exposed to 0 (static), 1, 2, 4, 8, 24, 48, or 72 hours of 25 dynes/cm<sup>2</sup> steady shear stress (n=3-8). Both CYP1A1 (A) and CYP1B1 (B) mRNA were maximally induced by 24-72 hours of shear stress. CYP1A1 protein (C) was usually detected only after 24 hours of shear stress. CYP1B1 (D and E) protein was maximally induced after 24 hours. Equal loading in C and D is indicated by reblotting the membranes with  $\beta$ -actin antibody. Fold changes are relative to static values. Significance was assessed using ANOVA followed by Tukey's post-hoc test. \*  $p < 0.05$  vs. 0-8 hours shear stress, ‡  $p < 0.05$  vs. indicated durations, #  $p < 0.05$  vs. 0-8 hours shear stress.

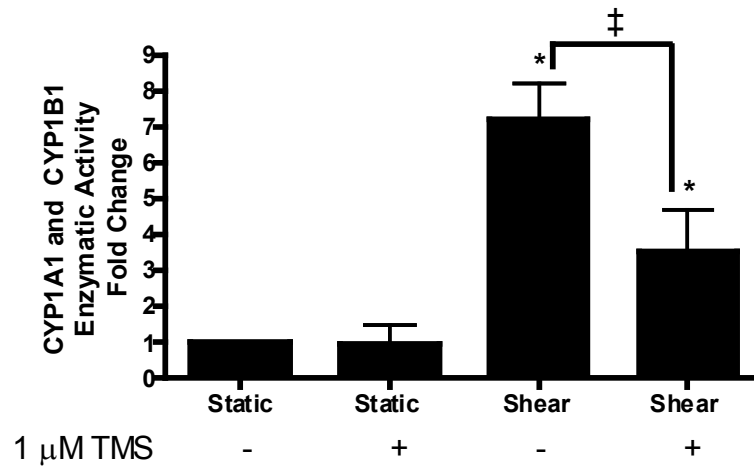


Figure 3.2 Effect of shear stress on CYP1A1 and CYP1B1 activity  
 Cells were exposed to 25 dynes/cm<sup>2</sup> or maintained under static conditions for 48 hours, and subsequently incubated under static conditions with 100 mM luciferin-CEE for an additional 3 hours (n=8). The CYP1B1 inhibitor (1 mM 2,3',4,5'-tetramethoxystilbene, TMS) was added to the media simultaneously with the luciferin-CEE in the indicated samples. Luminescence was normalized to total protein. Significance was assessed using ANOVA followed by Tukey's post-hoc test; \* p<0.05 vs. static conditions, ‡ p< 0.05 between shear stressed cells with and without TMS.

shear stressed cells assayed without the inhibitor. The activity of static controls treated with TMS was not significantly different from untreated static cells.

To determine whether expression level of these genes depended on shear stress magnitude, cells were exposed to 0 (static), 2, 5, 10, 15, or 25 dynes/cm<sup>2</sup> shear stress for 24 hours (Figure 3.3). CYP1A1 and CYP1B1 mRNA and CYP1B1 protein expression varied with shear stress magnitude. CYP1A1 protein was not detectable in cells subjected to shear stresses lower than 15 dynes/cm<sup>2</sup> (data not shown). Both CYP1A1 and CYP1B1 mRNA and CYP1B1 protein were up-regulated by as little as 2 dynes/cm<sup>2</sup> and maximally induced at 25 dynes/cm<sup>2</sup>.

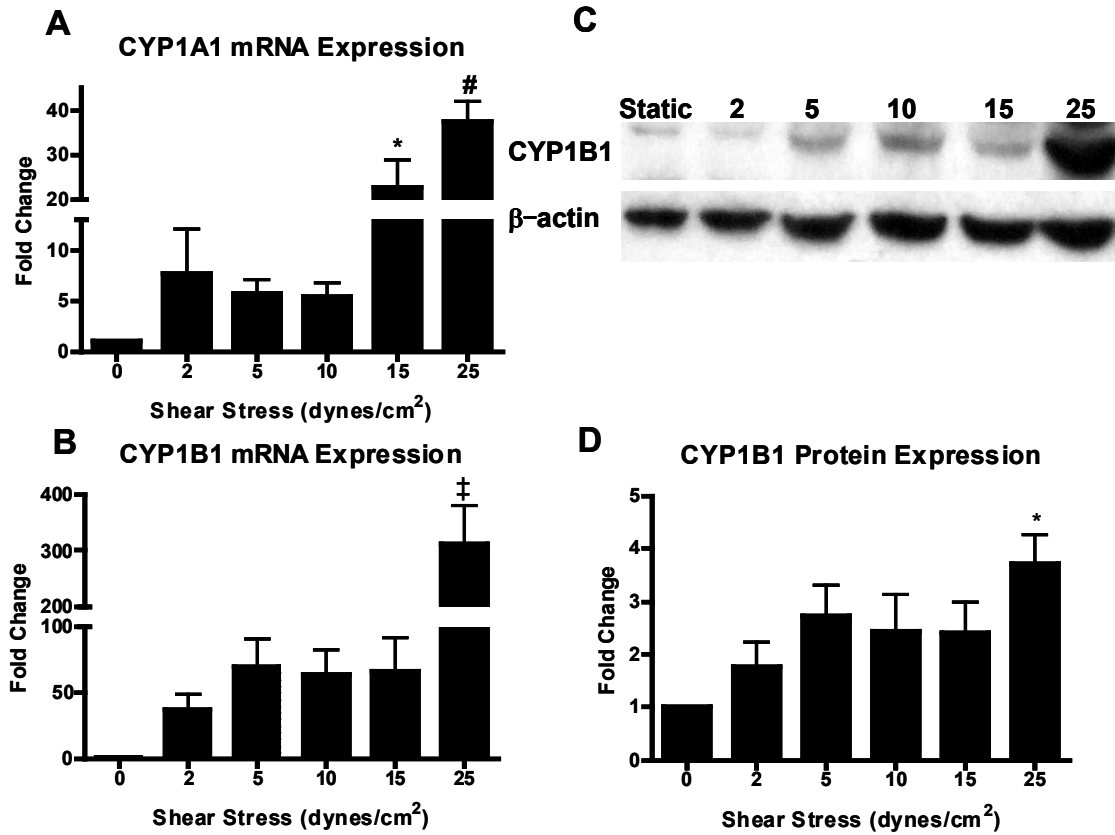


Figure 3.3 Effect of shear stress magnitude on CYP1A1 and CYP1B1 mRNA and protein expression  
 HUVEC were subjected to 0 (static), 2, 5, 10, 15, or 25 dynes/cm<sup>2</sup> shear stress for 24 hours (n=4-5). Both CYP1A1 (A) and CYP1B1 (B) mRNA expression and CYP1B1 protein (C and D) expression were maximal at 25 dynes/cm<sup>2</sup> shear stress. Significance was assessed using ANOVA followed by Tukey's post-hoc test. \* p<0.05 with respect to static conditions, # p<0.05 vs. 0 - 10 dynes/cm<sup>2</sup>, ‡ p<0.05 vs. 0 - 15 dynes/cm<sup>2</sup>.

The expression of CYP1A1 and CYP1B1 genes was investigated in HUVEC under reversing shear stress compared to steady shear stresses (15 dynes/cm<sup>2</sup> or 1 dyne/cm<sup>2</sup>) (Figure 3.4). The increased expression of both CYP1A1 and CYP1B1 mRNA by 15 dynes/cm<sup>2</sup> shear stress was significantly attenuated under reversing shear stress, and under steady shear stress of 1 dyne/cm<sup>2</sup> (the time-average of the reversing shear stress profile). CYP1A1 protein levels were highest at 15 dynes/cm<sup>2</sup>, and were reduced under reversing flow, 1 dyne/cm<sup>2</sup>, and static conditions. CYP1B1 protein levels were consistent with CYP1B1 mRNA levels. Similar results were observed in HAEC, with attenuation of CYP1A1 and CYP1B1 mRNA and protein under reversing shear stress and 1 dyne/cm<sup>2</sup> compared to 15 dynes/cm<sup>2</sup>.

To examine whether CYP1A1 or CYP1B1 modulate downstream gene expression, siRNA against CYP1A1 or CYP1B1 was transfected into HUVEC, which were then subjected to 24 hours of 25 dynes/cm<sup>2</sup> (Figure 3.5). Gene expression in these conditions was compared with that occurring in cells transfected with nonsilencing nonsense siRNA exposed to identical shear stress conditions. qRT-PCR was performed on target genes as well as genes previously shown to be regulated by AhR activation to determine if these effects were mediated by either CYP1A1 or CYP1B1. Knockdown of CYP1A1 resulted in significant decreases in CYP1B1 and thrombospondin-1 mRNA expression under shear stress. Knockdown of CYP1B1 did not result in significant gene expression changes of potential downstream genes examined (thrombospondin-1, CYP1A1) after shear stress.

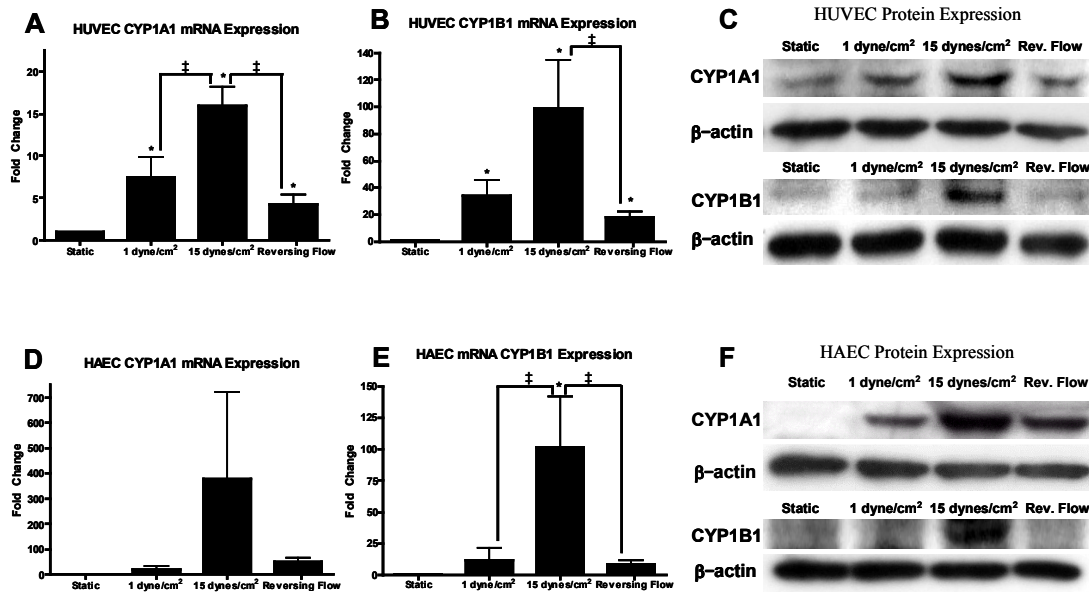


Figure 3.4 Effect of shear stress pattern on CYP1A1 and CYP1B1 mRNA and protein expression  
 HUVEC (n=5-9) or HAEC (n=4) were subjected to one of three different flow regimes: low shear stress (1 dyne/cm<sup>2</sup>), steady arterial shear stress (15 dynes/cm<sup>2</sup>), or carotid sinus reversing shear stress for 24 hours. CYP1A1 and CYP1B1 mRNA and protein expression in HUVEC (A-C) were highest under 15 dynes/cm<sup>2</sup> and greatly reduced under reversing shear stress. CYP1A1 and CYP1B1 had similar trends of expression in HAEC (D-F). Significance was assessed using ANOVA followed by Tukey's post-hoc test; \* p< 0.05 vs. static conditions, ‡ p< 0.05 between indicated conditions.

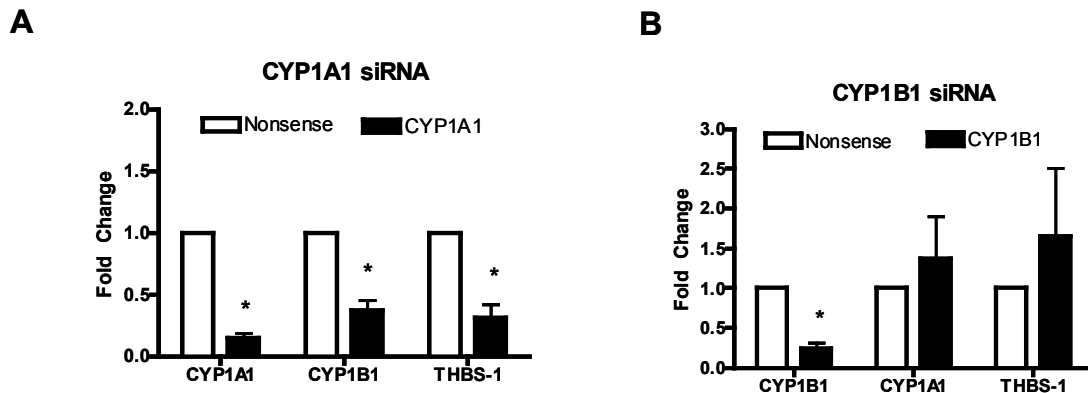


Figure 3.5 Effect of siRNA knockdown of CYP1A1 and CYP1B1 gene expression HUVEC were treated with either CYP1A1 (A) or CYP1B1 (B) siRNA 48 hours prior to 24 hours of 25 dynes/cm<sup>2</sup> shear stress (n=4). mRNA levels of CYP1A1, CYP1B1, and thrombospondin-1 were compared to cells treated with a non-silencing nonsense control and subjected to identical shear conditions. The knockdown of CYP1A1 caused significant decreases in CYP1B1 and thrombospondin-1. The knockdown of CYP1B1 caused no significant gene changes other than the target knockdown of CYP1B1. Significance measured using paired Students' t-test, \* p<0.05 between targeted knockdown and nonsense control.

Immunohistochemical staining of AhR and CYP1A1 protein was performed on fixed mouse aortas, which were then isolated into regions of the greater curvature, lesser curvature, and thoracic aorta (Figure 3.6). AhR was localized to the endothelial nuclei in the thoracic aorta, but in the region of the lesser curvature, the AhR was found in both the nuclei and the cytoplasm of the endothelial cells. Expression of CYP1A1 was increased in the thoracic aorta, but attenuated in the region of lesser curvature. Staining of the greater curvature showed similar trends in AhR localization and CYP1A1 expression to that of the thoracic aorta (data not shown). Negative control samples (without primary antibody) showed no positive staining (data not shown).

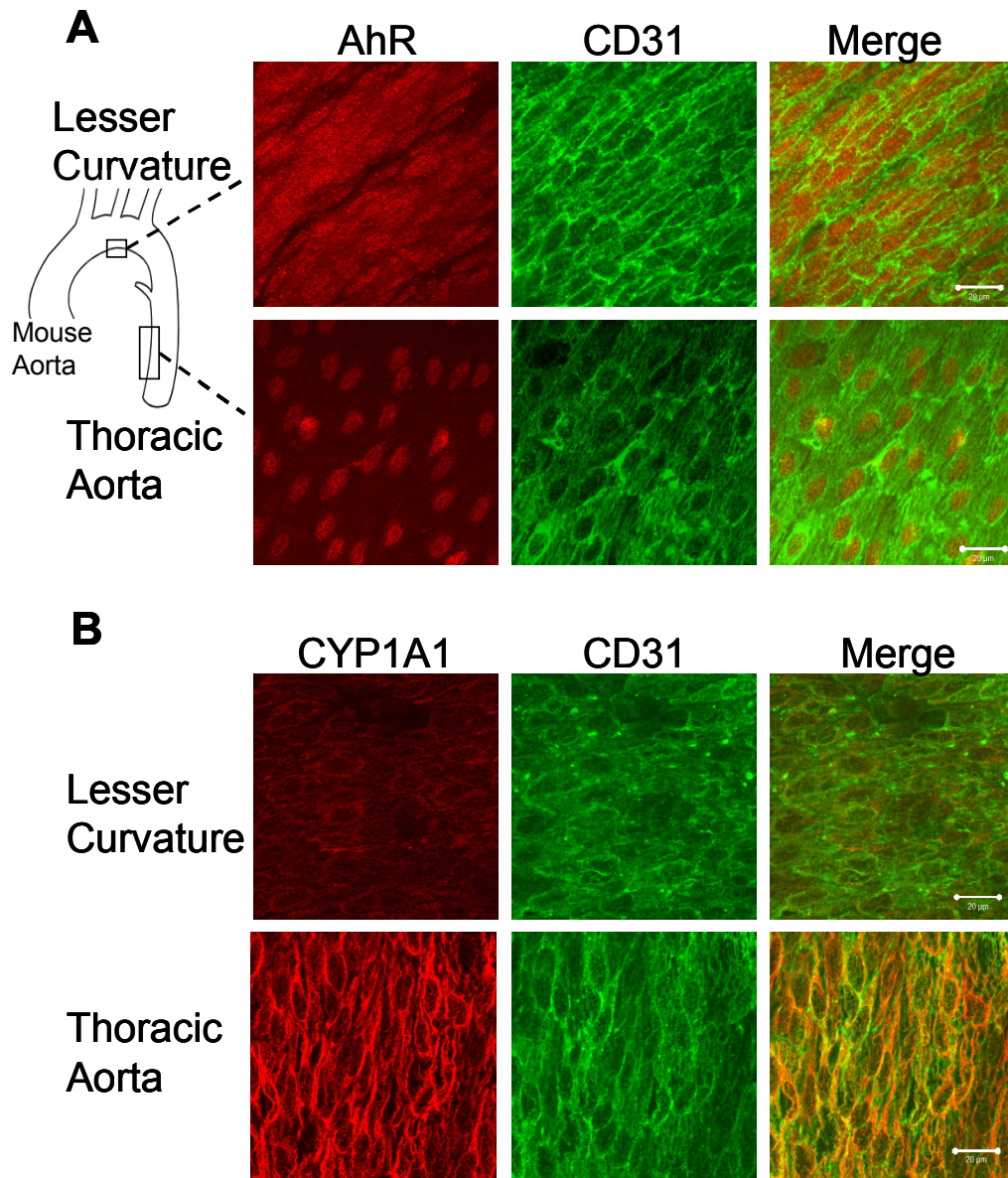


Figure 3.6 Expression of AhR and CYP1A1 protein in mouse aorta  
 Whole mouse aortas were stained for AhR (n=3) or CYP1A1 (n=7), and the lesser curvature and thoracic aorta were mounted *en face*. Endothelial cell integrity was confirmed with CD31 counterstaining. AhR (A) was expressed in the cytoplasm and nucleus in the region of lesser curvature, but was principally localized in the nucleus in the thoracic aorta. CYP1A1 (B) staining was strongest in the thoracic aorta, with attenuated staining in the region of lesser curvature. Bar is 20 micrometers.

Immunohistochemistry of CYP1A1 and CYP1B1 protein was performed on cross sections of human coronary artery from two individuals. The sections stained positively for CYP1A1 exclusively in the endothelium, whereas CYP1B1 was present in the endothelium, media, and adventitia (Figure 3.7).

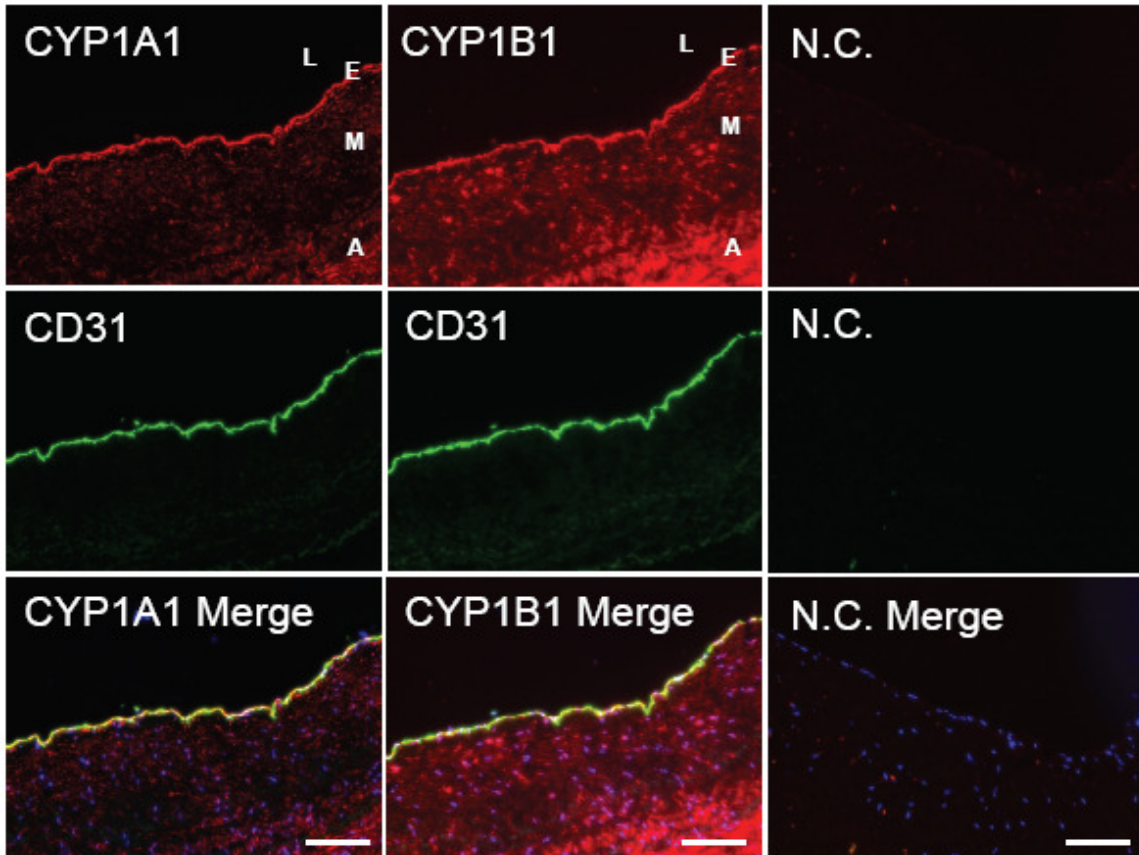


Figure 3.7 Expression of CYP1A1 and CYP1B1 protein in human coronary artery endothelial cells *in vivo*  
 Sectioned whole human coronary arteries were stained for either CYP1A1 or CYP1B1. Endothelial cells were identified using CD31. Merged images were counterstained with Hoechst (blue). CYP1A1 and CYP1B1 staining was strongest in the endothelium (E) with additional CYP1B1 expression in the media (M) and adventitia (A). Negative controls (N.C.) deleted the primary antibody. Bar is 20 micrometers. Lumen is at top of image (L).

### 3.4 Discussion

This study shows that both CYP1A1 and CYP1B1 gene expression are regulated by fluid shear stress in a time and magnitude-dependent manner. Both CYP1A1 and CYP1B1 mRNA and protein expression are strongly elevated in response to prolonged exposure to arterial levels of shear stress (15-25 dynes/cm<sup>2</sup>),<sup>65</sup> demonstrating that the increase of these two genes is not transiently induced by the initial application of shear stress (Figure 3.1). The continued elevation in expression of CYP1A1 and CYP1B1 out to 72 hours suggests that endothelial cells upregulate these two genes as an adaptation to chronic arterial levels of shear stress. It may be that high expression levels of CYP1A1 and CYP1B1 reflect a more physiological phenotype that is lost in statically cultured endothelial cells. This is consistent with our observation that these two genes are expressed in sections of human coronary arteries (Figure 3.7). Also consistent with our results, Dekker et al. showed maximal induction of CYP1B1 mRNA of HUVEC exposed to 25 dynes/cm<sup>2</sup> for 6 and 24 hours,<sup>21</sup> although our data showed an order of magnitude greater induction of this gene. Our finding that increased shear stress magnitude led to increased expression of CYP1A1 and CYP1B1 mRNA and protein (Figure 3.3) suggests that *in vivo* these genes would likely have higher expression levels in arterial than venous endothelial cells (human mean arterial shear stresses range from 10-30 dynes/cm<sup>2</sup>, whereas mean venous shear stresses range from 1-7 dynes/cm<sup>2</sup>).<sup>65</sup>

The reversing shear stress results (Figure 3.4) suggest that CYP1A1 and CYP1B1 gene expression would be higher in the arterial regions of the vasculature that have non-reversing flow than in those regions exposed to reversing flow; this hypothesis is confirmed by our mouse *en face* staining data (Figure 3.6) which showed decreases in

AhR nuclear localization and CYP1A1 expression in the lesser curvature of the mouse aorta, a region which experiences fluid shear stress reversal.<sup>63</sup> Development of lipid deposits at the lesser curvature in mice lacking low-density lipoprotein (LDL) receptors or apolipoprotein E<sup>63</sup> correlates disturbed flow with atherogenesis in this part of the aorta. Our results are also supported by Dai et al. who showed reduced CYP1A1 and CYP1B1 mRNA expression under reversing, athero-prone shear stress as compared to athero-protective, pulsatile non-reversing shear stress.<sup>16</sup> Since reversing flow has been hypothesized to be atherogenic and non-reversing flow to be athero-protective, CYP1A1 and CYP1B1 gene expression may be important in maintaining an athero-protective endothelial phenotype. There were no significant differences in CYP1A1 and CYP1B1 expression under 1 dyne/cm<sup>2</sup> steady shear stress compared to reversing shear stress, suggesting that this pathway is more sensitive to the time-averaged shear stress than to shear stress reversal.

Combined CYP1A1 and CYP1B1 enzymatic activity was increased significantly (7.2 fold) following shear stress (Figure 3.2). TMS, a specific CYP1B1 inhibitor,<sup>66</sup> reduced the measured activity in shear stressed cells by over 50 percent, indicating that both CYP1A1 and CYP1B1 contribute significantly to the dramatic change in activity. We also used alpha-naphthoflavone, in an effort to specifically block CYP1A1 activity, but found that it blocked all activity (data not shown). Although alpha-naphthoflavone has been used as a CYP1A1 inhibitor, it has been shown to equally inhibit CYP1B1.<sup>67</sup> The change in activity we observed under shear stress is nearly two-fold greater than the fold change reported by Han et al.<sup>58</sup> and is likely due to the more sensitive luciferase

activity assay. Our data also has the added advantage of distinguishing CYP1A1 from CYP1B1 through the use of a specific CYP1B1 inhibitor.

Recent studies have shown the existence of endogenous AhR-activating ligands.<sup>55-57, 68</sup> We previously reported that conditioned media from shear stressed cells increases CYP1A1 and CYP1B1 in naïve cells in static culture.<sup>69</sup> McMillan and Bradfield showed that in the absence of cells shear stress alone can directly modify LDL into an AhR ligand capable of up-regulating CYP1A1 and CYP1B1 when shear stress-conditioned media are applied to static cells.<sup>70</sup> Our finding that CYP1A1 and CYP1B1 expressions depend on shear stress magnitude (Figure 3.3) supports the hypothesis that shear stress produces a circulating AhR ligand in a shear stress magnitude dependent manner. Interestingly, the observation of regional differences in AhR nuclear localization in the mouse aorta (Figure 3.6) suggests a novel (and possibly synergistic) mechanism, in which the local hemodynamic environment directly affects the cellular response to circulating AhR ligands through a mechanotransduction-sensitive signaling pathway.

Gene expression of target genes, as well as thrombospondin-1 as a marker of AhR activation,<sup>56, 71</sup> were examined following siRNA treatment and shear stress exposure. In addition to knocking down CYP1A1, CYP1A1 siRNA treatment significantly decreased both CYP1B1 and thrombospondin-1 mRNA expression compared to the nonsense control (Figure 3.5). Since the CYP1A1 siRNA sequence is not complementary to CYP1B1 mRNA, a possible explanation is that CYP1A1 is necessary for endogenous AhR activation. Chiaro et al. have shown the existence of an auto-regulatory feedback loop between AhR and CYP1A1.<sup>57</sup> This study showed that AhR null mice had

dramatically reduced CYP1A1 mRNA expression and lower levels of AhR ligands in heart tissue compared to wild type animals, suggesting that in the heart CYP1A1 was necessary for activation of endogenous AhR ligands. Thrombospondin-1 has been recently shown in endothelial cells to be up-regulated by activated AhR through an AhR binding site in its promoter.<sup>56</sup> Isenberg et al. showed that thrombospondin-1 is an antagonist of NO-induced proliferation in HUVEC.<sup>72</sup> Given our observation that CYP1A1 knockdown decreased thrombospondin-1 expression and the observation by Han et al. that AhR activation is involved in shear stress cell cycle arrest,<sup>58</sup> increased CYP1A1 expression may decrease endothelial cell proliferation. Other shear stress responsive genes (Kruppel-like factor 2, endothelial nitric oxide synthase, and endothelin-1) were measured following CYP1A1 or CYP1B1 siRNA treatment but no significant differences in gene expression were found (data not shown). Taken together these results suggest that CYP1A1 and CYP1B1 gene expression affect the endothelial cell differently, and that CYP1A1 mediates gene expression through its involvement in AhR activation.

The presence of CYP1A1 and CYP1B1 expression in the endothelium of human coronary arteries (Figure 3.7) and AhR nuclear localization and CYP1A1 expression in mouse aortas (Figure 3.6) is consistent with the observation that fluid shear stress activates AhR resulting in the increased expression of CYP1A1 and CYP1B1 genes *in vitro*. To the author's knowledge, these are the first reports of constitutive CYP1A1 and CYP1B1 protein expression in endothelium of human arteries and of endogenous AhR nuclear localization in the mouse aorta. CYP1A1 has been shown to be inducible *in vivo* in vascular endothelium by many AhR ligands in many different species, including

human; however *in vivo* constitutive expression of CYP1A1 has not been reported.<sup>73</sup> Previous work by Dekker et al. did not detect CYP1B1 mRNA in human aorta sections using *in situ* hybridization.<sup>21</sup> Farin et al. showed constitutive expression of CYP1A1 in cultured HUVEC;<sup>74</sup> however Zhao et al. did not find constitutive expression of CYP1A1 or CYP1B1 in HUVEC.<sup>75</sup> Constitutive CYP1A1 expression was also observed in CD31 positive rat aortic endothelial cells.<sup>76</sup> Previous reports that CYP1A1 or CYP1B1 mRNA or protein were not constitutively expressed may be attributed to the use of the less-sensitive Northern blotting technique as compared to quantitative real-time PCR and to different sources of antibodies. Recent work has shown constitutive CYP1B1 expression in mouse corneal<sup>77</sup> and retinal endothelial cells<sup>78</sup> and human adult and fetal eyes.<sup>79</sup> In this study we also observed positive staining for CYP1B1 in the media and adventitia of human coronary arteries. Previous studies have shown that CYP1B1 is constitutively expressed in cultured human<sup>75, 80</sup> and mouse<sup>81</sup> vascular smooth muscle cells.

CYP1A1 and CYP1B1 genes and proteins represent potentially novel mechanosensitive pathways that merit additional detailed study. In the present study we also observed differences in CYP1A1 and CYP1B1 genes and proteins at different levels of shear stress (Figure 3.3) and between arterial steady shear stress and reversing shear stress (Figure 3.4), suggesting that the magnitude and time-average of shear stress may be important in the regulation of these two genes. The gene signaling capacities of CYP1A1 and CYP1B1 mRNA need additional investigation, in particular by focusing on the identity of substrates for these two genes, and a more detailed investigation of mechanisms of putative AhR/CYP feedback loops with cell regulatory functions.

Interestingly, both CYP1A1 and CYP1B1 can produce vasodilating compounds that could act as endothelial derived hyperpolarizing factors.<sup>26, 82, 83</sup>

The ability of cytochrome P450s to produce signaling and vasoreactive molecules from fatty acids and steroids, such as epoxyeicosatrienoic acids, has long been recognized in cardiovascular research. Epoxyeicosatrienoic acids are a group of P450 metabolites that are increased following shear stress.<sup>84, 85</sup> CYP1A1 and CYP1B1 represent two of the three reported cytochrome P450 genes (out of a total of 57 human P450 isoforms)<sup>86</sup> directly affected by shear stress (CYP27A1 has been shown recently to also be shear sensitive<sup>87</sup>). While it is possible that some of the previously observed changes in P450 metabolites by shear stress could be due to post-transcriptional modifications of other P450 enzymes or changes in substrate availability,<sup>88</sup> CYP1A1 and CYP1B1 may be important contributors to gene expression and metabolite profile changes in endothelial cells subjected to long-term shear stress. The possibility of lipid metabolism changes driven by CYP1A1 and CYP1B1, along with our *in vivo* data showing regional differences in AhR localization and CYP1A1 expression (Figure 3.6) that correlate with known sites of lipid deposition, strongly suggests that changes in CYP1A1 and CYP1B1 could affect atherosclerosis development and progression.

## CHAPTER 4: FREE INTRACELULAR ZINC IS REDUCED UNDER REVERSING SHEAR STRESS

### 4.1 Introduction

Zinc is a trace metal and essential nutrient. Within a cell, zinc binds with high affinity to metalloenzymes, structural proteins, and transcription factors, making the intracellular concentration of free (unbound) zinc typically very low.<sup>31</sup> Zinc has been estimated to be required for the function of more than 2000 transcription factors and 300 enzymes, making many signaling pathways dependent on zinc.<sup>89</sup> Large increases in extracellular zinc activate metal-regulatory transcription factor-1 (MTF-1) which increases transcription of proteins involved in zinc transport and binding, including metallothionein 1 (MT1), a zinc-binding protein, and zinc transporter-1, a zinc-specific transporter responsible for the efflux of zinc through the cell membrane.<sup>31</sup> Hence, the cell has a great ability to maintain a specific level of free zinc within the cell in response to changes in extracellular zinc.

Zinc has been shown to have anti-atherogenic properties, although the mechanisms remain unclear. Epidemiological studies of zinc have shown that in some populations low zinc serum levels are associated with coronary artery disease.<sup>32</sup> A postmortum study showed decreased zinc in the abdominal aorta in patients who died of cardiovascular disease as compared to other causes.<sup>90</sup> However, a more recent study showed elevated zinc in advanced lesions, which correlated strongly with lesion calcification.<sup>91</sup> Zinc was found to reduce the development of atherosclerosis in rabbits<sup>33-</sup>

<sup>35</sup> but not in apolipoprotein E (-/-) mice.<sup>92</sup> LDL (-/-) mice fed a zinc deficient diet had increased VLDL and HDL, however the mechanism for zinc regulation of lipoproteins is unknown.<sup>36</sup> LDL (-/-) mice with a zinc deficient diet also had increases in vascular cell adhesion molecule (VCAM-1) protein expression in the thoracic aorta, suggesting that zinc regulates inflammation.<sup>36</sup> Zinc deficiency has been shown to increase monocyte adhesion<sup>37</sup> and up-regulate nuclear factor  $\kappa$ B (NF- $\kappa$ B) in cultured endothelial cells,<sup>38</sup> even though NF- $\kappa$ B does not contain structural zinc.<sup>93</sup> Zinc binds to the active site of the pro form of matrix metalloproteinases (MMPs) to keep it inactive and is released before activation;<sup>94</sup> zinc has been shown to be an effective inhibitor of MMP-2 and MMP-9 activity in gingival tissue of the mouth.<sup>95</sup> Zinc has been shown to have antioxidant activity, and this could account for some of the anti-atherogenic properties observed.<sup>31</sup> Zinc has been shown to prevent oxidation of LDL by macrophages and endothelial cells.<sup>96</sup> Zinc has been shown to be required in the activation of the transcription factor nuclear factor, erythroid derived 2, like-2 (nrf-2) by hydrogen peroxide;<sup>31</sup> nrf-2 is responsible for the activation of antioxidant response element (ARE) genes such as hemeoxygenase-1 (HO-1).

Atherosclerosis is primarily localized to the carotid artery sinus, the coronary arteries, the abdominal aorta, and the superficial femoral arteries.<sup>39</sup> The vessel wall at these athero-prone locations is exposed to complex blood flow patterns including recirculation (reversing flow) in contrast to the non-reversing laminar shear stress that occurs throughout most of the vasculature, leading to the hypothesis that disturbed hemodynamic patterns are pro-atherogenic. Exposure to disturbed hemodynamics, when compared to non-reversing laminar shear stress, alter the gene expression profile and

ultimately the structure and function of endothelial cells, priming them for atherogenesis.<sup>3, 8</sup> A recent microarray study by our group showed the MT1 family, and MT2A to be differentially regulated by non-reversing pulsatile shear stress compared to steady shear stress.<sup>9</sup> Our unpublished microarray data, as well as published microarray data by Dai et al.,<sup>16</sup> showed increased MT1 and MT2A mRNA expression in HUVEC exposed to reversing shear stress compared to cells exposed to non-reversing shear stress. Regulation of metallothioneins by shear stress was also reported by Ohura et al. who showed a downregulation of metallothionein expression in cells exposed to turbulent flow in comparison to high steady laminar flow.<sup>18</sup> These differences indicate that metallothionein expression is highly sensitive to variations in shear stress.

We hypothesized that the reversing shear stress-induced increase in metallothionein protein expression could lead to a reduction in the free zinc levels in endothelial cells. In this study we examined the effects of reversing shear stress, arterial levels of high steady shear stress, low steady shear stress, and static culture conditions on the intracellular free zinc levels in endothelial cells. We also investigated the changes in metallothionein and Znt-1 protein expression under these different shear stress conditions. High steady shear stress dramatically increases the levels of free zinc in endothelial cells as compared to cells grown in static culture. This increase in free zinc is attenuated under reversing shear stress and low steady shear stress. The mechanosensitivity of intracellular free zinc to differences in shear stress supports the hypothesis that zinc is anti-atherogenic.

## 4.2 Methods

### *Cell Culture and Shear Stress*

HUVEC (Lonza) were grown and subjected to shear stress as previously described.<sup>41</sup> Briefly, cells were seeded at confluence on glass slides under static culture and then after 36 to 48 hours were subjected to 24 hours of one of four conditions: reversing shear stress (non-harmonic, 11 dynes/cm<sup>2</sup> maximum, -11 dynes/cm<sup>2</sup> minimum, -1 dyne/cm<sup>2</sup> average), steady arterial shear stress (15 dynes/cm<sup>2</sup>), low steady shear stress (1 dyne/cm<sup>2</sup>), and static culture. In the indicated experiments, 100 μM L-N<sup>G</sup>-Nitroarginine methyl ester (L-NAME) (Sigma) was added to the media at the beginning of application of shear stress to inhibit NO production.

### *Zinc Staining*

Following shear stress cells were rinsed with PBS (with calcium). Cells were incubated with 2.5 μM FluoZin-3 (Invitrogen), a zinc-sensitive cell-permeant dye,<sup>97</sup> in PBS for 15 minutes. Cells were rinsed with PBS and imaged directly on glass slides using a standard fluorescent microscope. For flow cytometry studies, following shear stress, cells were trypsinized, centrifuged, and then resuspended in 2.5 μM FluoZin-3 in PBS (without calcium) for 15 minutes. Cells were centrifuged and resuspended in PBS. Cells were analyzed on a BD LSR II flow cytometer (BD Biosciences) using a FITC filter and counting 10,000 events. The mean of the peak was used to compare between samples. To confirm uniform FluoZin-3 across samples loading identical cells were exposed to 200 μM ZnSO<sub>4</sub> and 50 μM pyrithione (a zinc ionophore). A zinc chelator,

N,N,N',N'-tetrakis-(2-pyridylmethyl)-ethylenediamine (TPEN) was used to confirm the zinc-specificity of FluoZin-3.

#### *Quantitative Real-time PCR*

Immediately after exposure to shear stress, total RNA and protein were extracted using TRI-zol (Invitrogen); RNA was further purified with DNase (Qiagen, Valencia, CA, USA) and RNeasy MinElute Cleanup Kit (Qiagen), according to manufacturers' instructions. The integrity and quantity of the RNA were verified with UV spectrophotometry, accepting only RNA with a 260/280 ratio greater than 1.9.

For quantitative real-time PCR (qRT-PCR), total RNA was reverse transcribed into cDNA with SuperScript II (Invitrogen) according the manufacturer's instructions. The resulting cDNA was purified through Micro Bio-Spin P-30 Chromatography Columns (BioRad) and diluted 1:20. qRT-PCR primers used were Znt-1 forward: 5'-tacatggaggtggctaaaacca-3', reverse: 5'-tgtcccacaacattgcttcaaa-3'); MT1E (forward: 5'-gcttgctctcactggtg-3', reverse: 5'-caggtgtgcaggtgttcta-3'); MT1F (MTF1 pre-designed PCR primer, Qiagen); MT1G (forward: 5'-cttctcgcttggaactcta-3', reverse: 5'-agggtcaagattgtagcaaa-3'); MT2A (forward: 5'-ccgactctagccgctctt-3', reverse: 5'-gtggaagtcgcttcttaca-3'); and 18S (QuantumRNA Classical II, Ambion). qRT-PCR reactions and analysis were performed on a MyiQ (BioRad, Hercules, CA, USA) using iQ SYBR Green Supermix (BioRad) according to the manufacturer's instructions. The qRT-PCR reactions and analysis were performed on a MyiQ (BioRad) with a 3 min initial denaturation step at 95°C; 45 cycles (30 cycles for 18 s) at 95°C for 5 s, 55°C for

10 s, 72°C for 60 s/kbp product and a ramped melting cycle. Samples were normalized by 18S expression. Fold changes were determined using the  $\Delta\Delta C_t$  method. .

Whole-cell protein was extracted immediately following shear stress using the Nuclear Extract kit (Active Motif). Protein concentration was quantified with DC Protein Assay (Bio-Rad) using BSA standards. Equal amounts of protein were resolved by SDS-PAGE in 10-20% tris-tricine precast polyacrylimide gels (BioRad) under reducing conditions with Laemmli sample buffer and electro-transferred onto polyvinyl difluoride membranes. Membranes were probed with rabbit anti-human MT1G, followed by donkey anti-rabbit immunoglobulin conjugated with horseradish peroxidase (GE Healthcare, Buckinghamshire, UK). Due to the strong homology across all metallothionein isoforms, it was assumed that the MT1G antibody was reactive against all human and mouse metallothionein isoforms.

#### *Mouse Aorta Immunohistochemistry*

C57BL/6 mice (6 to 8 week-old males, The Jackson Laboratory, Bar Harbor, ME, USA) were euthanized by CO<sub>2</sub> inhalation, and the aortas were perfusion-fixed with 10% formalin. The aortas were carefully cleaned *in situ*, and the arches and thoracic aortas were dissected and stained with rabbit-anti-human MT1G (1:100, Santa Cruz). Immunoreactive MT1G was detected with goat anti-rabbit IgG (1:250, Alexa Fluor 568, Invitrogen). Along with primary antibody, all samples were counterstained with antibody against CD31 using rat anti-mouse IgG (1:100, Santa Cruz), followed by counterstaining with goat anti-rat IgG (1:250, Alexa Fluor 488). The aortas were opened and separated into regions of lesser curvature, greater curvature, and thoracic artery. *En face* images

were collected with a LSM 510 META confocal microscope (Zeiss, Jena, Germany).<sup>63</sup>

The investigation conforms with the *Guide for the Care and Use of Laboratory Animals* published by the US National Institutes of Health (NIH Publication No. 85-23, revised 1996). Approval for use of animal studies was provided by the Emory University Institutional Animal Care and Use Committee.

### *Statistics*

Samples were analyzed using one-way ANOVA, followed by Newman-Keuls multiple comparison test.  $p < 0.05$  was considered significant.

## **4.3 Results**

Free zinc levels, as measured by FluoZin-3 staining, were increased in cells exposed to high steady shear stress (15 dynes/cm<sup>2</sup>), reversing shear stress, and low steady shear stress (1 dyne/cm<sup>2</sup>) as compared to cells exposed to static culture (Figure 4.1). Pseudocolor images indicated higher free zinc in endothelial cells exposed to high steady shear stress as compared to reversing shear stress and low steady shear stress (Figure 4.2).

To quantitate free zinc levels, cells were stained with FluoZin-3 and analyzed by flow cytometry (Figure 4.3). Consistent with the fluorescent images in Figure 4.1, cells exposed to 15 dynes/cm<sup>2</sup> had the highest free zinc levels, which was attenuated under 1 dyne/cm<sup>2</sup> and reversing shear stress. All shear stressed cells had increased free zinc when compared to cells grown in static culture. Equal loading of FluoZin-3 was

confirmed by exposing identical cells to exogenous zinc and a zinc ionophore (data not shown). Specificity of FluoZin-3 was confirmed by reduced fluorescence in the presence of the zinc chelator TPEN (data not shown). Free zinc levels were significantly attenuated in cells subjected to 15 dynes/cm<sup>2</sup> shear stress the presence of 100 μM L-NAME, an inhibitor of nitric oxide, suggesting that nitric oxide may regulate increases in free zinc (Figure 4.4).

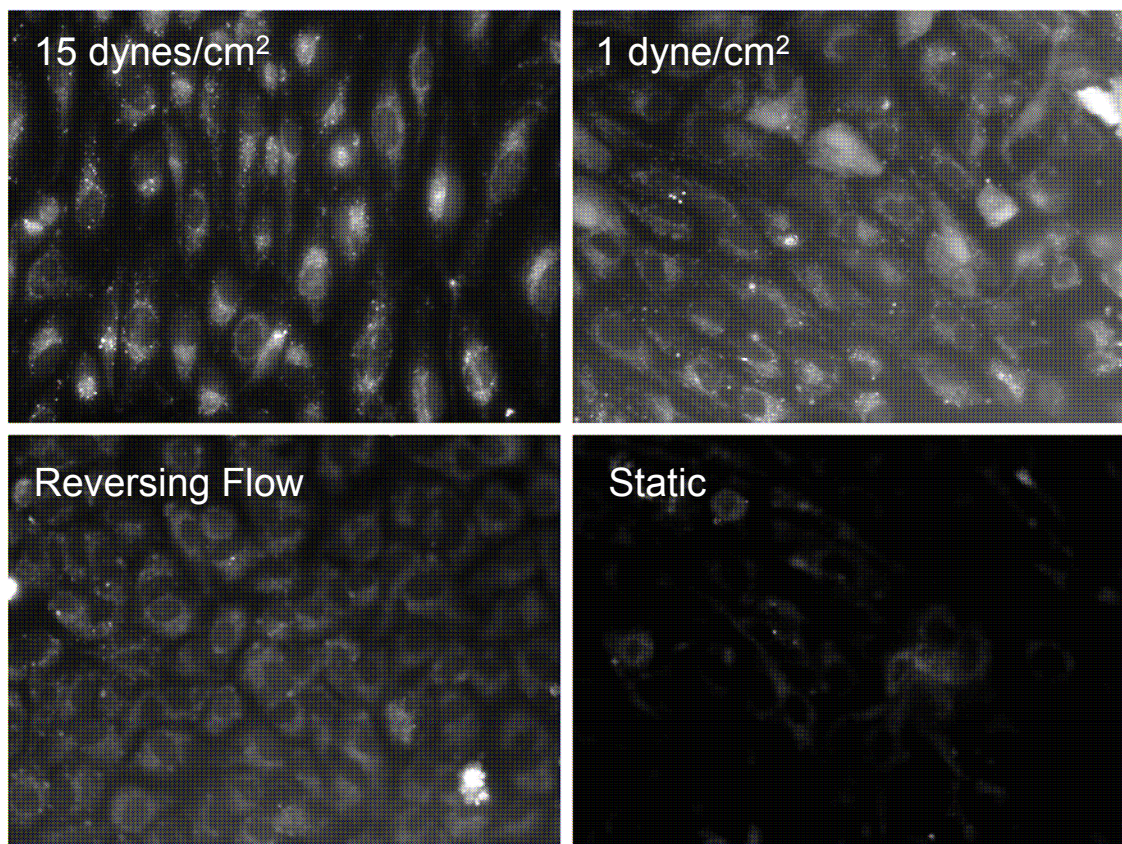


Figure 4.1 Free zinc levels in HUVEC after 24 hours shear stress  
HUVEC subjected to 24 hours shear stress treatment were stained with FluoZin-3 to show free zinc levels. Free zinc is highest under 15 dynes/cm<sup>2</sup>, attenuated under 1 dyne/cm<sup>2</sup> and reversing flow, and lowest under static conditions.

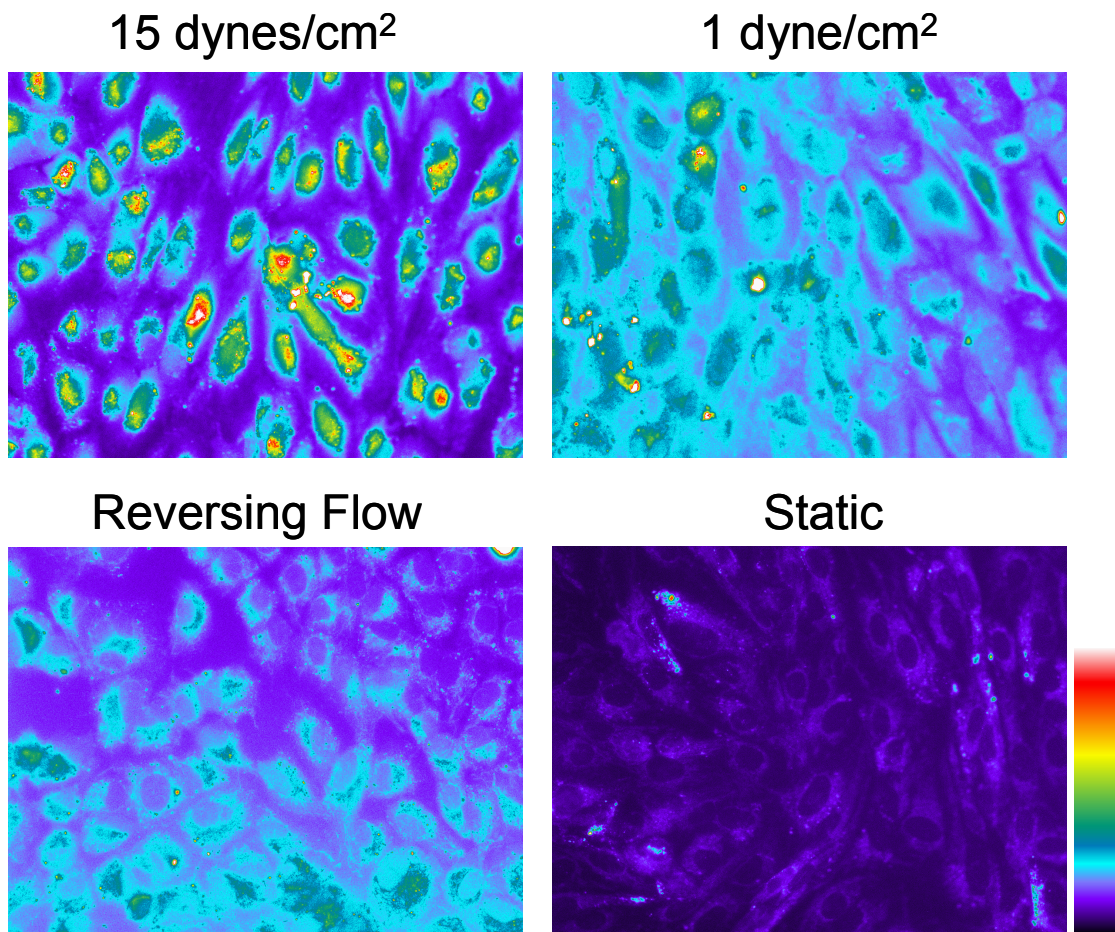


Figure 4.2 Pseudocolor of free zinc levels in HUVEC after 24 hours shear stress. Images in Figure 4.1 were converted to pseudocolor to show fluorescent intensity.

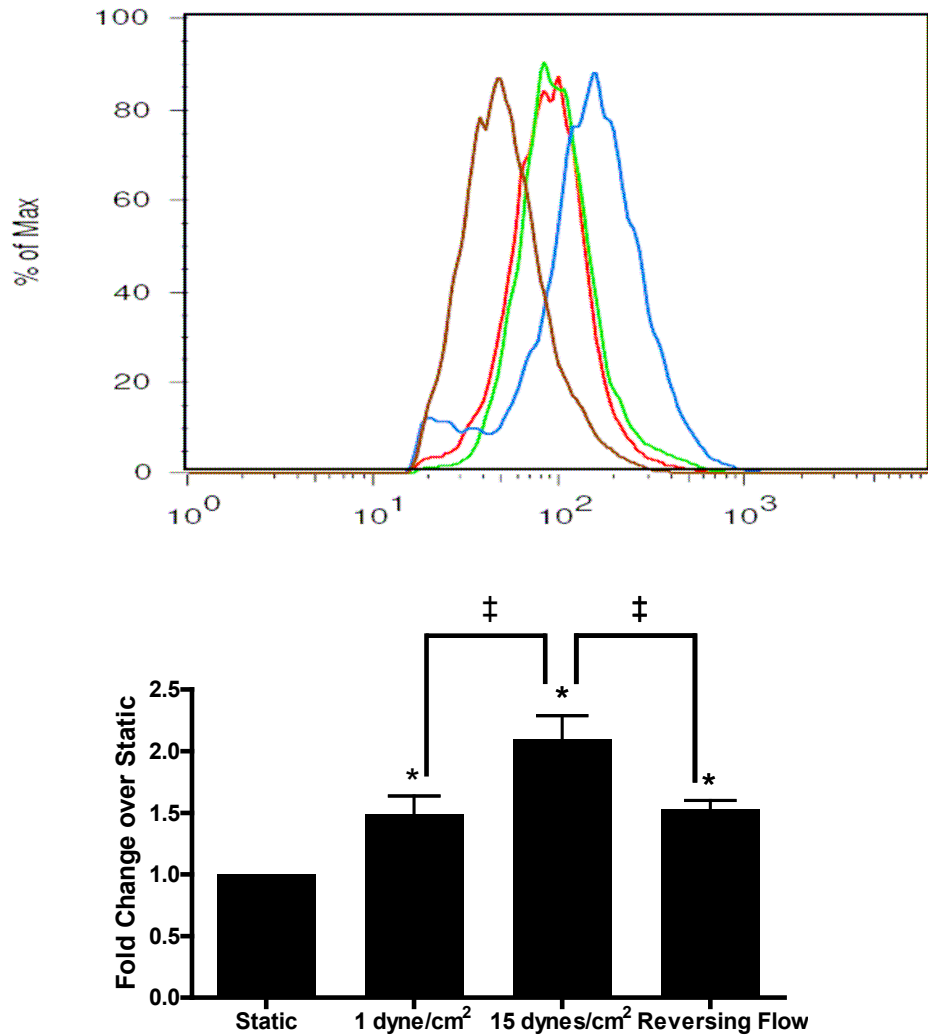


Figure 4.3 Flow cytometry measurement of free zinc in HUVEC. HUVEC subjected to 24 hours shear stress treatment were trypsinized, stained with FluoZin-3, and analyzed using flow cytometry to quantitate differences in free zinc levels. Top: A representative flow cytometry result showing free zinc is highest under 15 dynes/cm<sup>2</sup> (blue), attenuated under 1 dyne/cm<sup>2</sup> (green) and reversing flow (red), and lowest under static conditions (brown), similar to the results from the fluorescent images of FluoZin-3 stained cells. Bottom: The flow cytometry mean fluorescence of repeat experiments (n=6). \* significant between sample and static, ‡ significant between indicated conditions.

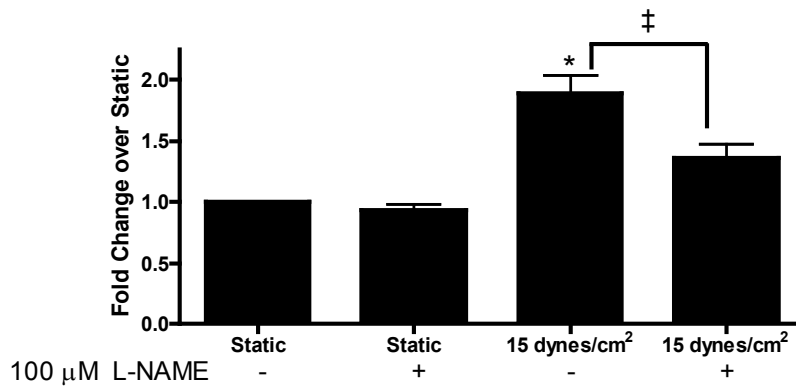


Figure 4.4 Inhibition of nitric oxide attenuates the free zinc increase by shear stress. Cells were grown in the presence or absence of 100  $\mu$ M L-NAME to inhibit nitric oxide (n=3). Inhibiting NO resulted in decreased free zinc only in endothelial cells exposed to shear stress (15 dynes/cm<sup>2</sup>). \* significant between sample and static, † significant between indicated conditions.

MT1E, MT1F, MT1G, MT2A, and Znt-1 mRNA were most highly expressed in endothelial cells exposed to reversing shear stress, and were also elevated in endothelial cells exposed to 1 dyne/cm<sup>2</sup> (Figure 4.5). MT1G was nearly undetectable in cells exposed to 15 dynes/cm<sup>2</sup> and static culture. Similar trends were observed in metallothionein protein expression.

Metallothionein protein expression was elevated in the region of lesser curvature in the mouse aorta when compared to the thoracic aorta (Figure 4.6). The staining pattern of metallothionein in the region of lesser curvature was throughout the cell, whereas in the thoracic aorta it was localized within the nucleus. Negative control samples (without primary antibody) showed no positive staining (data not shown).

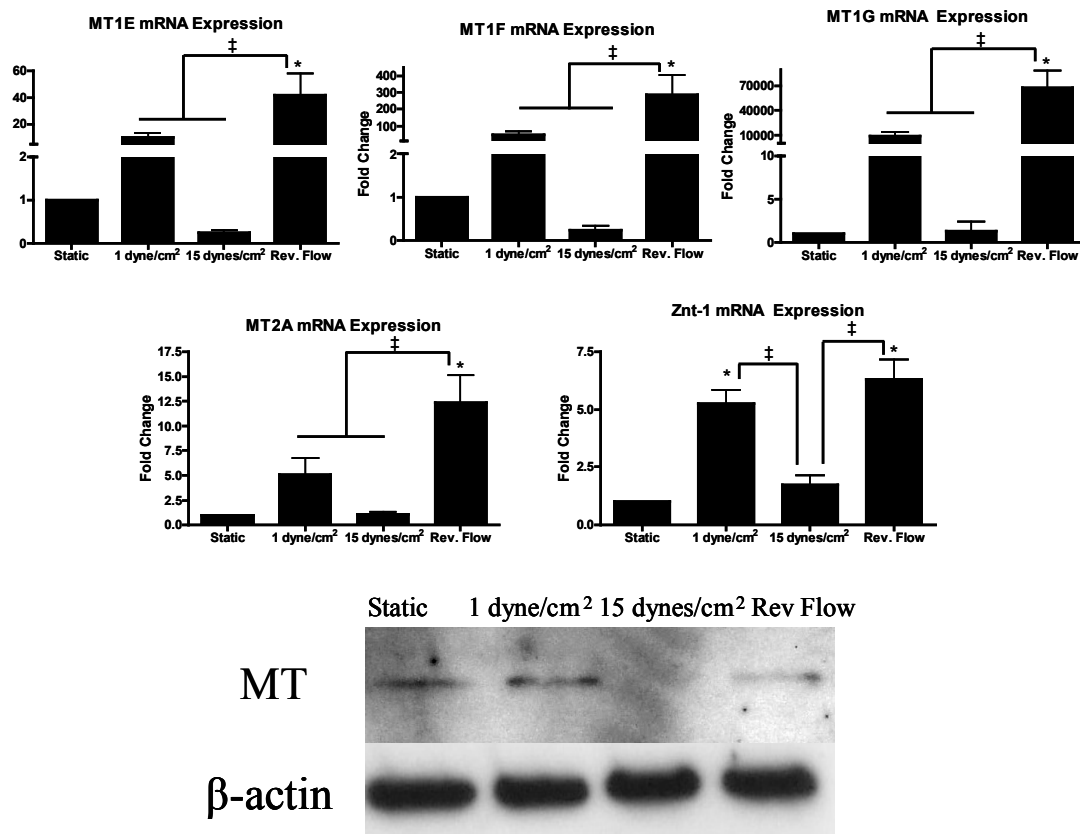


Figure 4.5 Metallothionein and Znt-1 expression is regulated by shear stress. Top: mRNA expression of MT1E, MT1F, MT1G, MT2A, and Znt-1 was increased in cells exposed to reversing shear stress and 1 dyne/cm<sup>2</sup> and attenuated under 15 dynes/cm<sup>2</sup> (n=5). MT1G was nearly undetectable in static and 15 dynes/cm<sup>2</sup>. \* significant between sample and static, † significant between indicated conditions. Bottom: Western blotting of metallothionein (MT) (n=2) shows increased expression of both proteins in cells exposed to reversing shear stress as compared to steady shear stress of 15 dynes/cm<sup>2</sup>.

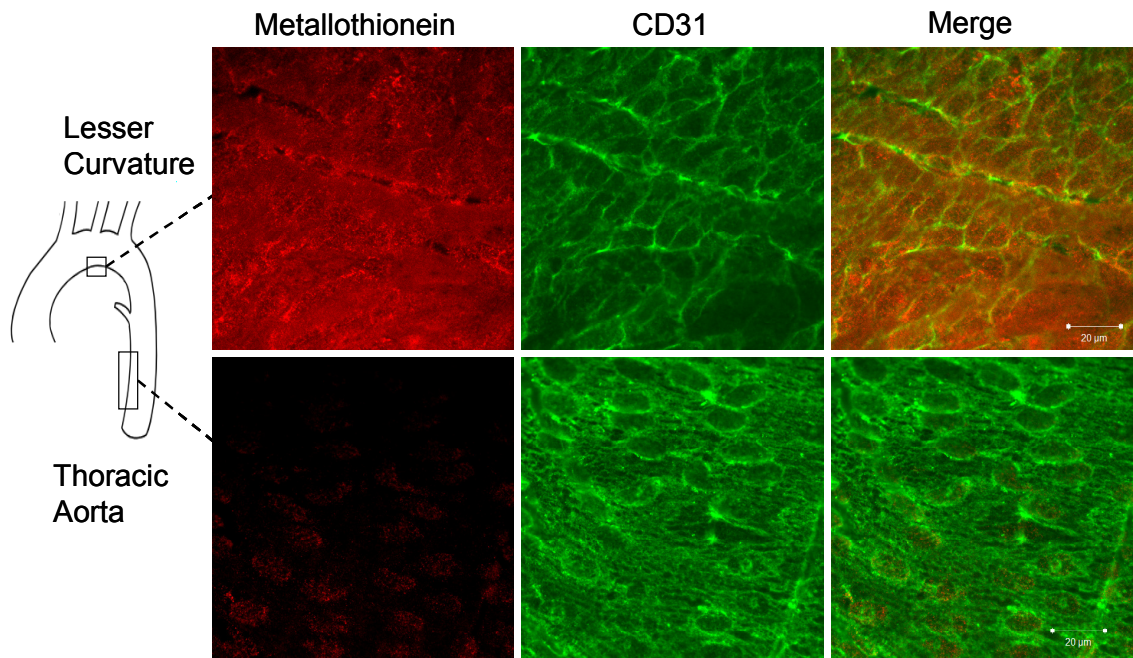


Figure 4.6 Expression of metallothionein protein in mouse aorta  
Whole mouse aortas were stained for metallothionein (n=3), and the lesser curvature and thoracic aorta were mounted *en face*. Endothelial cell integrity was confirmed with CD31 counterstaining.

#### 4.4 Discussion

This is the first report of free zinc being regulated by mechanical forces. We show that application of fluid shear stress leads to a dramatic increase in free zinc over static cultured cells (Figure 4.1 and Figure 4.3). Furthermore, the addition of L-NAME, a NO inhibitor, to cells subjected to 15 dynes/cm<sup>2</sup> caused a significant attenuation of the free zinc increase (Figure 4.4). Zinc release from metallothionein has previously been shown to be nitric oxide (NO) sensitive,<sup>98</sup> suggesting that shear stress-induced production of NO<sup>99</sup> accounts for some of the zinc increases observed (Figure 4.7). There are only minor differences in metallothionein and Znt-1 expression between static cultured cells and cells exposed to 15 dynes/cm<sup>2</sup> (Figure 4.5), and therefore we do not expect that changes in metallothionein or Znt-1 contribute to the increase in free zinc observed under 15 dynes/cm<sup>2</sup> as compared to static cultured cells.

Free zinc is significantly reduced in cells exposed to *in vitro* reversing shear stress, when compared to cells exposed to steady shear stress (Figure 4.3). The increased expression of metallothioneins and Znt-1 by reversing shear stress (Figure 4.5) offers a possible mechanism for this decrease; increases in metallothionein lead to increased protein binding of zinc and increases in Znt-1 lead to increased cellular efflux of zinc which together reduce the levels of intracellular free zinc (Figure 4.7). Changes in both metallothioneins 1 and 2A and in Znt-1 suggest the possibility that the transcription factor MTF-1 is activated in cells exposed to reversing flow. In addition to activation by metals such as zinc, MTF-1 has been shown to be activated in response to increased oxidative stress.<sup>100</sup> Since reversing shear stress leads to increased reactive oxygen

species<sup>101</sup> it is possible that oxidative stress could be contributing to the up-regulation of metallothionein and Znt-1 thereby affecting free zinc levels in the cell.

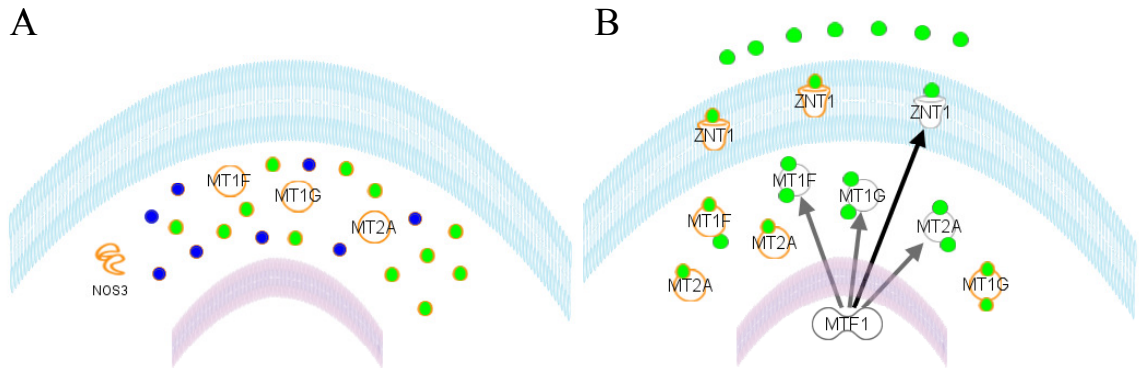


Figure 4.7 Possible mechanisms for shear stress mediated changes in free zinc  
 A: Under high steady shear stress (15 dynes/cm<sup>2</sup>), NO (blue circles) production is increased by NOS3 (eNOS). Increased NO production results in the release of zinc (green circles) from metallothioneins. B: Under reversing shear stress or low shear stress the transcription factor MTF-1 is activated, possibly by oxidative stress, and leads to the up-regulation of metallothioneins and Znt-1. The increased expression of metallothionein results in more intracellular zinc being bound to proteins and increased Znt-1 results in a larger cellular efflux of zinc, which in combination reduce the levels of intracellular free zinc.

Our *in vitro* results suggest that *in vivo* endothelial cells exposed to reversing wall shear stress (e.g. at sites prone to the development of atherosclerosis) have less intracellular free zinc. Although we were unable to successfully measure zinc in a freshly isolated mouse aorta, we did observe increased metallothionein expression in the lesser curvature of the mouse aortic arch as compared to the thoracic aorta (Figure 4.6), strongly suggesting that there are regional differences in free zinc in the mouse aorta. The wall of lesser curvature in mice lacking low-density lipoprotein (LDL) receptors or apolipoprotein E is prone to the development of lipid deposits, which is correlated to the

exposure of this site to reversing wall shear.<sup>63</sup> The reduced levels of free zinc in endothelial cells exposed to reversing shear stress may prime these cells towards an atherosclerotic state and may provide a possible mechanism for the observation that zinc is reduced in atherosclerotic plaques.

The implications of changes in free zinc are not fully understood, but we hypothesize that changes could affect the regulation of zinc-sensitive transcription factors and enzymes. In fact, recently it was shown that nrf-2, a transcription factor regulated by shear stress,<sup>102</sup> is activated by increased free zinc.<sup>31</sup> Zinc has also been shown to be important in reducing inflammation in endothelial cells *in vivo*<sup>36</sup> and *in vitro*<sup>37</sup> and atherosclerosis in rabbits.<sup>33-35</sup> A possible explanation for the protective effects of zinc is that zinc supplementation could lead to increases in free zinc levels within the cell and thus counteracting decreases in free zinc in endothelial cells exposed to reversing flow. In an effort to better understand the zinc-related shear stress signaling pathways, we performed shear stress experiments in the presence of N,N,N',N'-tetrakis-(2-pyridylmethyl)-ethylenediamine (TPEN), a zinc specific chelator (data not shown); however, in our hands the chelator did not reduce free zinc at sub-cytotoxic concentrations. Additional experiments are needed to better understand the effects of free zinc on endothelial gene expression and function.

## CHAPTER 5: CONCLUSIONS

### 5.1 Summary

In this thesis project the effects of pro-atherogenic versus anti-atherogenic shear stress on endothelial gene expression were examined using a novel flow system. Chapter 2 shows that reversing shear stress, in comparison to steady arterial shear stress, induces changes in morphology, cell proliferation, monocyte adhesion, and gene expression that may prime endothelial cells toward atherosclerosis. Through the use of a low average shear stress control, it was shown that many of the changes induced by reversing shear stress are due to the low average shear stress component of the flow profile, rather than the reversing or oscillatory component.

In Chapter 3 two shear stress responsive genes, CYP1A1 and CYP1B1, were examined using the new reversing shear stress system. Increased mRNA expression, protein expression, and enzymatic activity were observed under shear stress for both genes, whereas gene and protein expression was reduced under reversing shear stress. Knockdown of CYP1A1 with siRNA suggests CYP1A1 expression may be important in the initial activation of AhR. Differential expression of CYP1A1 and localization of AhR were observed in the mouse aorta, providing *in vivo* confirmation of the *in vitro* results. This study also provides the first confirmation of AhR, CYP1A1, and CYP1B1 protein expression in vascular endothelial cells. The differential regulation of CYP1A1 and CYP1B1 by pro- versus anti-atherogenic shear stress may offer a possible mechanism for the previously observed changes in lipid signaling under different forms of shear stress.

Chapter 4 examined the changes in free zinc levels induced by different shear stress regimens. Free zinc is strongly increased by steady shear stress over static cultured cells and is attenuated by reversing shear stress. The changes in zinc correlate with changes in metallothionein, zinc binding proteins, and Znt-1, a zinc exporter. This is the first report of free zinc levels being mechanosensitive, and leads to the hypothesis that changes in free zinc by shear stress may directly affect zinc-sensitive transcription factors and zinc-sensitive enzymes. The attenuation of free zinc under reversing shear stress, along with the increased metallothionein protein expression observed in the region of lesser curvature of the mouse aorta, may provide a possible explanation for previously published nutritional studies suggesting that reduced zinc levels can promote atherosclerosis.

The correlation of atherosclerosis to disturbed hemodynamics (reversing shear stress) suggests that these mechanical forces may be important in priming endothelial cells towards atherosclerosis. The studies herein show that reversing shear stress, when compared to steady arterial shear stress, alters a small set of genes that may promote the development of atherosclerosis. CYP1A1 and CYP1B1 represent additional genes regulated by fluid shear stress, which could be important in synthesizing or metabolizing lipid signaling molecules. Free zinc regulation by fluid shear stress suggests this pathway could be an important component in transducing mechanical forces into gene expression changes. By identifying genes and pathways differentially regulated by pro- versus anti-atherogenic shear stress, it may be possible to develop a better understanding of the development and progression of atherosclerosis and its localization to regions of disturbed flow.

## 5.2 Future Work

Reversing shear stress has been shown to cause an increase in cell proliferation as compared to steady arterial shear stress. Although microarray changes revealed changes in cell cycle related genes, a better understanding of the mechanism between shear stress and cell cycle control is needed. Previous studies have suggested shear stress-dependent cell cycle regulation occurs through p21.<sup>103</sup> Likely there are two mechanisms, one of cell proliferation suppression by any type of fluid shear stress and another that is specific only to high shear stress.

Additionally, the mechanism for increased monocyte adhesion on cells pre-treated with reversing shear stress is not clear. Because microarray results did not reveal any changes in expression of rolling or adhesion molecules, and Western blotting of VCAM-1 and ICAM-1 did not show increased protein expression in cells exposed to reversing shear stress, it may be possible that reversing shear stress induces post-translational or structural changes in adhesion molecules. Measurement of surface ICAM-1 and VCAM-1 expression will be performed with flow cytometry. Antibody blocking experiments of VCAM-1 and ICAM-1 will be performed to examine the role of these adhesion molecules in the increased monocyte adhesion. Another possibility is that the substrate used in the experiments, gelatin (a collagen-based substrate), could affect the endothelial cell response to shear stress. Recent work showed increased activation of NF- $\kappa$ B on endothelial cells exposed to shear stress that were cultured on fibronectin as compared to collagen,<sup>104</sup> making it possible that the gelatin substrate in these experiments suppressed additional inflammation that could occur under reversing shear stress. Finally, work has

been shown that the glycocalyx thickness is reduced *in vivo* at regions of atherosclerosis<sup>105</sup>; it is possible that reversing shear stress reduces glycocalyx, thereby exposing more adhesion receptors.

The lipid expression profile is dramatically changed by shear stress; some of these changes could be due to the upregulation of CYP1A1 and CYP1B1 expression and activity. *In vitro* CYP1A1 and CYP1B1 have been shown to be capable of producing potentially both vasoreactive and signaling compounds; however, the physiological substrates of CYP1A1 and CYP1B1 are unclear. A better understanding of the substrates of CYP1A1 and CYP1B1 would enable a better understanding of their roles in the endothelial cell and potential role in atherosclerosis. Also the mechanism of the sensitivity of AhR to different shear stress regimens merits additional study. Previous work showed shear-stressed modified LDL was responsible for the activation of AhR; however the differences in nuclear localization of AhR in the mouse aorta suggest that there is an additional mechanism beyond a circulating ligand. One possibility is that additional co-factors or AhR stability are mechanically regulated by shear stress. AhR activation has been shown to be dependent on caveolin-1;<sup>106</sup> caveolae changes under shear stress could alter AhR activity. Zinc has also been shown to affect AhR activation.<sup>107</sup>

Future experiments will seek to better understand the mechanism for zinc up-regulation by fluid shear stress in endothelial cells. To see if reversing shear stress differentially regulates Znt-1 protein expression, Znt-1 protein changes in response to shear stress will be detected by Western blotting and Znt-1 protein expression in the mouse aorta will be examined. Additional experiments are also planned to measure

MTF-1 activity in cells exposed to reversing and 15 dynes/cm<sup>2</sup> shear stress by using an electrophoretic mobility shift assay (EMSA) or examining changes in MTF-1 nuclear localization. Experiments using siRNA targeted knockdown of MTF-1 under reversing shear stress will also be performed to determine if MTF-1 is leading to the upregulation of metallothionein and Znt-1, and if blocking their upregulation would result in increases in free zinc similar to the levels observed under high steady shear stress.

To assess the potential protective role of zinc in the endothelial cell, reversing shear stress experiments will be performed with media supplemented with ZnSO<sub>4</sub>. These cells will be compared to cells exposed to reversing flow in unsupplemented media. After shear stress cells will be stained with FluoZin-3 to see if zinc supplementation leads to increased free intracellular zinc. Experiments to examine the protective effects of zinc will look for changes in transcription factors, such as NF-κB and nrf-2 that have been shown to be zinc sensitive.<sup>31, 38</sup> Additionally, the ability of zinc to prevent increased monocyte adhesion under reversing shear stress will be examined.

## APPENDIX A: CALCULATION OF WALL SHEAR STRESS

The measurement of fluid shear stress was accomplished through the use of latex beads filmed under high speed video microscopy (1000 frames per second). This appendix explains how the measured velocity of these individual beads was used to determine wall shear stress.

### Calculation of shear stress:

Navier-Stokes Equation

$$\rho \left( \frac{\partial v_x}{\partial t} + v_x \frac{\partial v_x}{\partial x} + v_y \frac{\partial v_x}{\partial y} + v_z \frac{\partial v_x}{\partial z} \right) = -\frac{\partial P}{\partial x} - \mu \left( \frac{\partial^2 v_x}{\partial x^2} + \frac{\partial^2 v_x}{\partial y^2} + \frac{\partial^2 v_x}{\partial z^2} \right) + \rho g_x$$

The Navier-Stokes Equation can be simplified for the fluid flow through a parallel plate chamber based on the following assumptions:

1. Steady state

$$\frac{\partial v_x}{\partial t} = 0$$

2. Fully developed flow

$$v_x \frac{\partial v_x}{\partial x} = 0 \quad \frac{\partial^2 v_x}{\partial x^2} = 0$$

3. Laminar flow

$$v_y \frac{\partial v_x}{\partial y} = 0 \quad v_z \frac{\partial v_x}{\partial z} = 0$$

4. Side wall effects can be ignored

$$\frac{\partial^2 v_x}{\partial z^2} = 0$$

5. No gravity in the x direction

$$pg_x = 0$$

The Navier-Stokes equation is then reduced to:

$$\frac{\partial P}{\partial x} = \mu \frac{\partial^2 v_x}{\partial y^2}$$

If the pressure drop is assumed to be constant over the entire length of the chamber, this can be reduced to

$$-\frac{\Delta P}{\mu L} = \frac{\partial^2 v_x}{\partial y^2}$$

Separate the variables and integrate to obtain:

$$-\frac{\Delta P}{\mu L} y + C_1 = \frac{\partial v_x}{\partial y}$$

Separate the variables again and integrate to obtain:

$$-\frac{\Delta P}{2\mu L} y^2 + C_1 y + C_2 = v_x$$

Use the following boundary conditions to solve for  $C_1$  and  $C_2$ .

$$\frac{\partial v_x}{\partial y} = 0 \text{ at } y = 0 \text{ and } v_x = 0 \text{ at } y = b/2$$

Inserting boundary condition 1:

$$-\frac{\Delta P}{\mu L}y + C_1 = \frac{\partial v_x}{\partial y}$$

$$-\frac{\Delta P}{\mu L}(0) + C_1 = 0$$

$$C_1 = 0$$

Boundary condition 2 can be used to solve for  $C_2$ :

$$-\frac{\Delta P}{2\mu L}y^2 + C_1y + C_2 = v_x$$

$$-\frac{\Delta P}{2\mu L}y^2 + C_2 = v_x$$

$$-\frac{\Delta P}{2\mu L}\left(\frac{b}{2}\right)^2 + C_2 = 0$$

$$C_2 = \frac{\Delta P b^2}{8\mu L}$$

$$v_x = -\frac{\Delta P}{2\mu L}y^2 + \frac{\Delta P b^2}{8\mu L}$$

Solve for the volumetric flow rate by substituting in the velocity equation to the following:

$$Q = \int_{-w/2}^{w/2} \int_{-b/2}^{b/2} v_x dydz$$

$$v_x = -\frac{\Delta P}{2\mu L} \left( y^2 - \frac{b^2}{4} \right)$$

$$Q = \int_{-w/2}^{w/2} \int_{-b/2}^{b/2} -\frac{\Delta P}{2\mu L} \left( y^2 - \frac{b^2}{4} \right) dydz$$

$$Q = \int_{-b/2}^{b/2} -\frac{\Delta P}{2\mu L} \left( y^2 - \frac{b^2}{4} \right) \left( \frac{w}{2} + \frac{w}{2} \right) dy$$

$$Q = \left( -\frac{\Delta P w}{6\mu L} y^3 + \frac{\Delta P w b^2}{8\mu L} y \right) \Bigg|_{y=-\frac{b}{2}}^{y=\frac{b}{2}}$$

$$Q = \frac{\Delta P w b^3}{12\mu L}$$

Solve for  $\Delta P$ :

$$\Delta P = \frac{12Q\mu L}{wb^3}$$

Solve for the shear rate at  $y = \pm b/2$ :

$$\gamma = \frac{\partial v_x}{\partial y} = \frac{\Delta P}{\mu L} y$$

$$\gamma = \frac{12Q\mu L}{wb^3} * \frac{1}{\mu L} * \frac{b}{2}$$

$$\gamma = \frac{6Q}{wb^2}$$

The shear stress,  $\tau$ , is the shear rate multiplied by the fluid viscosity.

$$\tau = \gamma\mu = \frac{6Q\mu}{wb^2}$$

### Relationship between fluid velocity and shear stress

To focus the high speed video camera at the center of the flow chamber, a mark was made on the glass slide and also on the surface of the flow chamber. The focus knob was marked at each position and then adjusted to the middle. The velocity at the middle of the chamber ( $y=0$ ) represents the maximum velocity, and the measured beads was assumed to be the maximum velocity of the fluid flow through the chamber.

$$v_x = -\frac{\Delta P}{2\mu L} y^2 + \frac{\Delta P b^2}{8\mu L}$$

$$y = 0$$

$$V_x^{\max} = \frac{\Delta P b^2}{8\mu L}$$

Using the previous derivation of shear stress, find a similar term for the average velocity:

$$Q = \frac{\Delta P w b^3}{12\mu L}$$

$$V_x^{\text{avg}} = \frac{Q}{A}$$

$$A = bw$$

$$V_x^{\text{avg}} = \frac{\frac{\Delta P w b^3}{12\mu L}}{bw} = \frac{\Delta P b^2}{12\mu L}$$

Finding the ratio of  $V_x^{\text{avg}}$  to  $V_x^{\max}$ :

$$\frac{V_x^{avg}}{V_x^{max}} = \frac{\frac{\Delta P b^2}{12 \mu L}}{\frac{\Delta P b^2}{8 \mu L}} = \frac{2}{3}$$

$$V_x^{max} = \frac{3}{2} V_x^{avg}$$

$$V_x^{max} = \frac{3}{2} \frac{\tau b}{6 \mu}$$

$$\tau = \frac{4 V_x^{max} \mu}{b}$$

## APPENDIX B: SUPPLEMENTARY MICROARRAY TABLES

Table B.1: Complete list of genes regulated by high shear component

[15d] vs [1d]	[RF] vs [1d]	Description
1.92	1.75	A_24_P401090
2.03	1.81	Homo sapiens fibroblast growth factor 18 (FGF18), mRNA [NM_003862]
3.13	2.27	Homo sapiens receptor (G protein-coupled) activity modifying protein 2 (RAMP2), mRNA [NM_005854]
1.67	1.81	Homo sapiens cDNA clone IMAGE:5300185. [BC039399]
-1.53	-1.92	Chromodomain-helicase-DNA-binding protein 6 (EC 3.6.1.-) (ATP- dependent helicase CHD6) (CHD-6) (Radiation-induced gene B protein). [Source:Uniprot/SWISSPROT;Acc:Q8TD26] [ENST00000373222]

Table B.2: Complete list of genes regulated by low shear stress

[15d] vs [1d]	[15d] vs [RF]	Description
3.26	4.25	A_23_P66347
1.79	1.86	A_24_P246636
9.49	11.05	A_32_P599
3.84	4.60	A_32_P93894
-2.56	-2.82	Homo sapiens arylacetamide deacetylase (esterase) (AADAC), mRNA [NM_001086]
2.23	2.42	Homo sapiens ADAM metalloproteinase with thrombospondin type 1 motif, 4 (ADAMTS4), mRNA [NM_005099]
-2.17	-2.39	Homo sapiens adrenergic, alpha-2A-, receptor (ADRA2A), mRNA [NM_000681]
-1.62	-1.84	Homo sapiens full length insert cDNA clone YW18A11. [AF086011]
-2.45	-2.78	Homo sapiens full length insert cDNA clone ZE03A08. [AF086511]
-1.51	-1.79	Homo sapiens amidohydrolase domain containing 2 (AMDHD2), mRNA [NM_015944]
-1.73	-2.46	Homo sapiens apolipoprotein B mRNA editing enzyme, catalytic polypeptide-like 3B (APOBEC3B), mRNA [NM_004900]
3.64	2.45	Homo sapiens apolipoprotein L, 3 (APOL3), transcript variant beta/a, mRNA [NM_145641]
1.60	1.58	Homo sapiens, clone IMAGE:4454331, mRNA. [BC019824]

<b>[15d] vs [1d]</b>	<b>[15d] vs [RF]</b>	<b>Description</b>
2.67	3.07	Homo sapiens HSPC047 protein, mRNA (cDNA clone MGC:34358 IMAGE:5178752), complete cds. [BC035371]
5.35	4.83	Homo sapiens B-cell CLL/lymphoma 2 (BCL2), nuclear gene encoding mitochondrial protein, transcript variant alpha, mRNA [NM_000633]
8.14	8.57	Homo sapiens bradykinin receptor B2 (BDKRB2), mRNA [NM_000623]
-1.67	-2.45	Homo sapiens brain expressed X-linked 2 (BEX2), mRNA [NM_032621]
2.76	2.47	UI-E-CK1-afh-p-15-0-UI.r1 UI-E-CK1 Homo sapiens cDNA clone UI-E-CK1-afh-p-15-0-UI 5', mRNA sequence [BM692484]
-1.64	-1.74	Homo sapiens chromosome 15 open reading frame 42 (C15orf42), mRNA [NM_152259]
-2.55	-3.30	Homo sapiens chromosome 17 open reading frame 53 (C17orf53), mRNA [NM_024032]
-1.59	-1.63	Homo sapiens chromosome 19 open reading frame 48 (C19orf48), mRNA [NM_199249]
1.76	1.52	Homo sapiens chromosome 1 open reading frame 107 (C1orf107), mRNA [NM_014388]
-4.18	-3.15	Homo sapiens chromosome 1 open reading frame 135 (C1orf135), mRNA [NM_024037]
8.30	13.43	Homo sapiens chromosome 20 open reading frame 42 (C20orf42), mRNA [NM_017671]
-1.67	-1.81	Homo sapiens chromosome 21 open reading frame 34 (C21orf34), transcript variant 1, mRNA [NM_001005732]
-1.51	-1.62	Homo sapiens chromosome 21 open reading frame 45 (C21orf45), mRNA [NM_018944]
1.83	1.52	Homo sapiens similar to 2010300C02Rik protein (MGC42367), mRNA [NM_207362]
-2.08	-2.86	Homo sapiens chromosome 5 open reading frame 34 (C5orf34), mRNA [NM_198566]
2.73	3.37	Homo sapiens chromosome 9 open reading frame 3 (C9orf3), mRNA [NM_032823]
3.06	3.18	Homo sapiens chromosome 9 open reading frame 3 (C9orf3), mRNA [NM_032823]
2.32	2.06	Homo sapiens coiled-coil domain containing 69 (CCDC69), mRNA [NM_015621]
-2.92	-3.78	Homo sapiens cyclin B3 (CCNB3), transcript variant 3, mRNA [NM_033031]

<b>[15d] vs [1d]</b>	<b>[15d] vs [RF]</b>	<b>Description</b>
3.90	4.68	Homo sapiens CD34 molecule (CD34), transcript variant 2, mRNA [NM_001773]
-1.68	-2.11	AGENCOURT_14360862 NIH_MGC_187 Homo sapiens cDNA clone IMAGE:30405414 5', mRNA sequence [CD511705]
1.56	1.61	Homo sapiens CD58 molecule (CD58), mRNA [NM_001779]
-1.85	-2.21	Homo sapiens cell division cycle 20 homolog (S. cerevisiae) (CDC20), mRNA [NM_001255]
-1.56	-2.06	Homo sapiens cell division cycle 25 homolog C (S. pombe) (CDC25C), transcript variant 1, mRNA [NM_001790]
-1.52	-1.61	Homo sapiens cyclin-dependent kinase 4 (CDK4), mRNA [NM_000075]
-1.52	-1.86	Homo sapiens chromatin licensing and DNA replication factor 1 (CDT1), mRNA [NM_030928]
-2.02	-2.91	Homo sapiens centromere protein E, 312kDa (CENPE), mRNA [NM_001813]
-2.01	-2.21	Homo sapiens chordin (CHRD), mRNA [NM_003741]
-1.65	-1.89	Homo sapiens Cbp/p300-interacting transactivator, with Glu/Asp-rich carboxy-terminal domain, 2 (CITED2), mRNA [NM_006079]
-4.19	-3.38	Homo sapiens C-type lectin domain family 1, member B (CLEC1B), mRNA [NM_016509]
-1.50	-1.90	CN391963 17000599942841 GRN_PRENEU Homo sapiens cDNA 5', mRNA sequence [CN391963]
4.56	3.49	Homo sapiens cannabinoid receptor 1 (brain) (CNR1), transcript variant 2, mRNA [NM_033181]
-3.86	-3.46	Homo sapiens carboxypeptidase A3 (mast cell) (CPA3), mRNA [NM_001870]
1.75	1.72	full-length cDNA clone CS0DC002YA18 of Neuroblastoma Cot 25-normalized of Homo sapiens (human) [CR624517]
2.07	1.92	Homo sapiens cysteine-rich protein 1 (intestinal) (CRIP1), mRNA [NM_001311]
5.47	14.75	Homo sapiens cytochrome P450, family 1, subfamily B, polypeptide 1 (CYP1B1), mRNA [NM_000104]
11.55	8.25	Homo sapiens dickkopf homolog 2 (Xenopus laevis) (DKK2), mRNA [NM_014421]
1.63	1.62	Homo sapiens DnaJ (Hsp40) homolog, subfamily C, member 3 (DNAJC3), mRNA [NM_006260]
2.00	1.98	Homo sapiens deoxyribonuclease I-like 1 (DNASE1L1), transcript variant 1, mRNA [NM_006730]

<b>[15d] vs [1d]</b>	<b>[15d] vs [RF]</b>	<b>Description</b>
2.33	2.06	Homo sapiens dihydropyrimidinase-like 2 (DPYSL2), mRNA [NM_001386]
1.53	1.73	Homo sapiens dual specificity phosphatase 8 (DUSP8), mRNA [NM_004420]
2.63	2.84	Homo sapiens endothelial differentiation, lysophosphatidic acid G-protein-coupled receptor, 6 (EDG6), mRNA [NM_003775]
1.74	1.56	U6 snRNA-specific terminal uridylyltransferase 1 (EC 2.7.7.52) (U6- TUTase) (RNA-binding protein 21) (RNA-binding motif protein 21). [Source:Uniprot/SWISSPROT;Acc:Q9H6E5] [ENST00000308436]
6.83	7.82	Homo sapiens ficolin (collagen/fibrinogen domain containing) 3 (Hakata antigen) (FCN3), transcript variant 1, mRNA [NM_003665]
3.45	3.14	Homo sapiens fibroblast growth factor 12 (FGF12), transcript variant 2, mRNA [NM_004113]
-2.81	-2.27	Homo sapiens fibrinogen-like 2 (FGL2), mRNA [NM_006682]
-1.65	-1.80	Homo sapiens fidgetin-like 1 (FIGNL1), transcript variant 2, mRNA [NM_022116]
1.85	1.97	Homo sapiens cDNA FLJ37399 fis, clone BRAMY2027587. [AK094718]
-1.65	-1.82	Homo sapiens FAD-dependent oxidoreductase domain containing 2 (FOXRED2), mRNA [NM_024955]
1.61	1.64	Homo sapiens fucokinase (FUK), mRNA [NM_145059]
-2.01	-1.82	Homo sapiens growth differentiation factor 15 (GDF15), mRNA [NM_004864]
-1.98	-2.36	Homo sapiens glia maturation factor, beta (GMFB), mRNA [NM_004124]
-2.08	-1.81	Homo sapiens glia maturation factor, beta (GMFB), mRNA [NM_004124]
3.90	4.17	Guanine nucleotide-binding protein alpha-14 subunit (G-protein alpha subunit 14). [Source:Uniprot/SWISSPROT;Acc:O95837] [ENST00000341700]
1.78	2.08	Homo sapiens guanine nucleotide binding protein (G protein), gamma transducing activity polypeptide 2 (GNGT2), mRNA [NM_031498]
2.37	3.01	Homo sapiens G protein-coupled receptor 68 (GPR68), mRNA [NM_003485]

<b>[15d] vs [1d]</b>	<b>[15d] vs [RF]</b>	<b>Description</b>
4.43	6.58	Homo sapiens G protein-coupled receptor 92 (GPR92), mRNA [NM_020400]
1.79	1.88	Homo sapiens mRNA for KIAA1237 protein, partial cds. [AB033063]
1.68	1.66	Homo sapiens heparanase (HPSE), mRNA [NM_006665]
5.21	5.87	Homo sapiens interleukin 3 receptor, alpha (low affinity) (IL3RA), mRNA [NM_002183]
4.60	6.20	Homo sapiens interleukin 3 receptor, alpha (low affinity) (IL3RA), mRNA [NM_002183]
-1.55	-1.99	Homo sapiens inhibin, beta A (activin A, activin AB alpha polypeptide) (INHBA), mRNA [NM_002192]
2.45	2.62	Homo sapiens potassium channel, subfamily K, member 3 (KCNK3), mRNA [NM_002246]
1.98	1.98	Homo sapiens KIAA1244 (KIAA1244), mRNA [NM_020340]
1.94	2.64	Homo sapiens KIAA1522 (KIAA1522), mRNA [NM_020888]
-1.67	-2.08	Homo sapiens kinesin family member 22 (KIF22), mRNA [NM_007317]
2.43	4.06	Homo sapiens Kruppel-like factor 2 (lung) (KLF2), mRNA [NM_016270]
2.75	2.22	Homo sapiens Kruppel-like factor 4 (gut) (KLF4), mRNA [NM_004235]
2.13	2.83	Homo sapiens low density lipoprotein receptor (familial hypercholesterolemia) (LDLR), mRNA [NM_000527]
2.35	2.81	Homo sapiens low density lipoprotein receptor (familial hypercholesterolemia) (LDLR), mRNA [NM_000527]
2.50	2.20	Homo sapiens LIM and senescent cell antigen-like domains 2 (LIMS2), mRNA [NM_017980]
-1.63	-2.09	Homo sapiens similar to CG12314 gene product (LOC201164), mRNA [NM_178836]
-1.51	-1.95	Homo sapiens calcium binding protein P22 pseudogene (LOC729603) on chromosome 6 [NR_003288]
2.62	4.00	Human parathyroid hormone-like peptide mRNA, 3' end. [M31157]
1.83	1.98	Homo sapiens MADS box transcription enhancer factor 2, polypeptide A (myocyte enhancer factor 2A) (MEF2A), mRNA [NM_005587]
1.93	2.12	Homo sapiens MADS box transcription enhancer factor 2, polypeptide A (myocyte enhancer factor 2A) (MEF2A), mRNA [NM_005587]

<b>[15d] vs [1d]</b>	<b>[15d] vs [RF]</b>	<b>Description</b>
-2.17	-2.54	Homo sapiens hypothetical protein MGC24975 (MGC24975), mRNA [NM_153359]
1.51	1.65	Homo sapiens muscle RAS oncogene homolog (MRAS), mRNA [NM_012219]
-40.13	-159.55	Homo sapiens metallothionein 1F (MT1F), mRNA [NM_005949]
-3.58	-5.52	Homo sapiens metallothionein 1G (MT1G), mRNA [NM_005950]
-3.93	-6.04	Homo sapiens metallothionein 1H (MT1H), mRNA [NM_005951]
-3.80	-5.65	H.sapiens mRNA for metallothionein isoform 1R. [X97261]
-22.47	-37.83	Homo sapiens metallothionein 1M (MT1M), mRNA [NM_176870]
-3.90	-6.19	Homo sapiens metallothionein 1X (MT1X), mRNA [NM_005952]
-2.18	-2.44	Homo sapiens v-myb myeloblastosis viral oncogene homolog (avian)-like 1 (MYBL1), mRNA [NM_001080416]
5.67	4.66	Homo sapiens myomesin family, member 3 (MYOM3), mRNA [NM_152372]
5.76	5.15	Homo sapiens myomesin family, member 3 (MYOM3), mRNA [NM_152372]
1.90	2.15	Homo sapiens neural precursor cell expressed, developmentally down-regulated 9 (NEDD9), transcript variant 1, mRNA [NM_006403]
-2.17	-2.06	Homo sapiens nexilin (F actin binding protein) (NEXN), mRNA [NM_144573]
-1.54	-1.84	Homo sapiens nuclear factor of kappa light polypeptide gene enhancer in B-cells inhibitor-like 2 (NFKBIL2), mRNA [NM_013432]
3.24	3.19	Homo sapiens neuronal guanine nucleotide exchange factor (NGEF), mRNA [NM_019850]
5.54	4.54	Homo sapiens natriuretic peptide receptor A/guanylate cyclase A (atriuretic peptide receptor A) (NPR1), mRNA [NM_000906]
2.28	1.97	Homo sapiens ornithine decarboxylase antizyme 3 (OAZ3), mRNA [NM_016178]
2.00	1.86	Homo sapiens ornithine decarboxylase antizyme 3 (OAZ3), mRNA [NM_016178]

<b>[15d] vs [1d]</b>	<b>[15d] vs [RF]</b>	<b>Description</b>
2.15	2.84	Homo sapiens cDNA FLJ16750 fis, clone ADRGL2011190, highly similar to cGMP-dependent 3',5'-cyclic phosphodiesterase (EC 3.1.4.17). [AK131525]
2.06	2.77	Homo sapiens phosphodiesterase 2A, cGMP-stimulated (PDE2A), mRNA [NM_002599]
1.67	1.61	Homo sapiens PDZ and LIM domain 3 (PDLIM3), mRNA [NM_014476]
-2.01	-2.44	Homo sapiens protein kinase, membrane associated tyrosine/threonine 1 (PKMYT1), transcript variant 2, mRNA [NM_182687]
1.62	1.99	Homo sapiens peripheral myelin protein 22 (PMP22), transcript variant 1, mRNA [NM_000304]
3.29	2.57	Homo sapiens prostaglandin D2 synthase 21kDa (brain) (PTGDS), mRNA [NM_000954]
2.63	4.32	Parathyroid hormone-related protein precursor (PTH-rP) (PTHrP) [Contains: PTHrP[1-36]; PTHrP[38-94]; Osteostatin (PTHrP[107-139])]. [Source:Uniprot/SWISSPROT;Acc:P12272] [ENST00000354417]
1.68	2.11	Homo sapiens parathyroid hormone-like hormone (PTHrP), transcript variant 1, mRNA [NM_198965]
1.83	2.60	Homo sapiens protein tyrosine phosphatase, receptor type, E (PTPRE), transcript variant 1, mRNA [NM_006504]
1.83	2.09	Homo sapiens protein tyrosine phosphatase, receptor type, E (PTPRE), transcript variant 1, mRNA [NM_006504]
1.69	2.03	Homo sapiens Ras association (RalGDS/AF-6) and pleckstrin homology domains 1 (RAPH1), transcript variant 2, mRNA [NM_025252]
1.60	2.06	Homo sapiens Ras association (RalGDS/AF-6) and pleckstrin homology domains 1 (RAPH1), transcript variant 1, mRNA [NM_213589]
-2.78	-2.57	Homo sapiens renin binding protein (RENBP), mRNA [NM_002910]
1.51	1.66	Homo sapiens shroom family member 1 (SHROOM1), mRNA [NM_133456]
-2.08	-2.19	Homo sapiens solute carrier family 30 (zinc transporter), member 3 (SLC30A3), mRNA [NM_003459]
1.56	1.65	Homo sapiens solute carrier family 6 (neurotransmitter transporter, taurine), member 6 (SLC6A6), mRNA [NM_003043]
4.27	5.32	Homo sapiens serine peptidase inhibitor, Kazal type 5 (SPINK5), mRNA [NM_006846]

<b>[15d] vs [1d]</b>	<b>[15d] vs [RF]</b>	<b>Description</b>
-1.91	-1.92	Homo sapiens suppressor of variegation 3-9 homolog 1 (Drosophila) (SUV39H1), mRNA [NM_003173]
-1.51	-1.77	Homo sapiens spectrin repeat containing, nuclear envelope 1 (SYNE1), transcript variant longer, mRNA [NM_033071]
7.18	6.10	Homo sapiens transforming growth factor, alpha (TGFA), mRNA [NM_003236]
2.80	3.84	Homo sapiens thrombomodulin (THBD), mRNA [NM_000361]
4.29	4.13	THC2617352
1.97	1.69	THC2631465
1.69	2.11	BC004696 Nedd9 protein Mus musculus (exp=-1; wgp=0; cg=0), partial (6%) [THC2657091]
-2.52	-3.03	Homo sapiens transmembrane and coiled-coil domains 2 (TMCO2), mRNA [NM_001008740]
-1.65	-1.53	Homo sapiens transmembrane protein 140 (TMEM140), mRNA [NM_018295]
-1.63	-2.26	Homo sapiens thyroid hormone receptor interactor 13 (TRIP13), mRNA [NM_004237]
1.53	1.70	Homo sapiens ubiquitin-conjugating enzyme E2F (putative) (UBE2F), mRNA [NM_080678]
11.13	8.63	Homo sapiens versican (VCAN), mRNA [NM_004385]
-1.99	-1.76	Homo sapiens zinc finger protein interacting with K protein 1 homolog (mouse) (ZIK1), mRNA [NM_001010879]
2.15	2.48	Homo sapiens cDNA FLJ37939 fis, clone CTONG2007613, highly similar to ZINC FINGER PROTEIN 185. [AK095258]

## REFERENCES

1. Lloyd-Jones D, Adams R, Carnethon M, De Simone G, Ferguson TB, Flegal K, Ford E, Furie K, Go A, Greenlund K, Haase N, Hailpern S, Ho M, Howard V, Kissela B, Kittner S, Lackland D, Lisabeth L, Marelli A, McDermott M, Meigs J, Mozaffarian D, Nichol G, O'Donnell C, Roger V, Rosamond W, Sacco R, Sorlie P, Stafford R, Steinberger J, Thom T, Wasserthiel-Smoller S, Wong N, Wylie-Rosett J, Hong Y. Heart Disease and Stroke Statistics--2009 Update. A Report From the American Heart Association Statistics Committee and Stroke Statistics Subcommittee. *Circulation*. 2008.
2. Davies PF. Hemodynamic shear stress and the endothelium in cardiovascular pathophysiology. *Nat Clin Pract Cardiovasc Med*. 2009;6(1):16-26.
3. Davies PF. Endothelial transcriptome profiles in vivo in complex arterial flow fields. *Ann Biomed Eng* 2008;36(4):563-570.
4. Glagov S, Zarins C, Giddens DP, Ku DN. Hemodynamics and atherosclerosis. Insights and perspectives gained from studies of human arteries. *Arch Pathol Lab Med*. 1988;112:1018-1031
5. Dobrin PB, Littooy FN, Endean ED. Mechanical factors predisposing to intimal hyperplasia and medial thickening in autogenous vein grafts. *Surgery*. 1989;105:393-400
6. Goldsmith HL, Turitto VT. Rheological aspects of thrombosis and haemostasis: basic principles and applications. ICTH-Report--Subcommittee on Rheology of the International Committee on Thrombosis and Haemostasis. *Thromb Haemost*. 1986;55:415-435.
7. Frangos JA, McIntire LV, Eskin SG. Shear stress induced stimulation of mammalian cell metabolism. *Biotech. Bioeng*. 1987;32:1053-1060.
8. Chien S. Effects of disturbed flow on endothelial cells. *Ann Biomed Eng*. 2008;36(4):554-562.
9. Yee A, Bosworth KA, Conway DE, Eskin SG, McIntire LV. Gene expression of endothelial cells under pulsatile non-reversing vs. steady shear stress; comparison of nitric oxide production. *Ann Biomed Eng*. 2008;36(4):571-579.
10. McCormick SM, Eskin SG, McIntire LV, Teng CL, Lu CM, Russell CG, Chittur KK. DNA microarray reveals changes in gene expression of shear stressed human umbilical vein endothelial cells. *Proc Natl Acad Sci U S A*. 2001;98:8955-8960.

11. Dai G, Kaazempur-Mofrad MR, Natarajan S, Zhang Y, Vaughn S, Blackman BR, Kamm RD, Garcia-Cardena G, Gimbrone MA, Jr. 41. Distinct endothelial phenotypes evoked by arterial waveforms derived from atherosclerosis-susceptible and -resistant regions of human vasculature. *Proc Natl Acad Sci U S A*. 2004;101:14871-14876
12. White CR, Frangos JA. The shear stress of it all: the cell membrane and mechanochemical transduction. *Philos Trans R Soc Lond B Biol Sci*. 2007;362(1484):1459-1467.
13. Frangos JA, Eskin SG, McIntire LV, Ives CL. Flow effects on prostacyclin production by cultured human endothelial cells. *Science*. 1985;227:1477-1479
14. Orr AW, Helmke BP, Blackman BR, Schwartz MA. Mechanisms of mechanotransduction. *Dev Cell*. 2006;10(1):11-20.
15. Eskin SG, McIntire LV. Hemodynamic effects on atherosclerosis and thrombosis. *Semin Thromb Hemost*. 1988;14:170-174
16. Dai G, Kaazempur-Mofrad MR, Natarajan S, Zhang Y, Vaughn S, Blackman BR, Kamm RD, Garcia-Cardena G, Gimbrone MA, Jr. Distinct endothelial phenotypes evoked by arterial waveforms derived from atherosclerosis-susceptible and -resistant regions of human vasculature. *Proc Natl Acad Sci U S A*. 2004;101(41):14871-14876.
17. Perktold K, Rappitsch G. Computer simulation of local blood flow and vessel mechanics in a compliant carotid artery bifurcation model. *J Biomech*. 1995;28(7):845-856.
18. Ohura N, Yamamoto K, Ichioka S, Sokabe T, Nakatsuka H, Baba A, Shibata M, Nakatsuka T, Harii K, Wada Y, Kohro T, Kodama T, Ando J. Global analysis of shear stress-responsive genes in vascular endothelial cells. *J Atheroscler Thromb*. 2003;10(5):304-313.
19. McCormick SM, Eskin SG, McIntire LV, Teng CL, Lu CM, Russell CG, Chittur KK. DNA microarray reveals changes in gene expression of shear stressed human umbilical vein endothelial cells. *Proc. Natl. Acad. Sci. U. S. A*. 2001;98(16):8955-8960.
20. Garcia-Cardena G, Comander J, Anderson KR, Blackman BR, Gimbrone MA, Jr. Biomechanical activation of vascular endothelium as a determinant of its functional phenotype. *Proc. Natl. Acad. Sci. U. S. A*. 2001;98(8):4478-4485.
21. Dekker RJ, van Soest S, Fontijn RD, Salamanca S, de Groot PG, VanBavel E, Pannekoek H, Horrevoets AJ. Prolonged fluid shear stress induces a distinct set of endothelial cell genes, most specifically lung Kruppel-like factor (KLF2). *Blood*. 2002;100(5):1689-1698.

22. Parmar KM, Larman HB, Dai G, Zhang Y, Wang ET, Moorthy SN, Kratz JR, Lin Z, Jain MK, Gimbrone MA, Jr., Garcia-Cardena G. Integration of flow-dependent endothelial phenotypes by Kruppel-like factor 2. *J Clin Invest*. 2006;116(1):49-58.
23. Fledderus JO, van Thienen JV, Boon RA, Dekker RJ, Rohlena J, Volger OL, Bijmens A-PJJ, Daemen MJAP, Kuiper J, van Berkel TJC, Pannekoek H, Horrevoets AJG. Prolonged shear stress and KLF2 suppress constitutive pro-inflammatory transcription through inhibition of ATF2. *Blood*. 2007;109(10):4249-4257.
24. Barouki R, Morel Y. Repression of cytochrome P450 1A1 gene expression by oxidative stress: mechanisms and biological implications. *Biochem Pharmacol*. 2001;61(5):511-516.
25. Murray GI, Melvin WT, Greenlee WF, Burke MD. Regulation, function, and tissue-specific expression of cytochrome P450 CYP1B1. *Annu Rev Pharmacol Toxicol*. 2001;41:297-316.
26. Choudhary D, Jansson I, Stoilov I, Sarfarazi M, Schenkman JB. Metabolism of retinoids and arachidonic acid by human and mouse cytochrome P450 1b1. *Drug Metab Dispos*. 2004;32(8):840-847.
27. Chambers D, Wilson L, Maden M, Lumsden A. RALDH-independent generation of retinoic acid during vertebrate embryogenesis by CYP1B1. *Development*. 2007;134(7):1369-1383.
28. Vincent AL, Billingsley G, Buys Y, Levin AV, Priston M, Trope G, Williams-Lyn D, Heon E. Digenic inheritance of early-onset glaucoma: CYP1B1, a potential modifier gene. *Am J Hum Genet*. 2002;70(2):448-460.
29. Vasilioi V, Gonzalez FJ. Role of CYP1B1 in Glaucoma. *Annu Rev Pharmacol Toxicol*. 2007;48:333-358.
30. Libby RT, Smith RS, Savinova OV, Zabaleta A, Martin JE, Gonzalez FJ, John SW. Modification of ocular defects in mouse developmental glaucoma models by tyrosinase. *Science*. 2003;299(5612):1578-1581.
31. Cortese MM, Suschek CV, Wetzel W, Kroncke KD, Kolb-Bachofen V. Zinc protects endothelial cells from hydrogen peroxide via Nrf2-dependent stimulation of glutathione biosynthesis. *Free Radic Biol Med*. 2008;44(12):2002-2012.
32. Singh RB, Gupta UC, Mittal N, Niaz MA, Ghosh S, Rastogi V. Epidemiologic study of trace elements and magnesium on risk of coronary artery disease in rural and urban Indian populations. *J Am Coll Nutr*. 1997;16(1):62-67.

33. Jenner A, Ren M, Rajendran R, Ning P, Huat BT, Watt F, Halliwell B. Zinc supplementation inhibits lipid peroxidation and the development of atherosclerosis in rabbits fed a high cholesterol diet. *Free Radic Biol Med.* 2007;42(4):559-566.
34. Ren M, Rajendran R, Ning P, Tan Kwong Huat B, Choon Nam O, Watt F, Jenner A, Halliwell B. Zinc supplementation decreases the development of atherosclerosis in rabbits. *Free Radic Biol Med.* 2006;41(2):222-225.
35. Alissa EM, Bahijri SM, Lamb DJ, Ferns GA. The effects of coadministration of dietary copper and zinc supplements on atherosclerosis, antioxidant enzymes and indices of lipid peroxidation in the cholesterol-fed rabbit. *Int J Exp Pathol.* 2004;85(5):265-275.
36. Reiterer G, MacDonald R, Browning JD, Morrow J, Matveev SV, Daugherty A, Smart E, Toborek M, Hennig B. Zinc deficiency increases plasma lipids and atherosclerotic markers in LDL-receptor-deficient mice. *J Nutr.* 2005;135(9):2114-2118.
37. Shen H, Oesterling E, Stromberg A, Toborek M, MacDonald R, Hennig B. Zinc deficiency induces vascular pro-inflammatory parameters associated with NF-kappaB and PPAR signaling. *J Am Coll Nutr.* 2008;27(5):577-587.
38. Hennig B, Meerarani P, Toborek M, McClain CJ. Antioxidant-like properties of zinc in activated endothelial cells. *J Am Coll Nutr.* 1999;18(2):152-158.
39. Wootton DM, Ku DN. Fluid mechanics of vascular systems, diseases, and thrombosis. *Annu Rev Biomed Eng.* 1999;1:299-329.
40. Yee A, Sakurai Y, Eskin SG, McIntire LV. A validated system for simulating common carotid arterial flow in vitro: alteration of endothelial cell response. *Ann Biomed Eng.* 2006;34(4):593-604.
41. Conway DE, Sakurai Y, Weiss D, Vega JD, Taylor WR, Jo H, Eskin SG, Marcus CB, McIntire LV. Expression of CYP1A1 and CYP1B1 in human endothelial cells: regulation by fluid shear stress. *Cardiovasc. Res.* 2009.
42. Chow S, Rodgers P. Applet For Drawing 3 Set Area-Proportional Venn Diagrams. Available at: <http://www.cs.kent.ac.uk/people/staff/pjr/EulerVennCircles/EulerVennApplet.html>. Accessed 9/25/08, 2008.
43. Chappell DC, Varner SE, Nerem RM, Medford RM, Alexander RW. Oscillatory shear stress stimulates adhesion molecule expression in cultured human endothelium. *Circ. Res.* 1998;82(5):532-539.

44. Sorescu GP, Sykes M, Weiss D, Platt MO, Saha A, Hwang J, Boyd N, Boo YC, Vega JD, Taylor WR, Jo H. Bone morphogenic protein 4 produced in endothelial cells by oscillatory shear stress stimulates an inflammatory response. *J. Biol. Chem.* 2003;278(33):31128-31135.
45. Brooks AR, Lelkes PI, Rubanyi GM. Gene expression profiling of human aortic endothelial cells exposed to disturbed flow and steady laminar flow. *Physiol Genomics.* 2002;9(1):27-41.
46. Davies PF. Endothelial transcriptome profiles in vivo in complex arterial flow fields. *Ann. Biomed. Eng.* 2008;36(4):563-570.
47. Chen BP, Li YS, Zhao Y, Chen KD, Li S, Lao J, Yuan S, Shyy JY, Chien S. DNA microarray analysis of gene expression in endothelial cells in response to 24-h shear stress. *Physiol Genomics.* 2001;7(1):55-63.
48. Mann GJ, Musgrove EA, Fox RM, Thelander L. Ribonucleotide reductase M1 subunit in cellular proliferation, quiescence, and differentiation. *Cancer Res.* 1988;48(18):5151-5156.
49. Payton M, Coats S. Cyclin E2, the cycle continues. *Int. J. Biochem. Cell Biol.* 2002;34(4):315-320.
50. Dehde S, Rohaly G, Schub O, Nasheuer HP, Bohn W, Chemnitz J, Deppert W, Dornreiter I. Two immunologically distinct human DNA polymerase alpha-primase subpopulations are involved in cellular DNA replication. *Mol. Cell. Biol.* 2001;21(7):2581-2593.
51. Dekker RJ, van Thienen JV, Rohlena J, de Jager SC, Elderkamp YW, Seppen J, de Vries CJ, Biessen EA, van Berkel TJ, Pannekoek H, Horrevoets AJ. Endothelial KLF2 links local arterial shear stress levels to the expression of vascular tone-regulating genes. *Am J Pathol.* 2005;167(2):609-618.
52. Wang N, Miao H, Li YS, Zhang P, Haga JH, Hu Y, Young A, Yuan S, Nguyen P, Wu CC, Chien S. Shear stress regulation of Kruppel-like factor 2 expression is flow pattern-specific. *Biochem Biophys Res Commun.* 2006;341(4):1244-1251.
53. Sorescu GP, Song H, Tressel SL, Hwang J, Dikalov S, Smith DA, Boyd NL, Platt MO, Lassegue B, Griendling KK, Jo H. Bone morphogenic protein 4 produced in endothelial cells by oscillatory shear stress induces monocyte adhesion by stimulating reactive oxygen species production from a nox1-based NADPH oxidase. *Circ. Res.* 2004;95(8):773-779.
54. Michaelis UR, Fleming I. From endothelium-derived hyperpolarizing factor (EDHF) to angiogenesis: Epoxyeicosatrienoic acids (EETs) and cell signaling. *Pharmacol Ther.* 2006;111(3):584-595.

55. Denison MS, Nagy SR. Activation of the aryl hydrocarbon receptor by structurally diverse exogenous and endogenous chemicals. *Annual Review of Pharmacology and Toxicology*. 2003;43(1):309-334.
56. Dabir P, Marinic TE, Krukovets I, Stenina OI. Aryl hydrocarbon receptor is activated by glucose and regulates the thrombospondin-1 gene promoter in endothelial cells. *Circ Res*. 2008;102(12):1558-1565.
57. Chiaro CR, Patel RD, Marcus CB, Perdew GH. Evidence for an aryl hydrocarbon receptor-mediated cytochrome p450 autoregulatory pathway. *Mol Pharmacol*. 2007;72(5):1369-1379.
58. Han Z, Miwa Y, Obikane H, Mitsumata M, Takahashi-Yanaga F, Morimoto S, Sasaguri T. Aryl hydrocarbon receptor mediates laminar fluid shear stress-induced CYP1A1 activation and cell cycle arrest in vascular endothelial cells. *Cardiovasc Res*. 2008;77(4):809-818.
59. Vidal JD, Vandevoort CA, Marcus CB, Lazarewicz NR, Conley AJ. 2,3,7,8-tetrachlorodibenzo-p-dioxin induces CYP1B1 expression in human luteinized granulosa cells. *Arch Biochem Biophys*. 2005;439(1):53-60.
60. Cali JJ, Ma D, Sobol M, Simpson DJ, Frackman S, Good TD, Daily WJ, Liu D. Luminogenic cytochrome P450 assays. *Expert Opin Drug Metab Toxicol*. 2006;2(4):629-645.
61. Pollenz RS, Sattler CA, Poland A. The aryl hydrocarbon receptor and aryl hydrocarbon receptor nuclear translocator protein show distinct subcellular localizations in Hepa 1c1c7 cells by immunofluorescence microscopy. *Mol Pharmacol*. 1994;45(3):428-438.
62. Soucek P, Martin MV, Ueng YF, Guengerich FP. Identification of a common cytochrome P450 epitope near the conserved heme-binding peptide with antibodies raised against recombinant cytochrome P450 family 2 proteins. *Biochemistry*. 1995;34(49):16013-16021.
63. Suo J, Ferrara DE, Sorescu D, Guldberg RE, Taylor WR, Giddens DP. Hemodynamic shear stresses in mouse aortas: implications for atherogenesis. *Arterioscler Thromb Vasc Biol*. 2007;27(2):346-351.
64. Sorescu D, Weiss D, Lassegue B, Clempus RE, Szocs K, Sorescu GP, Valppu L, Quinn MT, Lambeth JD, Vega JD, Taylor WR, Griendling KK. Superoxide production and expression of nox family proteins in human atherosclerosis. *Circulation*. 2002;105(12):1429-1435.
65. Kao S-H, McIntire LV. Rheology. In: Loscalzo J, Schafer AI, eds. *Thrombosis and hemorrhage*. 3rd ed. Philadelphia: Lippincott Williams & Wilkins; 2003:294-314.

66. Kim S, Ko H, Park JE, Jung S, Lee SK, Chun YJ. Design, synthesis, and discovery of novel trans-stilbene analogues as potent and selective human cytochrome P450 1B1 inhibitors. *J Med Chem.* 2002;45(1):160-164.
67. Shimada T, Yamazaki H, Foroozesh M, Hopkins NE, Alworth WL, Guengerich FP. Selectivity of polycyclic inhibitors for human cytochrome P450s 1A1, 1A2, and 1B1. *Chem Res Toxicol.* 1998;11(9):1048-1056.
68. Song J, Clagett-Dame M, Peterson RE, Hahn ME, Westler WM, Sicinski RR, DeLuca HF. A ligand for the aryl hydrocarbon receptor isolated from lung. *Proc Natl Acad Sci U S A.* 2002;99(23):14694-14699.
69. Eskin SG, Turner NA, McIntire LV. Endothelial Cell Cytochrome P450 1A1 and 1B1: Up-Regulation by Shear Stress. *Endothelium.* 2004;11(1):1-10.
70. McMillan BJ, Bradfield CA. The Aryl hydrocarbon receptor is activated by modified low-density lipoprotein. *Proc Natl Acad Sci U S A.* 2007;104(4):1412-1417.
71. Guo J, Sartor M, Karyala S, Medvedovic M, Kann S, Puga A, Ryan P, Tomlinson CR. Expression of genes in the TGF-beta signaling pathway is significantly deregulated in smooth muscle cells from aorta of aryl hydrocarbon receptor knockout mice. *Toxicol Appl Pharmacol.* 2004;194(1):79-89.
72. Isenberg JS, Ridnour LA, Perruccio EM, Espey MG, Wink DA, Roberts DD. Thrombospondin-1 inhibits endothelial cell responses to nitric oxide in a cGMP-dependent manner. *Proc Natl Acad Sci U S A.* 2005;102(37):13141-13146.
73. Rifkind AB. CYP1A in TCDD toxicity and in physiology-with particular reference to CYP dependent arachidonic acid metabolism and other endogenous substrates. *Drug Metab Rev.* 2006;38(1-2):291-335.
74. Farin FM, Pohlman TH, Omiecinski CJ. Expression of Cytochrome P450s and Microsomal Epoxide Hydrolase in Primary Cultures of Human Umbilical Vein Endothelial Cells. *Toxicology and Applied Pharmacology.* 1994;124(1):1-9.
75. Zhao W, Parrish AR, Ramos KS. Constitutive and inducible expression of cytochrome P450IA1 and P450IB1 in human vascular endothelial and smooth muscle cells. *In Vitro Cell Dev Biol Anim.* 1998;34(9):671-673.
76. Thum T, Haverich A, Borlak J. Cellular dedifferentiation of endothelium is linked to activation and silencing of certain nuclear transcription factors: implications for endothelial dysfunction and vascular biology. *FASEB J.* 2000;14(5):740-751.
77. Choudhary D, Jansson I, Rezaul K, Han DK, Sarfarazi M, Schenkman JB. Cyp1b1 Protein in the Mouse Eye during Development: An Immunohistochemical Study. *Drug Metab Dispos.* 2007;35(6):987-994.

78. Tang Y, Scheef EA, Wang S, Sorenson CM, Marcus CB, Jefcoate CR, Sheibani N. CYP1B1 expression promotes the proangiogenic phenotype of endothelium through decreased intracellular oxidative stress and thrombospondin-2 expression. *Blood*. 2008.
79. Doshi M, Marcus C, Bejjani BA, Edward DP. Immunolocalization of CYP1B1 in normal, human, fetal and adult eyes. *Exp Eye Res*. 2006;82(1):24-32.
80. Dubey RK, Gillespie DG, Zacharia LC, Barchiesi F, Imthurn B, Jackson EK. CYP450- and COMT-Derived Estradiol Metabolites Inhibit Activity of Human Coronary Artery SMCs. *Hypertension*. 2003;41(3):807-813.
81. Kerzee JK, Ramos KS. Constitutive and inducible expression of Cyp1a1 and Cyp1b1 in vascular smooth muscle cells: role of the Ahr bHLH/PAS transcription factor. *Circ Res*. 2001;89(7):573-582.
82. Zeldin DC. Epoxygenase Pathways of Arachidonic Acid Metabolism. *J Biol Chem*. 2001;276(39):36059-36062.
83. Schwarz D, Kisselev P, Ericksen SS, Szklarz GD, Chernogolov A, Honeck H, Schunck WH, Roots I. Arachidonic and eicosapentaenoic acid metabolism by human CYP1A1: highly stereoselective formation of 17(R),18(S)-epoxyeicosatetraenoic acid. *Biochem Pharmacol*. 2004;67(8):1445-1457.
84. Huang A, Sun D, Jacobson A, Carroll MA, Falck JR, Kaley G. Epoxyeicosatrienoic acids are released to mediate shear stress-dependent hyperpolarization of arteriolar smooth muscle. *Circ Res*. 2005;96(3):376-383.
85. Liu Y, Zhang Y, Schmelzer K, Lee TS, Fang X, Zhu Y, Spector AA, Gill S, Morisseau C, Hammock BD, Shyy JY. The antiinflammatory effect of laminar flow: the role of PPARgamma, epoxyeicosatrienoic acids, and soluble epoxide hydrolase. *Proc Natl Acad Sci U S A*. 2005;102(46):16747-16752.
86. Guengerich FP. Cytochrome p450 and chemical toxicology. *Chem Res Toxicol*. 2008;21(1):70-83.
87. Zhu M, Fu Y, Hou Y, Wang N, Guan Y, Tang C, Shyy JY, Zhu Y. Laminar shear stress regulates liver X receptor in vascular endothelial cells. *Arterioscler Thromb Vasc Biol*. 2008;28(3):527-533.
88. Aguiar M, Masse R, Gibbs BF. Regulation of cytochrome P450 by posttranslational modification. *Drug Metab Rev*. 2005;37(2):379-404.
89. Beattie JH, Kwun IS. Is zinc deficiency a risk factor for atherosclerosis? *Br J Nutr*. 2004;91(2):177-181.

90. Vlad M, Caseanu E, Uza G, Petrescu M. Concentration of copper, zinc, chromium, iron and nickel in the abdominal aorta of patients deceased with coronary heart disease. *J Trace Elem Electrolytes Health Dis.* 1994;8(2):111-114.
91. Stadler N, Stanley N, Heeneman S, Vacata V, Daemen MJ, Bannon PG, Waltenberger J, Davies MJ. Accumulation of zinc in human atherosclerotic lesions correlates with calcium levels but does not protect against protein oxidation. *Arterioscler Thromb Vasc Biol.* 2008;28(5):1024-1030.
92. Paul A, Calleja L, Joven J, Vilella E, Ferre N, Camps J, Girona J, Osada J. Supplementation with vitamin E and/or zinc does not attenuate atherosclerosis in apolipoprotein E-deficient mice fed a high-fat, high-cholesterol diet. *Int J Vitam Nutr Res.* 2001;71(1):45-52.
93. Hainaut P, Mann K. Zinc binding and redox control of p53 structure and function. *Antioxid Redox Signal.* 2001;3(4):611-623.
94. Visse R, Nagase H. Matrix metalloproteinases and tissue inhibitors of metalloproteinases: structure, function, and biochemistry. *Circ Res.* 2003;92(8):827-839.
95. de Souza AP, Gerlach RF, Line SR. Inhibition of human gingival gelatinases (MMP-2 and MMP-9) by metal salts. *Dent Mater.* 2000;16(2):103-108.
96. Wilkins GM, Leake DS. The oxidation of low density lipoprotein by cells or iron is inhibited by zinc. *FEBS Lett.* 1994;341(2-3):259-262.
97. Gee KR, Zhou ZL, Qian WJ, Kennedy R. Detection and imaging of zinc secretion from pancreatic beta-cells using a new fluorescent zinc indicator. *J Am Chem Soc.* 2002;124(5):776-778.
98. Bernal PJ, Leelavanichkul K, Bauer E, Cao R, Wilson A, Wasserloos KJ, Watkins SC, Pitt BR, St Croix CM. Nitric-oxide-mediated zinc release contributes to hypoxic regulation of pulmonary vascular tone. *Circ Res.* 2008;102(12):1575-1583.
99. Ranjan V, Xiao Z, Diamond SL. Constitutive NOS expression in cultured endothelial cells is elevated by fluid shear stress. *Am J Physiol.* 1995;269(2 Pt 2):H550-555.
100. Andrews GK. Regulation of metallothionein gene expression by oxidative stress and metal ions. *Biochem Pharmacol.* 2000;59(1):95-104.
101. Hwang J, Saha A, Boo YC, Sorescu GP, McNally JS, Holland SM, Dikalov S, Giddens DP, Griendling KK, Harrison DG, Jo H. Oscillatory shear stress stimulates endothelial production of O<sub>2</sub><sup>-</sup> from p47phox-dependent NAD(P)H

- oxidases, leading to monocyte adhesion. *J Biol Chem.* 2003;278(47):47291-47298.
- 102.** Hosoya T, Maruyama A, Kang MI, Kawatani Y, Shibata T, Uchida K, Warabi E, Noguchi N, Itoh K, Yamamoto M. Differential responses of the Nrf2-Keap1 system to laminar and oscillatory shear stresses in endothelial cells. *J Biol Chem.* 2005;280(29):27244-27250.
- 103.** Lin K, Hsu PP, Chen BP, Yuan S, Usami S, Shyy JY, Li YS, Chien S. Molecular mechanism of endothelial growth arrest by laminar shear stress. *Proc Natl Acad Sci U S A.* 2000;97(17):9385-9389.
- 104.** Orr AW, Sanders JM, Bevard M, Coleman E, Sarembock IJ, Schwartz MA. The subendothelial extracellular matrix modulates NF-kappaB activation by flow: a potential role in atherosclerosis. *J Cell Biol.* 2005;169(1):191-202.
- 105.** van den Berg BM, Spaan JA, Rolf TM, Vink H. Atherogenic region and diet diminish glycocalyx dimension and increase intima-to-media ratios at murine carotid artery bifurcation. *Am J Physiol Heart Circ Physiol.* 2006;290(2):H915-920.
- 106.** Lim EJ, Majkova Z, Xu S, Bachas L, Arzuaga X, Smart E, Tseng MT, Toborek M, Hennig B. Coplanar polychlorinated biphenyl-induced CYP1A1 is regulated through caveolae signaling in vascular endothelial cells. *Chem Biol Interact.* 2008;176(2-3):71-78.
- 107.** Shen H, Arzuaga X, Toborek M, Hennig B. Zinc Nutritional Status Modulates Expression of Ahr-Responsive P450 Enzymes in Vascular Endothelial Cells. *Environ Toxicol Pharmacol.* 2008;25(2):197-201.